Novel strategies for monitoring intervertebral disc degeneration and regeneration

Novel strategies for monitoring intervertebral disc degeneration and regeneration

A catalogue record is available from the Eindhoven University of Technology Library

ISBN: 978-90-386-3692-4

This thesis was prepared with the LaTeX documentation system.
Reproduction: Ipskram Drukkers B.V., Enschede, The Netherlands.

The research was supported by the European Community's Seventh Framework Programme (FP7, 2007-2013) under grant agreement no. HEALTH-F2-2008-201626.

Novel strategies for monitoring intervertebral disc degeneration and regeneration

PROEFSCHRIFT

ter verkrijging van de graad van doctor aan de Technische Universiteit Eindhoven, op gezag van de rector magnificus prof.dr.ir. C.J. van Duijn, voor een commissie aangewezen door het College voor Promoties, in het openbaar te verdedigen op dinsdag 7 oktober 2014 om 16:00 uur

door

Roman Dittmar

geboren te Leipzig, Duitsland

Dit proefschrift is goedgekeurd door de promotoren en de samenstelling van de promotiecommissie is als volgt:

voorzitter:	prof.dr.ir. P. A.J. Hilbers
1^e promotor:	prof.dr. K. Ito
copromotor(en):	dr. C.C. van Donkelaar
leden:	prof.dr. J. Iatridis (Mount Sinai School of Medicine New York)
	prof.dr. M. A. M. J. van Zandvoort (RWTH Aachen)
	dr. L.B. Creemers (Universiteit Utrecht)
	dr. M. Merkx

Contents

Summary

Novel strategies for monitoring intervertebral disc degeneration and regeneration

Within Europe, disorders related to intervertebral disc degeneration are one of the most common and costly of clinical problems and yet diagnosis is very poor. Furthermore, disc structural changes evident on e.g. MRI images arise from cellular and biochemical events which occurred months to years earlier. Examples of such early events include decreased cell viability, increased proteolytic enzyme activity and a change in the composition and organization of the disc's collagen network. Therefore, the general objective of this Ph.D project is to develop novel diagnostic strategies for assessing the condition of tissue and cells in the intervertebral disc to potentially allow an earlier diagnosis of disc degeneration and the monitoring of the efficacy of regenerative therapies. For this purpose, advanced microscopy techniques and novel fluorescent probes were applied and/or developed to enable quantitative measurements of known disc degeneration markers.

In a first study, we sought to determine the potential of non-invasively assessing cell viability in 3D constructs using cellular auto-fluorescence. Current cell viability assays are rather invasive as they require potentially harmful dyes and in some cases even the disintegration of scaffold/tissue prior to quantifying living and dead cells. Recent studies showed that the metabolic state of living cells can be non-destructively probed by measuring cellular auto-fluorescence originating from endogenous proteins. In chapter 2, we demonstrate that also live and dead cells can be discriminated inside 3D constructs by measuring their auto-fluorescence using advanced microscopy tools. Both two-photon and confocal microscopy images of cell seeded collagen gels were acquired and the cellular auto-fluorescence emission was analyzed. Live and dead cells systematically emitted auto-fluorescent light with different spectral characteristics. Based on these spectral differences, cells were classified as viable or dead. Since no dyes were required to stain cells, cell viability could be determined without disintegrating the constructs resulting in an accurate and non-invasive cell viability assessment. Thus, monitoring cellular auto-fluorescence utilizing advanced microscopy tools would potentially allow longitudinal cell viability measurements, e.g. in tissue engineering studies.

To become a useful technique for longitudinally evaluating the effects of regenerative stimuli on cell viability in pre-clinical or even clinical settings, monitoring cellular auto-fluorescence must first prove its applicability in mature tissue containing

a dense extracellular matrix. Recording auto-fluorescent light in such tissues may be considerably more difficult due to increased light scattering, interfering collagen auto-fluorescence and low metabolic activity of intervertebral disc cells. Therefore, in chapter 3, we assessed the feasibility and accuracy of measuring cell viability using cellular auto-fluorescence in an intervertebral disc explant model that better resembles the disc's in-vivo environment. Nucleus pulposus explants were isolated and cultured in media with different glucose supplementation to induce different degrees of cell death. After culture, samples were split and cell viability was assessed using conventional staining and auto-fluorescence measurements using two-photon microscopy. Results show that also living and dead nucleus pulposus cells exhibit distinct spectral differences in their auto-fluorescence emission. Moreover, cell viability values of cultured nucleus pulposus explants as measured by cellular auto-fluorescence were not significantly different from those obtained by conventional (fluorescent) staining. Thus, viability assessments using cellular auto-fluorescence are not limited to 3D constructs. In fact, cell viability can be non-invasively and accurately assessed even in highly light scattering nucleus pulposus tissue in-situ containing low metabolically active live cells and dead cells.

A second biomarker relevant for potentially detecting early intervertebral disc degeneration and monitoring regeneration is the organization of the disc's collagen network. Healthy intervertebral discs consist of a specific, spatially heterogeneous collagen fiber orientation in the annulus fibrosus. Mean fiber angle is 30 with respect to the transverse plane of the spine. However, this mean fiber orientation varies both in radial direction (disc periphery to center) and circumferentially (from anterior to posterior location). While it is well established that severely degenerated intervertebral discs suffer from dramatic changes to their collagen network, less is known about effects of degeneration on the tissue architecture in moderately degenerated discs. Therefore, in chapter 4, we hypothesized that degeneration also affects the collagen fiber organization of moderately degenerated human intervertebral discs and quantified the annulus fibrosus collagen orientation using Second Harmonic Generation microscopy with subsequent image analysis. Results indicate that moderately degenerated human discs are characterized by a spatially homogeneous collagen fiber orientation in contrast to that reported for healthy intervertebral discs. Mean collagen orientation did not change strongly in radial or in circumferential direction supporting the hypothesis that the disc tissue architecture is affected during (early) degeneration. As the mechanical properties of the annulus fibrosus and consequently of the entire disc depend on the collagen fiber organization, these findings support the hypothesis that moderately degenerated discs are subjected to an altered mechano-biological environment which in its turn may induce more or accelerate degenerative changes in the intervertebral disc.

Finally, in chapter 5, we describe the development and characterization of a novel-fluorescent probe for detecting and monitoring matrix metalloproteinase 13 (MMP-13) activity, a catabolic enzyme involved in intervertebral disc degeneration. Both levels and activities of MMP-13 are rather low or negligible in the normal steady-state, however during disc degeneration increased or unbalanced levels and activities of MMP-13 are widely thought to mediate disc matrix breakdown particularly in the nucleus pulposus. Based on existing probe designs, a novel probe was synthesized consisting of a peptide linker that functions as a specific substrate to MMP-13 and a fluorescence donor and quencher. In the absence of active MMP-13, no fluorescent light is emitted since the energy of the donor is transferred to the quencher by fluorescence

resonance energy transfer. When the peptide linker is cleaved by active MMP-13, the fluorescence donor separates from the quencher and, therefore, the energy transfer from donor to quencher seizes resulting in a detectable fluorescence signal. Probe performance parameters of measuring active MMP-13 in buffer solution and in 3D constructs largely complied with relevant guidelines and fluorescent probe detection limit is similar to that of the gold standard technique, i.e. ELISA. Moreover, no significant differences in measuring active MMP-13 levels were found between the novel probe and ELISA indicating the good accuracy of this novel method for assaying active MMP-13. However, while measurements in buffer demonstrated the selectivity of the fluorescent probe for active MMP-13, results from 3D cell culture indicate that the probe may be subjected to non-specific cleavage and therefore selectivity is lost. Since other fluorescent probes exhibit a very similar design, these results may raise concerns regarding the feasibility of measuring cell-produced MMP-13 utilizing such probes and may therefore prompt the re-evaluation of current probe designs.

Chapter 1

General Introduction

1.1 Clinical relevance

The spine and its function have been studied for centuries dating back to Hippocrates (460-377 B.C.). One of the earliest spinal surgeries was performed by Paulus of Aegina in the 7th century (Emch and Modic, 2011) demonstrating that low back and spine related discomforts have plagued mankind for ages. Knowledge about spinal structures and pathologies readily increased over the years including disorders related to intervertebral discs (IVDs), the pads of fibrocartilage located in between the vertebral bodies of the spine. For example, in 1911 Joel Goldhwaite already described the relationship between herniated IVD material and low back pain (Emch and Modic, 2011). It is estimated that eight to nine out of ten adults experience back pain at some point in their life (Kandel et al., 2008; Zhang et al., 2009). Consequently, low back pain is a major public health problem in Western societies with both the direct and indirect costs of low back pain exceeding $100 billion/year in the United States alone (Kepler et al., 2013). People with acute low back pain normally recover rather quickly, however reports indicate that about $10 - 15\%$ develop chronic symptoms (Balague et al., 2012).

1.2 Intervertebral disc structure

The human spine comprises twenty-three IVDs that separate the vertebral bodies and provide flexibility (Fig. 1.1A). They are the main joints of the spinal column allowing bending, flexion and torsion and mainly function to absorb shocks and transmit loads (Roughley, 2004).

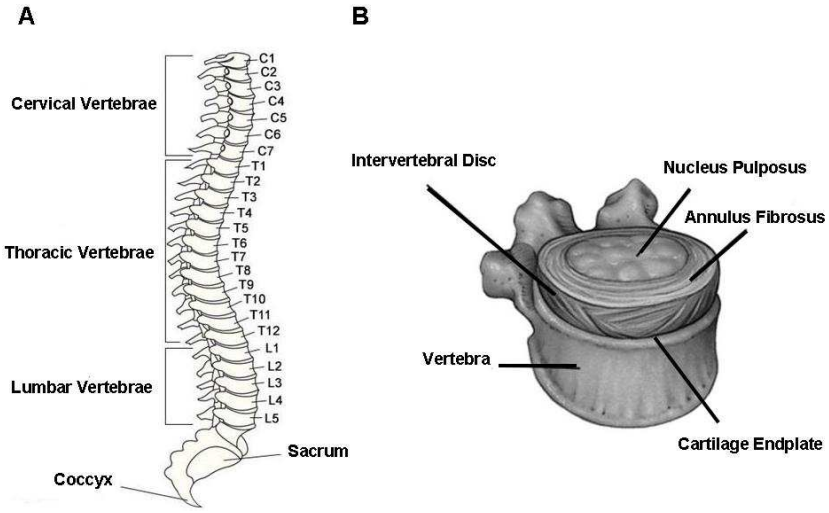

Figure 1.1: A) Schematic representation of the human spine and its twenty-three vertebral bodies. B) Intervertebral discs (IVDs) comprise three structurally different parts: the nucleus pulposus (NP), the annulus fibrosus (AF) and the cartilage endplates.

IVDs are not uniform in thickness. Instead, discs are considerably thinner at posterior position than at anterior location and disc thickness ranges between 6-14 mm depending on the spinal level (Eijkelkamp et al., 2001). Three structurally different parts characterize IVDs: the nucleus pulposus (NP), the annulus fibrosus (AF) and the cartilage endplates (Fig. 1.1B).

The more gelatinous core of the disc, the NP, is surrounded by the AF (Urban and Roberts, 2003; Adams and Roughley, 2006), a thick outer ring of fibrous cartilage. Both the AF and NP are sandwiched inferiorly and superiorly by the cartilage endplates of the vertebral bodies contributing to the intrinsically complex disc structure (Urban and Roberts, 2003; Roughley, 2004; Adams and Roughley, 2006). Compositional differences of the AF and NP are summarized in Table 1.1. IVDs consist mainly of water, collagen, proteoglycans and non-collagenous proteins (e.g. elastin). This biochemical composition varies with location within the disc, spinal level and age (Urban and Roberts, 2003). Water content increases from the AF to the NP as does proteoglycan content (Antoniou et al., 1996; Adams and Roughley, 2006). In contrast, collagen content decreases from the disc periphery towards the center and there is a transition from predominantly collagen type I found in the outer AF to collagen type II in the NP (Bron et al., 2009; Kepler et al., 2013). Collagen content is largest in the NP of cervical discs and lowest in lumbar discs, whereas the proteoglycan content shows the opposite behavior (Roughley, 2004). Furthermore, older discs are typically less hydrated as both the water content and proteoglycan content decreases in the NP and to a lesser extent in the AF (Adams and Roughley, 2006).

Table 1.1: Major differences between healthy AF and NP (adapted from Kepler et al. (2013) and Bron et al. (2009)).

Feature	**AF**	**NP**
Cell Shape	Elongated, fibroblast-like	Spherical, chondrocyte-like
Dominant collagen type	Collagen I	Collagen II
Collagen content	High (50-70% dry weight)	Low (20% dry weight)
Proteoglycan content	Low (10-20% wet weight)	High (50% wet weight)
Water content	Moderate (70% wet weight)	High (80-90% wet weight)

Aside from the biochemical composition, also the cell population varies with location and age within IVDs. Mature IVDs typically contain ca. 9x106 cells/cm^3 in the AF, which is about twice the cell density found in the NP (Roughley, 2004; Bron et al., 2009). In the outer AF, cells exhibit an elongated morphology resembling fibroblasts and are interconnected by very long processes (Bruehlmann et al., 2002; Bron et al., 2009). Towards the central part of the AF, these cell processes are reduced until cells are completely isolated without any apparent physical, intercellular connectivity within the inner AF (Bron et al., 2009; Bruehlmann et al., 2002). Here, cells typically resemble chondrocytes, i.e. they have a spherically shaped morphology that is very similar to cells in the NP (Bron et al., 2009). At birth, notochordal cells predominantly make

up the NP. However, with growth, the majority of these notochordal cells disappears and cells inside the NP assume a round, chondroctye-like morphology (Risbud et al., 2010). Until recently, it was presumed that adult IVDs lose their notochordal cells, yet evidence indicates that some notochordal cells may remain in the NP during adulthood and play a role in delaying the onset of degenerative changes within the IVD (Risbud et al., 2010).

Finally, the AF and NP are characterized by differences in their collagen fiber organization (Urban and Roberts, 2003). The NP extracellular matrix exhibits a rather isotropic organization. Collagen type II fibers are randomly arranged and embedded in a proteoglycan-rich, highly hydrated gel (Urban and Roberts, 2003; Bron et al., 2009). Instead, the AF comprises a highly anisotropic collagen architecture (Fig. 1.2). A series of 15 (posterior) to 25 (lateral) concentric rings, or lamellae, make up the AF with layers consisting mostly of type I collagen fibers (Marchand and Ahmed, 1990). These fibers are oriented at approximately $\pm 60^o$ to spinal axis or $\pm$ 30^o to the transverse plane, alternating in adjacent lamellae (Cassidy et al., 1989; Marchand and Ahmed, 1990). The interlamellar spaces contain predominantly proteoglycans and an array of linking elements, e.g. elastin, creating cohesion between the separate layers (Bron et al., 2009).

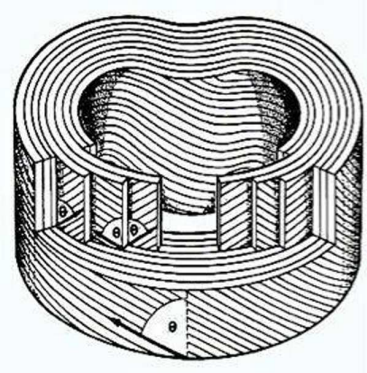

Figure 1.2: Collagen fiber organization in the AF (adapted from Neumann). Fibers are arranged in multiple concentric rings termed lamellae. Collagen orientation θ alternates $\pm$ 60^o with respect to the spinal axis in adjacent lamellae.

1.3 Intervertebral disc degeneration

While the exact cause for low back pain remains unknown, a significant association between IVD degeneration and low back pain has been observed (Urban and Roberts, 2003; Adams and Roughley, 2006). Many different and interdependent factors have been implicated in the onset and progression of disc degeneration. Aging, decreased nutrient supply, unphysiologic loading, lack of exercise and even the use of non-Swedish and non-Japanese cars have been blamed for contributing to IVD degeneration and herniation (Kepler et al., 2013). In recent years, however, the involvement of genetic factors in disc degeneration has become evident which may account for up to 70% of an individual's risk of IVD degeneration (Battie et al., 1995). Regardless of the actual

underlying causes for these degenerative processes, IVD degeneration is characterized by a number of commonly observed changes to the disc biochemistry and biology that include changes to the IVD extracellular matrix organization, a decreased cell viability and increased catabolic enzyme levels and activity (Urban and Roberts, 2003; Roughley, 2004). These characteristic alterations are discussed in more detail in the next sections.

1.3.1 Structural changes

Degeneration affects all areas of IVDs but evidence indicates that the first (detectable) changes occur in the disc endplates and inside the NP (Boos et al., 2002). Gross structural and morphological changes include reduced disc height, inward buckling of the AF, increase of radial disc bulging and tears in the AF, disorganization of the extracellular matrix and loss of the demarcation between the AF and NP (Adams and Roughley, 2006). Water content specifically in the NP decreases, resulting in thinner discs (Antoniou et al., 1996; Urban and Roberts, 2003). Not surprisingly, a reduced disc height observed on for example radiological images is one of the main clinical indicators for detecting disc degeneration (Haughton, 2006; Balague et al., 2012). This decreased water content is likely caused by a fragmented proteoglycan network unable to retain water (Buckwalter, 1995; Urban and Roberts, 2003). Already during childhood proteoglycans start to fragment and with increasing age both proteoglycan and water content in the NP decrease concomitantly resulting in a reduced NP swelling pressure (Buckwalter, 1995; Adams and Roughley, 2006). In contrast, absolute levels of collagen in the NP remain rather unaffected by degeneration, yet types and distribution of collagens change (Roughley, 2004). With increasing age and degeneration, the NP becomes more fibrous and disorganized as collagen type II is replaced by collagen type I (Urban and Roberts, 2003; Adams and Roughley, 2006). In addition, the collagen network becomes increasingly cross-linked and so-called non-enzymatic glycation reactions cause IVDs to change appearance from white to yellow-brown (Duance et al., 1998; Urban and Roberts, 2003; Degroot et al., 2004). As the NP becomes more fibrotic, the clear distinction between the AF and NP is lost (Bron et al., 2009). In later stages of degeneration, radial and circumferential tears especially inside the AF start to appear (Vernon-Roberts et al., 2007). The AF collagen network becomes less organized with annular lamellae becoming thicker and interrupted, i.e. they seize to circumvent the entire disc and start to bifurcate (Boos et al., 2002; Urban and Roberts, 2003). Also, blood vessels and nerve fibers start to enter IVDs (Boos et al., 2002; Roughley, 2004; Adams and Roughley, 2006).

1.3.2 Cell viability

One hallmark of IVD degeneration is a decreased cellularity because of apoptosis or programmed cell death particularly in the NP (Kepler et al., 2013; Ding et al., 2013). Different factors including decreased nutrient supply, un-physiologic loading and aging presumably all contribute to the decreased cell viability observed in degenerated discs (Vernon-Roberts et al., 2008; Ding et al., 2013). Specifically in the NP, nutrient supply is very critical, since NP cells are supplied entirely by diffusion via capillaries that originate in the disc endplates (Urban and Winlove, 2007). Thus, cell death in the NP may be caused by an impaired nutrient diffusion due to structural changes,

e.g. the calcification of end plates, leading to a fall in endplate permeability (Urban and Roberts, 2003; Urban and Winlove, 2007). In vitro, NP cell viability has been shown to be very sensitive to glucose levels (Bibby and Urban, 2004) and a decrease in oxygen levels and pH can lower extracellular matrix synthesis ultimately affecting NP composition (Bibby et al., 2005). This further suggests that nutrient supply to the NP is critical and impaired nutrient diffusion may explain the observed changes in the NP of degenerating IVDs in vivo, e.g. a decline in cell density, loss of proteoglycan organization and concentration, decreased synthetic activity and upregulated catabolic enzyme activity, ultimately leading to loss of disc structure and function (Grunhagen et al., 2011). Endplate fractures can also induce both apoptotic and necrotic cell death in NP and AF tissue (Feng et al., 2006). Similarly, various research groups have shown both in vitro and in vivo that mechanical loading affects cell survival and hence un-physiological loading due to for instance structural changes may induce or accelerate cell death (Ding et al., 2013).

1.3.3 Enzyme activity

In healthy IVDs, there is a well-controlled balance between anabolic and catabolic enzyme activity that maintains extracellular matrix synthesis and break-down (Vo et al., 2013). So-called matrix-metalloproteinases (MMPs) are thought to be heavily involved in extracellular matrix degradation within the disc and, therefore, an imbalance in their production and activation may cause or accelerate disc degeneration (Roughley, 2004; Maitre et al., 2007). MMPs are zinc-dependent proteinases that are produced in a latent form and require activation, often by other MMPs, to become active (Visse and Nagase, 2003; Nagase et al., 2006). Depending on their preferred substrate, protein structure and sub-cellular location, MMPs are often categorized into different groups: collagenases, gelatinases, stromelysins and membrane-type MMPs (Visse and Nagase, 2003) (Table 1.2). All major extracellular matrix constituents including proteoglycans and collagen can be broken down by different types of MMPs and gene-expression of MMP-1, -2, -3, -7, -8, -9, -10, -12, -13 and -14 has been found upregulated in degenerative discs (Vo et al., 2013) (Table 1.2). In healthy IVDs MMP gene expression appears minimal, and the various proteases are likely involved in normal matrix turnover of non-degenerate IVDs (Maitre et al., 2007; Vo et al., 2013). However, with aging and degeneration, MMP levels and activity may increase to facilitate break-down and remodeling of the extracellular matrix (Weiler et al., 2002; Bachmeier et al., 2009; Vo et al., 2013).

Out of all extracellular matrix degrading enzymes, MMP-13 is of particular interest since it is suspected to play a major role in the depletion of the disc's collagen network. Both MMP-13 gene and protein expression is elevated in degenerated discs while immunohistochemical studies of healthy IVDs showed no signs of MMP-13 presence (Maitre et al., 2007; Vo et al., 2013). Thus, MMP-13 may be crucially involved in catabolizing the NP and inner AF as it exhibits the strongest affinity for collagen type II of any MMP (Vo et al., 2013).

Table 1.2: Expression of major MMPs in healthy and degenerate human IVDs (adapted from Vo et al. (2013)).

Name	**Main matrix substrates**	**Expression in non-degenerate IVD**	**Increased expression in degenerate IVD**
Collagenases			
MMP-1	Collagen 1-3, 7, 10	No	Yes
MMP-8	Same as MMP-1	Yes	Yes
MMP-13	Same as MMP-1 (highest affinity for Collagen 2)	No	No
Gelatinases			
MMP-2	Aggrecan	Yes	Yes
MMP-9	Aggrecan	Unclear	Yes
Stromelysins MMP-3	Proteoglycans	Unclear	Yes
MMP-10	Proteoglycans	Yes	Yes
Membrane type MMP-7	Proteoglycans	Yes	Yes

1.4 IVD regeneration

Currently, many surgical interventions aim at removing damaged or altered IVD tissue in order to treat patients suffering from (chronic) low back pain due to (severely) degenerated discs (Kandel et al., 2008). However, the potential of treating disc related disorders by surgery is very limited and its overuse has been criticized (Balague et al., 2012). For instance, spinal fusion, a common surgical technique with 200,000 cases in 2002 in the U.S. alone (Boden, 2002), did not show better clinical outcomes than intensive conservative treatment (e.g. physiotherapy) but more complications (Fairbank et al., 2005; Brox et al., 2010; Balague et al., 2012). Likewise, other surgical treatments including total or partial IVD replacements do not perform better and show similar outcomes as compared to spinal fusion (Blumenthal et al., 2005; Hellum et al., 2011; Balague et al., 2012) illustrating limitations of surgery to treat degenerative disc disease. Hence, in recent years, new treatment modalities have started to emerge that promise to overcome these limitations by restoring physiological function through inducing biological repair in (painful) degenerated IVDs (Kandel et al., 2008; Masuda and Lotz, 2010; Iatridis et al., 2013). Different regenerative approaches exist ranging from growth factor injection and cell transplantation to IVD tissue engineering and some have shown potential to at least slow down degenerative changes in pre-clinical models of IVD degeneration (Masuda and Lotz, 2010; Bae and Masuda, 2011; Zhang et al., 2011). Depending on the severity of IVD degeneration, different regenerative strategies may be effective (Zhang et al., 2011) (Fig. 1.3). In the early stage of

disc degeneration, protein factors such as growth factors or proteinase inhibitors may be effective. In the intermediate stage of degeneration, cell or gene therapy may be required, while in the advanced stage of disc degeneration, tissue engineering approaches may be suitable. However, all biological disc repair strategies, i.e. growth factor injection, cell therapy and tissue engineering, are still in their infancy and more research is mandatory before these therapies may become clinically applicable (Kandel et al., 2008; Zhang et al., 2011). The various biological repair approaches are discussed in more detail in the sections below.

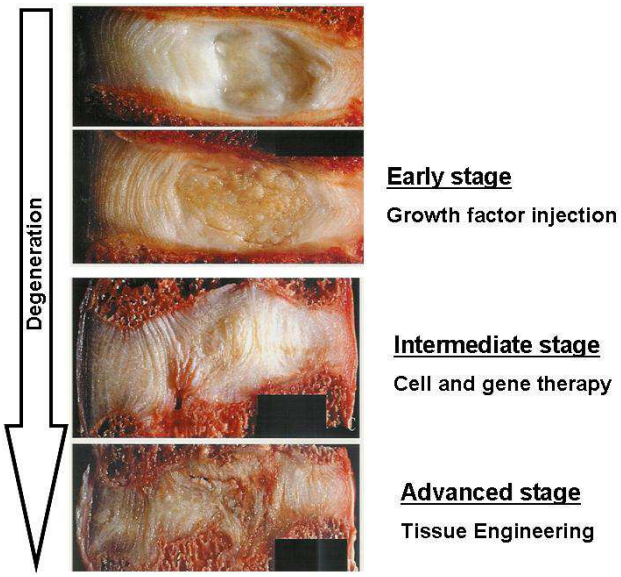

Figure 1.3: Human IVDs in increasing stages of degeneration as classified by Thompson grading (Thompson et al., 1990)(adapted from Zhang et al.). Depending on the severity of degeneration, different regenerative therapies may be required.

1.4.1 Growth factors

Injection of bioactive proteins, i.e. growth factors, and other biological agents into the IVD is thought to stimulate cell growth and evoke an anabolic response that may revoke disc degenerative changes (Masuda and An, 2004; Yoon and Patel, 2006). Among these proteins are bone morphogenetic proteins (BMPs), a family of growth factors that have been found to induce bone and cartilage formation (Zhang et al., 2011). Both NP and AF cells respond to BMP exposure, yet in different manners. Whereas NP cells have been shown to increase proteoglycan synthesis when stimulated by BMP-2 and BMP-7, AF cells respond to BMP-2, BMP-13, and Sox9 by up-regulating collagen production (Zhang et al., 2011). First clinical trials of BMP-7 (also known as osteogenic protein 1) and BMP-14 have started, yet it will take years to determine whether intradiscal injection of these proteins will have therapeutic potential in humans (Zhang et al., 2011). A completely different strategy to at least slow down disc degeneration is followed by research groups that investigate inhibitors of MMPs

and other catabolic agents, i.e. cytokines (Yoon and Patel, 2006; Bae and Masuda, 2011). For instance, interleukin-1 (IL-1) and tumor necrosis factor - α (TNF-α) are known to stimulate the expression and activity of MMPs including MMP-13 and which can result in decreased proteoglycan production by disc cells (Zhang et al., 2011). Therefore, cytokine inhibitors are being tested to potentially decrease MMP production and consequently stop or slow down the catabolic breakdown of the disc extracellular matrix (Yoon and Patel, 2006). Likewise, inhibitors of MMP activity are being investigated to decrease matrix breakdown more downstream.

1.4.2 Cell and gene therapy

As mentioned before, degenerated discs are characterized by decreased cell viability (Ding et al., 2013). Especially in later stages of degeneration, the number of cells potentially receptive to growth factor stimulation diminishes and, therefore, the injection of these bioactive agents may have limited efficacy (Zhang et al., 2011). Cell therapy may offer better treatment potential by directly injecting cells into degenerated discs to halt or revoke degenerative processes. Transplanted cells are thought to produce for example extracellular matrix constituent including collagens and proteoglycans to restore the functional integrity of degenerated IVDs (Meisel et al., 2007). Various cell sources have been proposed for IVD cell therapy, e.g. autologous disc cells and articular chondrocytes (Zhang et al., 2011), and recently Yoshikawa et al. (2010) reported some initial clinical success using transplanted mesenchymal stem cells.

In gene therapy, new genes are transferred into cells or tissues utilizing viral vectors that express different anabolic growth factors that stimulate disc cells to increase production of extracellular matrix proteins (Zhang et al., 2011). Furthermore, cell and gene therapy may be combined into cell-based gene therapy by transplanting transfected cells into degenerated IVDs (Leo et al., 2004; Zhang et al., 2005). This may increase the safety of gene transfer therapy since only the transplanted cells will be transfected with the respective vector and cells adjacent to the injection site will not be infected (Zhang et al., 2011).

1.4.3 Tissue Engineering

At the most advanced stage of degeneration, the tissue engineering approach appears promising to restore IVD function (Kandel et al., 2008; Masuda and Lotz, 2010; Iatridis et al., 2013; Hudson et al., 2013). Depending on the location, size and severity of the defect, different tissue engineering strategies exist to repair degenerated IVDs including NP replacement, AF repair and total IVD replacement (Hudson et al., 2013). Generally, tissue engineering involves seeding cells onto a carrier or scaffold and applying appropriate biochemical and mechanical stimuli to induce the formation of an extracellular matrix similar to that of the target tissue (Kandel et al., 2008). As for cell therapy approaches, there are different potential cell sources for IVD tissue engineering, e.g. mesenchymal stem cells (Masuda and Lotz, 2010). Similarly, a multitude of potential scaffold materials exists to support the formation of the different IVD components such as chitosan, alginate, collagen and fibrin (Kandel et al., 2008) just to list a few. NP tissue engineering has focused on two general methods: injectable materials for minimally invasive procedures, and implantable scaffolds for

more extensive repairs (Hudson et al., 2013; Iatridis et al., 2013). Injectable therapies do not always follow the traditional tissue engineering approach as the may involve injecting biomaterials without cells and focus primarily on providing a mechanical replacement for the degraded NP (Halloran et al., 2008; Hudson et al., 2013; Coric and Mummaneni, 2008; Iatridis et al., 2013). Instead, tissue engineered NP implants aim to provide both the mechanical and biochemical properties of the native NP and therefore include both a scaffold for mechanical support and cells for biological functionality. Defects and injuries also characterize the degenerated AF. Specifically in more advanced stages of degeneration radial and circumferential tears especially inside the AF start to appear (Vernon-Roberts et al., 2007) and different annular repair strategies are under investigation. Similar to the NP, a wide range of materials have been investigated for repairing the AF with special attention to mimicking the highly organized, multilamellar AF structure (Nerurkar et al., 2009; Iatridis et al., 2013; Hudson et al., 2013). Finally, the two approaches of NP replacement and AF repair are joined in whole tissue engineered IVDs (Iatridis et al., 2013; Hudson et al., 2013; Bowles et al., 2011). While NP and AF tissue engineering therapies generally aim to augment the existing disc, whole tissue engineered IVDs are designed to completely replace degenerated discs. Not surprisingly, popular materials and cell sources utilized in NP and AF tissue engineering are often combined to provide suitable scaffolds and biological function for total disc replacements (Iatridis et al., 2013; Hudson et al., 2013).

1.5 Monitoring IVD regeneration and degeneration

In pre-clinical (animal) models of IVD degeneration different techniques exists that allow monitoring markers of disc regeneration and (early) degeneration including (decreased) cell viability, (increased) levels and activity of catabolic enzymes and changes to the disc's collagen network. Traditionally, histological and immunohistochemical or related techniques have been used to evaluate cells and tissues in such pre-clinical model systems (Appel et al., 2013). Examples include Calcein-AM/Propidium Iodide or trypan blue staining for determining cell viability (Gantenbein-Ritter et al., 2008), gelatin zymography and enzyme-linked immunosorbent assays (ELISAs) for measuring enzyme levels and activity (van Beurden and den Hoff, 2005) and fast green, safranin and alcian blue staining for collagen and proteoglycans (Boos et al., 2002; van Dijk et al., 2011). These examples and other techniques provide researchers with a wealth of information and have led to tremendous advances in both developing (novel) regenerative therapies and evaluating their efficacy. Clinically, aside from the patient's history and physical examination, physicians often employ imaging techniques, specifically Magnetic Resonance Imaging (MRI), to diagnose and monitor structural, degenerative changes to the IVD that presumably cause pain syndromes (Haughton, 2006; Finch, 2006; Emch and Modic, 2011). Due to its wealth of anatomic detail, tissue contrast and lack of ionizing radiation, MRI of degenerated IVDs may be used for different purposes: diagnostic, predictive, assessment of severity and recovery, management planning and therapeutic targeting (Balague et al., 2012). As such, MRI contributed tremendously to our understanding of low back pain and IVD degeneration.

However, current methods for monitoring IVD regeneration also have significant lim-

itations that may prevent the effective application of (novel) regenerative therapies to treat IVD degeneration. Often these techniques are destructive, e.g. histological methods require sectioning of the tissue/sample prior to staining and evaluation, or, like ELISAs, they are only applicable to digested tissues and fluids. Moreover, these techniques often do not provide information on cellular functionality (Appel et al., 2013). Due to their destructive nature, they only possess limited usage for longitudinal measurements that allow an evaluation at multiple time points or even a continuous assessment. For instance, cell viability of transplanted cells into IVD explants cannot be assessed without applying either destructive methods (trypan blue assay) or (fluorescent) staining techniques that may affect cellular function (Gantenbein-Ritter et al., 2008). Consequently, explants are usually discarded after viability determination and the fate of transplanted cells cannot be monitored longitudinally over time. Likewise, current clinical MRI protocols are limited to detecting gross anatomical changes and cannot be employed to determine for example cell viability or subtle changes to the disc's collagen network. Moreover, degenerative changes that are clearly evident on MRI do not always result in a definite diagnosis as similar changes are often seen in asymptomatic individuals as well (Finch, 2006; Balague et al., 2012). Furthermore, anatomical or structural alterations arise from cellular and biochemical processes which occurred months to years earlier. In fact, only the long-term downstream consequences of these early degenerative processes may be detected using (clinical) MRI (Finch, 2006; Emch and Modic, 2011). Therefore, diagnoses may be too late for preventative or regenerative interventions (Urban and Winlove, 2007; Emch and Modic, 2011).

1.6 Aims and outline thesis

Thus, while the specifics of a given regenerative strategy may vary, its success may largely depend on developing new methods and improving existing techniques that would enable non-destructive and longitudinal monitoring of the effects of regenerative stimuli. Specifically, these methods should target characteristic cellular and biochemical processes involved in IVD homeostasis including cell viability, enzyme levels and activity and extracellular matrix composition and organization. As such, these methods may be especially suitable for monitoring IVD regeneration and degeneration in experimental pre-clinical models. However, if translated into clinics, they may also allow an earlier diagnosis of markers and pathologies involved in IVD degeneration that cannot be detected using current (clinical) MRI protocols. This may lead to a better understanding of the underlying causes of disc degenerative disease and potentially result in better clinical outcomes, i.e. improved diagnoses of disc related disorders.

The work in this thesis therefore introduces some new strategies for monitoring cellular and biochemical processes involved in IVD regeneration and degeneration. Special attention was given to develop and apply techniques that would enable detecting changes to parameters of disc homeostasis: cell viability, (catabolic) enzyme levels and activity and disc extracellular matrix organization. The outline of this thesis is as follows:

In chapter 2, advanced microscopy is applied to non-invasively measure cell viability using cellular auto-fluorescence. The feasibility and accuracy of this technique is assessed in 3D constructs typically used in tissue engineering studies. Next, the

accuracy of the same technique is determined in an explant model of IVD tissue that can be utilized for pre-clinical testing of regenerative therapies (Chapter 3).

Likewise, advanced optical methods can be employed to assess changes to the IVD extracellular-matrix. Specifically, changes to the disc's collagen network may represent interesting targets for improved diagnosis and in chapter 4 we use Second Harmonic Generation microscopy to quantify such changes in moderately degenerated human IVDs.

In chapter 5 the development and characterization of a novel-fluorescent probe to detect active matrix metalloproteinase 13 (MMP-13), an enzyme involved in collagen catabolism, is described. Since increased levels and activity of MMPs are thought to be signs of degenerative processes, this probe may be utilized to diagnose and monitor such processes.

Finally, conclusions and limitations of the developed methods and future perspectives are discussed in chapter 6.

Chapter 2

Assessment of cell viability in 3D scaffolds using cellular auto-fluorescence

After assessing cell viability (CV), tissue engineered constructs are often discarded, as current CV assays commonly require specific (fluorescent) dyes to stain cells and may need scaffold/tissue digestion prior to quantifying the live and dead cells. Here, we demonstrate and evaluate how cellular auto-fluorescence can be exploited to facilitate a non-invasive CV estimation in 3D scaffolds using two advanced microscopy methods. Mixtures of live and dead C2C12 myoblasts (0%, 25%, 50%, 75%, and 100% live cells) were prepared and CV was determined before seeding cells into collagen carriers using the trypan blue (TB) assay. Cell seeded collagen gels were produced by mixing collagen solution with the live/dead cell mixtures. After polymerization, two-photon microscopy and confocal microscopy images of the CSCG were acquired. Live and dead cells systematically emit auto-fluorescent light with different spectral characteristics. Viable cells showed predominantly blue fluorescence with peak emission around 470 nm, whereas dead cells appeared to mainly emit green fluorescent light with peak intensity around 560 nm. For two-photon microscopy, live and dead cells were distinguished spectrally. For confocal images, the intensity ratio of images taken with band-pass filters was used to distinguish live from dead cells. CV values obtained with both two-photon microscopy and confocal imaging did not significantly differ from those acquired with the established TB method. In comparison to two-photon microscopy, confocal microscopy was found to be less accurate in assessing the exact CV in constructs containing mostly live or dead cells. In summary, monitoring cellular auto-fluorescence using advanced microscopy techniques allows CV assessment requiring no additional dyes and/or scaffold digestion and thus may be especially suitable studies where CV is measured at multiple times points.

The content of this chapter is based on the publication: Dittmar, R., Potier, E., van Zandvoort, M. and Ito, K.: 2012, Assessment of cell viability in three-dimensional scaffolds using cellular auto-fluorescence, *Tissue Engineering Part C Methods*, **18(3):198-204**.

2.1 Introduction

Cell viability (CV) is an important parameter in tissue engineering and culture studies to evaluate the effect of environmental conditions on cell behavior. Currently, several methods to determine CV in three-dimensional (3D) scaffolds exist (Gantenbein-Ritter et al., 2008; Rauch et al., 2006). Common to all CV assays is their rather invasive nature, e.g. by requiring specific dyes to specifically stain live and dead cells. Some assays may even need the scaffold/tissue to be digested prior to staining and quantifying the live and dead cells. For instance, the most accurate CV estimation technique for 3D scaffolds1, the trypan blue (TB) method, can only be utilized after scaffold degradation. The TB dye is mixed with the cell solution and selectively enters dead cells allowing the quantification of live (uncolored) and dead (colored) cells. Due to the required staining and/or scaffold digestion, tissue engineered constructs are often discarded after CV evaluation as the utilized dyes may influence cellular activity, e.g. gene expression patterns. One potential method that promises to overcome these limitations is the monitoring of cell auto-fluorescence using advanced fluorescence microscopy techniques such as two-photon microscopy (TPM) and confocal microscopy. Auto-fluorescence is a known cellular property. Cells possess a number of endogenous fluorophores that in summation provide sufficient signal for obtaining fluorescence microscopy images (Huang et al., 2002; Heikal, 2010; Li and Seeger, 2010; Rocheleau et al., 2004). The most important endogenous fluorophore is nicotinamide adenine dinucleotide (NADH). Among other functions, NADH plays an important role in the energy metabolism of cells, i.e. in the production of adenosine triphosphate (ATP) (Heikal, 2010; Ying, 2008; Wang et al., 2009). NADH has its peak fluorescence emission at 470 nm, while its oxidized form, NAD+, is nonfluorescent (Heikal, 2010; Ying, 2008; Kierdaszuk et al., 1996). The intracellular levels of NADH and NAD+ are thus direct markers of the cell reduction-oxidation state. Consequently, changes in cellular fluorescence are observable when cells increase or decrease their ATP production or when cells are subjected to perturbations in their metabolic pathways. Both (confocal) fluorescence microscopy and TPM have been successfully applied to assess the metabolic state of cells by measuring differences in auto-fluorescence resulting from changes in cellular metabolic activity, i.e. different levels of NADH (Huang et al., 2002; Rocheleau et al., 2004; Eng et al., 1989; Ghukasyan and Kao, 2009; Hennings et al., 2009; Pogue et al., 2001; Tiede et al., 2007). Most studies, however, utilized this method to visualize and/or determine different metabolic states of living cells, e.g. by determining different cellular reduction-oxidation (redox) states (Skala et al., 2007; Tiede et al., 2007; Kirkpatrick et al., 2005; Mujat et al., 2008; Park et al., 2006; Quesada et al., 2006). Some studies described auto-fluorescence and redox changes of apoptotic and necrotic cells (Eng et al., 1989; Pogue et al., 2001; Levitt et al., 2006; Brewer et al., 2002; Pogue et al., 2001). While these reports indicate the potential of using differences in cellular auto-fluorescence to distinguish live from dead cells, according to our knowledge, only Hennings et al (Hennings et al., 2009) applied it to differentiate viable from necrotic (thermally induced) cells. In their report, fixed, paraffin embedded tissue sections were visualized using a fluorescence microscope. Aside from not being applicable to monitor cell viability in living three-dimensional constructs or tissues, their results are limited by utilizing formaldehyde to fix tissue sections, which may influence cellular auto-fluorescence (K. and H., 1994). Also, to our knowledge, no systematic investigation exists addressing the usage of auto-fluorescence to assess CV in 3D constructs. Using cell populations of known percent viability

seeded into collagen gels, we first evaluated the feasibility of using TPM and confocal microscopy to distinguish live from dead cells based on differences in auto-fluorescence. Secondly, we compared two microscopy methods for quantitative determination of CV with the established trypan blue (TB) viability assay.

2.2 Materials and Methods

2.2.1 Cell source and expansion

C2C12 murine myoblasts (ECACC, Salisbury, UK) were cultured at 37^oC, 5% CO_2 and at full humidity in growth medium containing 85% high-glucose Dulbecco's modified eagle medium (Invitrogen, Breda, The Netherlands), 15% fetal bovine serum (Lonza, Belgium), 1% penicillin-streptomycin (Lonza, Belgium) and 1% non-essential amino acids (Invitrogen, Breda, The Netherlands). Every $2-3$ days cells were passaged.

2.2.2 Preparation of cell viability mixtures

Cells were detached using 1% trypsin, centrifuged (250 g, 5 min) and re-suspended in phosphate-buffered saline (PBS). To prepare dead cells, 1 ml of 1 N HCl was added to 9 ml of cell suspension (10 min incubation at room temperature)(Gantenbein-Ritter et al., 2008). Afterwards, dead cells were washed twice with 10 ml PBS. Subsequently, the concentration of the live and dead cell solutions was determined using the TB assay in standard fashion. Briefly, the TB dye enters selectively dead cells coloring them dark blue and subsequently live and dead cells were hand-counted using a Neubauer improved hemocytometer. The two solutions were then mixed at 0/100%, 25/75%, 50/50%, 75/25%, and 100/0% live/dead ratios. After mixing, the actual produced live/dead ratio (MIX) was measured in triplicate (TB assay).

2.2.3 Preparation of cell seeded collagen gels (CSCGs)

CSCGs were produced by mixing $255\mu l$ of acid-solubilized rat-tail tendon collagen type I solution (2 mg/ml final collagen concentration, BD Biosciences, USA), $245\mu l$ growth medium, and $6\mu l$ of 1 N NAOH and the prepared cell solutions of known live/dead ratio at $7x10^6$ cells/ml (n = 5/MIX). Subsequently, the collagen-cell mixtures were cast into the wells ($\sim$ 18 mm diameter) of a 24-well plate ($500\mu l$ collagen-cell mix/well). Gels were allowed to polymerize for 30 min at 37^oC before 2 ml of growth medium was added. The construct was put back into the incubator and left to continue polymerization for 2 h before imaging. Two separate sets of cell mixtures were produced to make two separate set of gels, one for TPM and the other for confocal microscopy.

2.2.4 Two-photon and confocal microscopy

Two photon images of the CSCGs were acquired on a Zeiss LSM 510 META NLO laser scanning microscope and confocal images were obtained on a Zeiss LSM 510 laser scanning microscope with a 62x, 1.2 numerical aperture water immersion objective (Carl Zeiss GmbH, Jena, Germany). Images were taken approximately $20 - 40\mu m$ deep into the CSCG. For TPM, the excitation light source was a mode-locked Ti:Sapphire Chameleon laser (Coherent Inc., Santa Clara, California) tuned to an excitation wavelength of 730 nm. The laser output was set to 5%. Fluorescence emission was discriminated with a 650 nm short-pass dichroic mirror and transmitted to the appropriate detector unit. Confocal imaging utilized 458 nm excitation with the laser output set to 100%. The emitted fluorescent light was discriminated with a 458 nm main dichroic mirror and transmitted to the appropriate detector unit.

Two photon spectral images were measured by diverting the emitted auto-fluorescence to a diffraction grating and detecting 19 wavelength bands centered from 405 to 608 nm (in steps of approx. 10.7 nm) using the META detector of the microscope. The spectrally separated light is transmitted to 19 photo-multiplier tubes (PMTs) of the META detector and the number of photons per spectral band is counted. Subsequently, the microscope's internal software generates a spectral image by analyzing the frequency of photons detected in each individual PMT. Per pixel, the tube detecting the majority of photons is determined and a color, i.e. pixel value, is assigned, representative of the spectral band the PMT is detecting. For instance, if the majority of photons are measured in the PMT covering 549-560 nm, the pixel is colored in green since this spectral band is within the green visible spectrum. Emission spectra were obtained by manually outlining regions-of-interest (ROI) on the spectral images using the ROI selection tool of the microscope image-analysis software (Zeiss LSM Image Browser). The emission spectra were extracted from the ROIs presumed to represent the cell cytoplasm and mitochondria. Post-processing of the spectra data included averaging and calculation of standard deviations using the MATLAB software environment (The Mathworks, Natick, MA, USA).

Confocal image pairs were acquired by consecutively imaging CSCGs through a 475-525 nm band-pass filter (image 1) and a 560-615 nm band-pass filter (image 2), respectively. A custom written MATLAB script was used to identically outline the same cells visualized on image 1 and 2 and their corresponding intensities (pixel values) were obtained and averaged. An intensity ratio per imaged cell was determined by dividing the cell's averaged intensity from image 1 by the averaged intensity from image 2.

2.2.5 Threshold determination for confocal microscopy images

Receiver operating characteristics (ROC) analysis (Hennings et al., 2009) was performed to identify a threshold ratio to distinguish live from dead cells on confocal images. Intensity ratios of cells in the CSCGs with 0% and 100% CV were obtained and a ROC curve was calculated (PASW Statistics Release 18.0.0, SPSS, Inc., Chicago, IL, www.spss.com). The intensity ratio corresponding to the maximum sum of sensitivity and specificity on the calculated ROC curve was identified as the threshold ratio.

2.2.6 Cell viability assessment

The number of live and dead cells per two-photon spectral image (n = 20 images/CSCG with at least 100 cells imaged) of each gel (n = 5/MIX) was counted. Likewise, the number of live and dead cells per confocal intensity image pair (n = 30 image pairs/gel with at least 150 cells imaged) of each gel (n = 5/MIX) was determined. Subsequently, all living and dead cells were summarized and cell viability per imaged gel was defined as:

$$CV = \frac{l}{l+d} \tag{2.1}$$

where l and d are the total number of visualized living and dead cells per carrier, respectively.

2.2.7 Statistical analysis

The measured CV values obtained with the two different CV assessment methods were examined for significant differences compared to their corresponding TB assays using two separate two-way analysis of variance tests. The dependent variable was defined as the measured CV values. The two factors were defined as the method to assess CV (microscopic and TB) and the targeted CV sub-groups (0%, 25%, 50%, 75% and 100%). If no significant interaction effect was found, a one-way analysis of variance test with Tukey-HSD post-hoc testing was employed to search for significant differences in either targeted CV or CV assessment method within the other factor level. Otherwise, an independent t-test with Bonferroni correction for number of applied comparisons ($k = 5$) was used to test for significant differences between each specific CV assessment method and targeted CV sub-group. Statistical significance was assumed for $p < 0.05$. All statistical tests were performed using PASW Statistics Release 18.0.0 (SPSS, Inc., Chicago, IL, www.spss.com)

2.3 Results

2.3.1 Cell classification using auto-fluorescence

Two-photon excitation resulted in live and dead cells systematically emitting fluorescent light with different spectral characteristics. Viable cells showed predominantly blue fluorescence with peak emission around 470 nm, the typical emission wavelength of NADH (Fig. 2.1A and C). In contrast, dead cells appeared to mainly emit green fluorescent light with peak intensity around 560 nm (Fig. 2.1B and C).

Emission spectra of live and dead cells largely overlapped for emission wavelengths between 400-500 nm. In the spectral range above 500 nm, the spectra showed an opposite behavior. While the averaged fluorescent intensity of live cells rapidly decreased with increasing wavelength, the dead cells' fluorescence intensity increased and remained elevated. These spectral differences resulted in live cells appearing blue and dead cells appearing green on the color-coded two-photon images, allowing an easy and direct cell

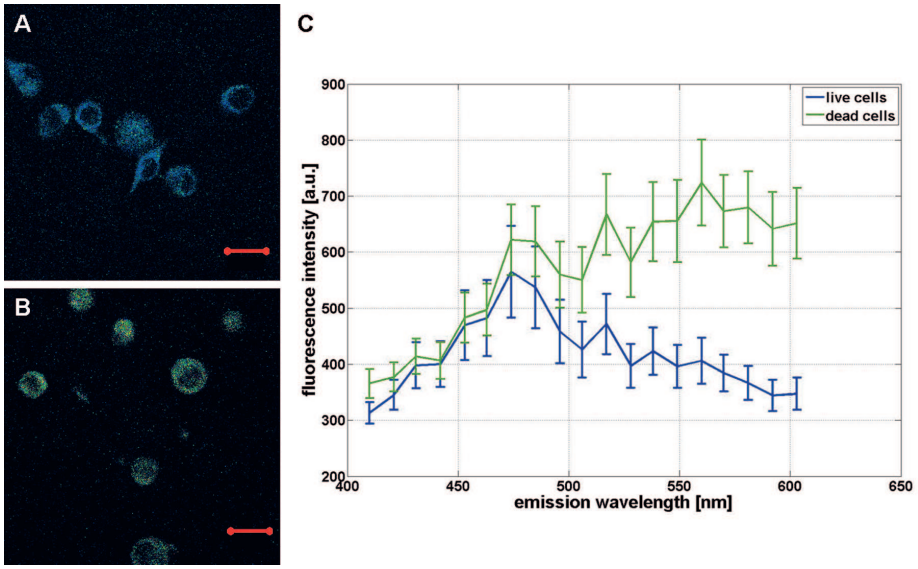

Figure 2.1: Characteristic two-photon spectral images of CSCGs with A) 100% CV and B) 0% CV. Bar is 20μm, Magnification 630x. C) Respective emission spectra of 50 live (green) and 50 dead (red) cells illustrating distinct spectral differences between live and dead cells. Values are mean ± standard deviations.

classification (Fig. 2.1A and B). In a few exceptions, the color-coding was ambiguous and the emission spectra of the cells in question were examined. For classification, the spectra were normalized to their intensity at 470 nm. Cells with peak intensity at 470 nm were categorized as living and cells with peak intensity at 560 nm as dead, respectively. In all observed cases, this extra check successfully categorized cells as either live or dead. The observed spectral differences in the emitted fluorescent light of live and dead cells were also reflected in the intensity ratios obtained from the confocal image pairs. On average, live cells had larger intensity ratios than dead cells due to their decreased fluorescence emission above 500 nm (Fig. 2.2A).

The small overlap in the distribution of intensity ratios of live and dead cells indicated a good potential to classify them using a threshold intensity ratio. The ROC curve shows how the sensitivity and specificity of such a classification rule changes with different settings of a threshold ratio (Fig. 2.2B). The best combination of sensitivity and specificity was attained for a threshold ratio of 0.68, corresponding to 91% sensitivity and 93% specificity. In other words, 771 of the 847 live cells imaged in the CSCGs with 100% CV had their intensity ratio above the threshold ratio (91% sensitivity), while 813 of the 847 dead cells visualized in the CSCG with 0% CV had their ratio below the threshold (93% specificity). Consequently, when assessing viability using confocal ratio imaging, cells with intensity ratio above the threshold value were classified as viable, whereas cells with a lower intensity ratio were classified as dead.

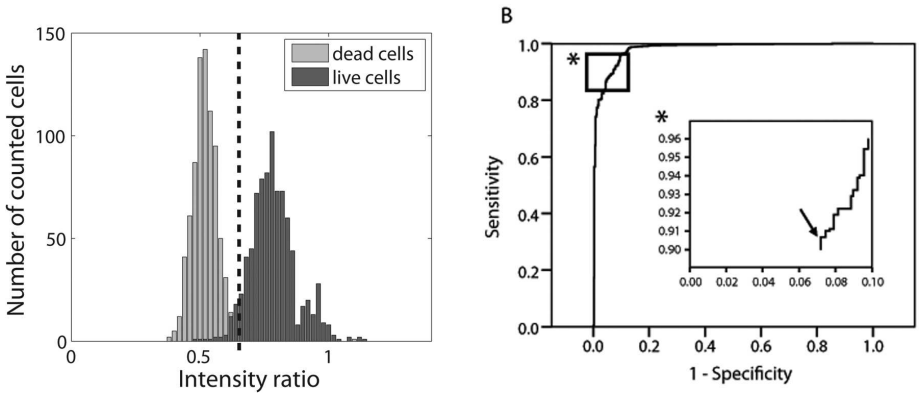

Figure 2.2: A) Histogram of intensity ratios of the CSCGs with 0% and 100% CV. Dashed line represents the threshold ratio of 0.68 as calculated by ROC analysis. B) Corresponding ROC curve for classifying intensity ratios via a ratio threshold. (*) Detail of the ROC curve; arrow in the insert denotes where the sum of sensitivity (number of correctly identified live cells/total number of live cells) and specificity (number of correctly identified dead cells/total number of dead cells) is maximized (91% and 93%, respectively) which corresponds to a threshold of 0.68.

2.3.2 Viability assessment

The CV values determined using the TB assay and the measured CV using two-photon spectral imaging and confocal ratio imaging all matched well the targeted CV (Fig. 2.3 and 2.4).

The obtained values of all three methods showed a clear gradient from 0% to 100% CV with significant effect of the cell viability mixture. More importantly, both microscopy techniques showed similar accuracy in determining CV as the TB method. In the case of TB assay vs. two-photon spectral imaging, no significant differences in assessing CV were found between the two methods. There was, however, a significant interaction effect, which was attributed to significantly different CV values ($p < 0.01$) for CSCGs containing 100% live cells (Fig. 2.3). However, this is an artifact, of less than 100% CV as measured by TB and very low within group variance, as the methods themselves did not have a significant effect. In the second case, confocal microscopy vs. TB assay, also no significant differences in measuring CV was found between the two techniques. Furthermore, no significant interaction between the two CV assessment methods was determined. Yet, the individual set of CV values obtained with confocal microscopy did not show significant differences between the 0% vs. 25%, and 75% vs. 100% targeted CV sub-groups. In other words, confocal microscopy failed to distinguish between CSCGs containing 0% vs. 25%, and 75% vs. 100% targeted CVs. In contrast, all TB viability groups were significantly different from each other (Fig. 2.4).

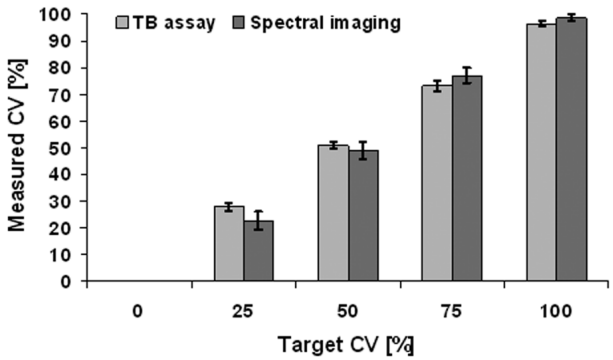

Figure 2.3: Measured cell viabilities as evaluated using two methods, Trypan blue assay and two-photon spectral imaging, for five different targeted cell mixtures (0%, 25%, 50%, 75% and 100% living cells). Values are means ± standard deviations, n = 5.

2.4 Discussion

Rather than showing only differences in intensity, the auto-fluorescence emission of live and dead cells was found to be characterized by distinct spectral differences. Analysis of two-photon fluorescence emission spectra showed that live cells emit predominantly blue fluorescent light with peak intensity around 470 nm, the typical emission wavelength of NADH (Fig. 2.1). In contrast, dead cells emit mainly green fluorescent light with peak intensity at 560 nm (Fig. 2.1). Using advanced microscopy methods, these spectral differences could be exploited to accurately differentiate viable from dead cells and to assess the CV of cell seeded 3D constructs. In fact, CV values obtained with either two-photon spectral imaging or confocal ratio imaging were not significantly different from those acquired with the established TB viability assay. In comparison to TPM, confocal microscopy was found to be less accurate in measuring CV of CSCGs containing mostly live or dead cells. This illustrates the dependency of confocal ratio imaging on defining a good intensity ratio threshold to categorize cells. The exact underlying mechanism that causes the measured differences in auto-fluorescence emission remains to be investigated. Initially, we hypothesized that dead cells emit fluorescent light with stronger intensity. The increase was attributed to larger intracellular NADH levels presumably resulting from the absence of oxidative phosphorylation in non-viable cells. Indeed, examination of the measured emission spectra of dead cells shows that the fluorescence intensity is elevated compared to viable cells as the area under the spectrum represents the measured (averaged) total fluorescence intensity (Fig. 2.1C). However, the determined increase cannot be solely attributed to larger NADH levels since the major differences were observed for emission wavelengths greater than 500 nm. For this spectral region, NADH emits negligible amounts of fluorescent light (Huang et al., 2002; Heikal, 2010; Wang et al., 2009; Kierdaszuk et al., 1996; Eng et al., 1989; Tiede et al., 2007). One possible explanation for the observed differences in emission spectra is the presence of flavoproteins (FP). Like NADH, this class of proteins exists in any cell type and FPs are known to play crucial roles in cellular energy metabolism (Huang et al., 2002; Heikal, 2010; Wang et al., 2009; Eng et al.,

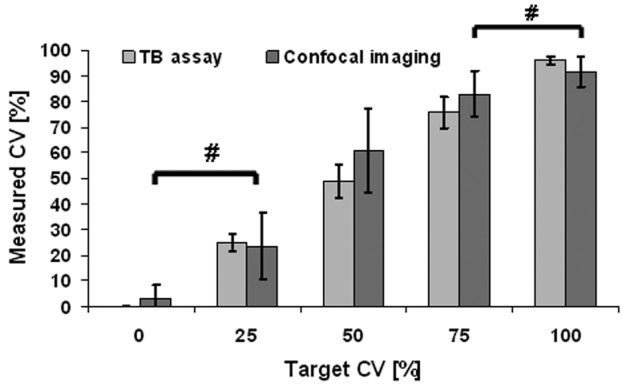

Figure 2.4: Measured cell viabilities as evaluated using two methods, Trypan blue assay and confocal ratio imaging, for five different targeted cell mixtures. Values are means +/- standard deviations, n = 5. denotes $p > 0.05$ between target CV categories within the confocal CV assessment method

1989; Tiede et al., 2007). However, FPs are characterized by emitting predominantly green fluorescent light with peak intensities typically around 530 nm (Wang et al., 2009; Eng et al., 1989; Tiede et al., 2007). In viable cells both signals, i.e. fluorescence from NADH and FP, contribute to the cellular auto-fluorescence. Since the concentration of NADH is typically much larger than that of FP, the fluorescence emission of live cells is characterized by a dominant NADH signal (Heikal, 2010; Wang et al., 2009). Dead cells appear to be subjected to a much larger FP contribution to the measured fluorescence emission. Our results indicated that the measured fluorescence intensity per wavelength continuously increases, peaking at 560 nm which is well within the characteristic spectral range of FPs. Apparently, cell death causes changes in the relative concentrations of NADH and FP. As cells become necrotic, they lose the integrity of their mitochondrial membranes leaving proteins or compounds unprotected to oxidation (Pogue et al., 2001). Unlike NADH, FPs are fluorescent in their oxidized form and do not fluoresce in their reduced state (Wang et al., 2009; Eng et al., 1989). Thus, the enhanced FP contribution to the total fluorescence signal of dead cells may be explained by increased levels of oxidized FP present in non-viable cells. Supporting our findings are the results of Hennings et al.(Hennings et al., 2009) who distinguished live from heat-fixed (necrotic) cells based on differences in fluorescence intensity. In their study, dead cells exhibited increased fluorescence intensity as compared to viable cells. However, they did not determine the spectral characteristics of the emitted fluorescent light and hence it remains unclear whether the observed differences were caused by changes in NADH and/or FP levels. In contrast, Pogue et al (Pogue et al., 2001) and Eng et al (Eng et al., 1989) found the fluorescence emission of dead cells decreased relative to living cells. One explanation for this discrepancy may be an oscillation in the emitted fluorescent light during cell apoptosis or necrosis, as shown by Ghukasyan et al. (Ghukasyan and Kao, 2009). Initially, the cellular fluorescence emission increased, yet within several hours after cell death it decreased below its initial value and remained low. These results, however, are contradicted by Georgakoudi et al.(Georgakoudi et al., 2005) who reported an increased fluorescence intensity of apoptotic cells within the same time range. Taken together, these findings illustrate the

ongoing uncertainness about the proper interpretation of auto-fluorescence variations found in live and dead cells (Wang et al., 2009). However, regardless of an actual increase or decrease in fluorescence intensity, all studies reported significant variations in the auto-fluorescence emission of live and dead cells. Hence, these differences can be employed to distinguish cells as in the present study while recognizing the need to clarify the underlying processes.

In a previous study, the TB staining method was found to be the most accurate in assessing CV in 3D scaffolds1. However, it can only be used with scaffolds/tissue that can be digested without killing any cells. Our results indicate that both TPM and confocal microscopy can be employed to determine CV with similar accuracy and without disintegrating the constructs. Since no dyes with unknown effects on cellular processes, e.g. gene expression, are required, CV can be measured longitudinally over time and constructs can be utilized for other analyses without discarding them after assessment. The TB method is advantageous to the two other methods in terms of simplicity, needed infrastructure, and required lab time and will therefore most likely remain the gold standard for assessing CV *in vitro*. However, both microscopy techniques are in principle applicable for determining CV *in situ* in scaffolds/tissue and possibly *in vivo*. In addition to non-invasively measuring CV, information on cell distribution and morphology is also provided. Choosing the appropriate microscopy method for one's experiment depends among others on the availability of the microscopy equipment. Two-photon spectral imaging requires specialized equipment, e.g. a detector unit capable of extracting spectral information of the emitted fluorescent light. Thus, although less accurate than TPM in determining CV, confocal microscopy represents a valid alternative technique using more generally available equipment.

The current study relies heavily on the accuracy of the CV estimated using the TB assay. This could be considered as a potential bias. However, this source of error should be minimal as the viability was determined prior to seeding the cells and the TB method is considered to be an accurate CV estimation technique. Here, measuring (differences in) auto-fluorescence using advanced microscopy methods was found to accurately assess CV in 3D scaffolds. A few factors may have influenced the good accuracy of two-photon spectral imaging and confocal ratio imaging that could be considered bias. First of all, only a reasonable number of gels (n = 5 for each live/dead cell mixture) were imaged. Visualization of more gels with subsequent CV assessment could potentially show that the microscopy techniques and the TB assay do not express the same accuracy because the power of the statistical analysis would increase. However, such small differences requiring such large sample sizes are often not actually meaningful differences in CV. Estimating the viability exploiting cellular auto-fluorescence depends heavily on visualizing representative numbers of live and dead cells. However, cells from a limited number of regions within the CSCG were visualized possibly overlooking zones of accumulated live or dead cells. Here, all visualized gels were characterized by a relatively even live/dead cell distribution and prior to imaging the CSCGs, a trial study was performed to estimate how many cells were needed to be visualized in order to obtain a representative CV measurement.

Measuring CV using TPM and confocal microscopy also depends heavily on cells being clearly classifiable as either live or dead. Here, only few cells could not be directly categorized on the spectral two-photon images, i.e. they did not distinctively appear blue (live) or green (dead). Still, classification was achieved by examining the peak intensities in their normalized emission spectra. Confocal microscopy in

conjunction with calculating intensity ratios allowed distinguishing live from dead cells, yet some cells were falsely categorized. To facilitate a more accurate CV estimation, different band pass filters could be chosen. Here, we were limited by our confocal microscopy set-up to utilize a 475-525 nm band pass filter and a 560-615 nm band pass filter, respectively. Apparently, for some cells, the auto-fluorescence emission in these spectral bands partially matches and hence some calculated intensity ratios led to live cells being identified as dead and vice versa. The observed spectral differences could be better taken advantage of by obtaining confocal image pairs through more narrow band pass filters, e.g. through 460-500 nm and 560-600 nm band pass filters. A different set of filters would possibly result in more distinct intensity ratio distributions of live and dead cells and consequently allow a more accurate cell classification.

In this study, a high numerical aperture (NA) objective was required to capture the weak auto-fluorescence emission, but its depth penetration is limited to $280\mu m$. Future in situ or *in vivo* applications using auto-fluorescence to assess CV will want to consider employing objectives with high enough NA and large enough working distances to image a representative cell population within the tissue/construct. On inverted microscopes, smaller magnifying objectives with high NA could be utilized as they are characterized by larger working distances. Alternatively, for upright confocal or TPM set-ups, water-dipping lenses with high NA could be used due to their even larger working distances (typically above 2 mm). However, even the most advanced TPM set-ups do not penetrate even low light-scattering tissues deeper than 1 mm (Theer et al., 2003). Therefore, any clinical application of TPM or confocal microscopy to estimate CV requiring deeper tissue penetration will likely rely on the development of endoscopic probes (Wu et al., 2009). Finally, another issue that might complicate the potential usage of both microscopy techniques is the presence of various cell types in tissues. Intracellular contents of endogenous fluorophores may vary between cell types and species. However, numerous studies on measuring cell metabolism/activity using auto-fluorescence of various cell types from different species have been published; examples include cancer cells (Skala et al., 2007; Georgakoudi et al., 2002; Chernyavskiy et al., 2009; Chen et al., 2008; Yu and Heikal, 2009), liver cells (Rajwa et al., 2007), cornea cells (Park et al., 2006; Masters, 2009), skin cells (Bader et al., 2011; Palero et al., 2007; Masters et al., 1997; Chen et al., 2006), stem cells (Chen et al., 2010), brain cells (Drezek et al., 2001; Kwan et al., 2009) and heart cells (Huang et al., 2002; Eng et al., 1989). In these studies, relatively small differences in cellular auto-fluorescence were successfully utilized to determine various metabolic states of live cells. As differences in auto-fluorescence between live and dead cells are likely larger than between metabolically active and inactive cells, we believe that it is possible to assess the viability of constructs seeded with other cell types than the one in our study. Since each cell population is likely characterized by their individual auto-fluorescence emission, reference spectra and typical intensity ratio threshold values must be obtained for the different cell types.

2.5 Conclusion

The results indicate the potential of using differences in auto-fluorescence to distinguish live from dead cells and accurately assess CV in 3D scaffolds. Utilizing advanced microscopy techniques, no dyes were required to stain live and dead cells and CV could

be determined without disintegrating the cell seeded constructs. In terms of accuracy, both two-photon spectral and confocal ratio imaging perform well as compared to the established TB viability assay, with confocal microscopy being slightly less accurate. Therefore, both microscopy techniques show good potential to be used in (tissue engineering) studies where CV is measured at multiple times points.

Chapter 3

In Situ Label-Free Cell Viability Assessment of Nucleus Pulposus Tissue

Regenerative medicine approaches aiming at treating degenerating intervertebral discs, a major cause of back pain, are increasingly tested in ex-vivo disc explant models mimicking in-vivo conditions. For assessing the efficacy of regenerative therapies, cell viability is commonly measured requiring specific labels to stain cells. Here, we demonstrate and evaluate how cellular auto-fluorescence can be utilized to non-invasively assess viability in disc tissue in-situ using label-free two-photon microscopy. Live and dead bovine disc cells (0% and 100% cell viability) from the nucleus pulposus were seeded into collagen gels and auto-fluorescence was characterized. Subsequently, nucleus pulposus explants were cultured for 6 days in media with different glucose supplementation (0, 0.25, 0.5 and 1 g/l) to induce different degrees of cell death. Then, samples were split and viability was assessed using label-free two-photon microscopy and conventional staining. Results show that live and dead nucleus pulposus cells systematically emit auto-fluorescent light with distinct characteristics. Cell viability values obtained with label-free microscopy did not significantly differ from those acquired with staining. In summary, monitoring auto-fluorescence facilitates accurate cell viability assessment in nucleus tissue requiring no additional dyes. Thus, this technique may be suitable for pre-clinical testing of regenerative therapies in nucleus pulposus cultures.

.

The content of this chapter is based on the publication: Dittmar, R., van Dijk, B. G. M., van Zandvoort, M. A. M. J. and Ito, K.: 2014, In Situ Label-Free Cell Viability Assessment of Nucleus Pulposus Tissue, *J. Orthop. Res.*, **32(4):545-550**

3.1 Introduction

Current treatments for chronic low back pain have limited long-term success and fail to address the underlying cause of the disease, which is strongly associated with intervertebral disc (IVD) degeneration (Masuda and Lotz, 2010). Degeneration affects all areas of IVDs, but evidence indicates that the earliest changes occur in the disc endplates and in the center of IVDs, the nucleus pulposus (Boos et al., 2002) (NP). Thus, in recent years, regenerative therapies have started to emerge that target specifically the NP and, therefore, aim to treat disc degeneration at an early stage to prevent low back pain from occurring (Masuda and An, 2004). To develop possible therapies and to test their efficacy, experimental ex-vivo models of the (degenerated) NP are needed. A major benefit of such NP explant systems over cell culture is that the effect of cell and growth factor-based therapies can be assessed in an in-vitro environment mimicking in-vivo conditions. Regardless of the system chosen, a few parameters including cell viability (CV) are often measured to determine the efficacy of regenerative therapies (van Dijk et al., 2011). CV, the percentage of live cells in a tissue/sample containing both live and dead cells, is an important parameter in explant culture studies to evaluate the effect of environmental conditions on cell behavior. Commonly, current standard CV assays require specific labels to stain live and dead cells. Due to such (fluorescent) labels, samples are often discarded, as the utilized staining may influence cellular behavior, e.g. gene expression patterns.

Recently, we demonstrated that two-photon microscopy could accurately assess CV in three-dimensional (3D) scaffolds, without staining, based on differences in auto-fluorescence emission spectra of live and dead fibroblasts (Dittmar et al., 2012). Cellular auto-fluorescence arises from the presence of several endogenous fluorophores, i.e. Nicotinamide Adenine Dinucleotide (NADH) and Flavoproteins (FPs). Live fibroblasts emitted predominantly blue fluorescent light with peak intensity around 470 nm, typical for NADH. In contrast, dead fibroblasts emitted mainly green fluorescent light with peak intensity at 560 nm, attributed to FPs. However, to become a useful technique for extra-cellular matrix rich tissues, e.g. disc tissue, articular cartilage, etc., label-free two-photon microscopy must first prove its applicability for assessing CV in tissue explants that better resemble the in-vivo environment. Recording auto-fluorescent light in tissues in-situ may be considerably more difficult due to increased light scattering caused by a dense extracellular matrix (Durr et al., 2011). Furthermore, mature collagenous tissues such as IVD tissue are known to exhibit strong auto-fluorescence originating from collagen (Hoell et al., 2006). As collagen auto-fluorescence partially overlaps NADH emission, label-free two-photon imaging of live and dead cells may be negatively affected. Moreover, cells in the IVD, specifically in NP, are known to be notoriously low in metabolic activity (Gruber et al., 2013). As levels of NADH and FPs are related to cellular energy metabolism, it is unclear whether live and dead NP cells would be distinguishable. All these factors, i.e. a dense matrix, collagen auto-fluorescence and low metabolic activity, present a significant challenge for applying label-free two-photon microscopy to assess CV in NP tissue in-situ.

Hence, the objectives of this study were to first determine the feasibility of differentiating viable NP cells from dead NP cells based on (potential) differences in auto-fluorescence. Isolated NP cells of known CV were seeded into collagen gels and subsequently the auto-fluorescence emission of the unlabeled cells was characterized. Second, the potential and accuracy of measuring CV in dense NP tissue was assessed.

Excised NP explants were cultured in media with different glucose supplementation to induce different degrees of cell death followed by assessing CV utilizing both label-free imaging and conventional staining.

3.2 Materials and Methods

3.2.1 Tissue harvesting and NP cell isolation

NP explants were harvested from bovine caudal discs within 2 hours of slaughter. Bovine tails were obtained from the local abattoir according to local regulations. Discs (n = 5 donors, total 20 discs) were opened transversally, underneath the end-plate, and NP explants were punched with an 8-mm-diameter biopsy punch (Kruuse, UK) from the center of the disc. Standard medium (SM) was prepared from basic Dulbecco's modified Eagle's medium powder (Sigma, The Netherlands) in milli-Q filtered water (8.3 g/l), supplemented with 15.9 mg/l Phenol Red (Sigma), 2% L-glutamine (Lonza, Switzerland), 1% pyruvate (Sigma), 1% penicillin/streptomycin (Lonza), 3.7 g/l sodium bicarbonate (Sigma) and 100 mg/l ascorbic acid (Sigma). For auto-fluorescence characterization, NP explants were chopped finely and put into a culture flask containing 30 ml SM with 1 g/l glucose and 2 mg/ml collagenase II (Sigma). After overnight digestion, released cells were passed through a 70 m pore size cell strainer and washed in SM with 1 g/l glucose and re-suspended in PBS. Cells were counted using a hemocytometer, and CV was tested using trypan blue staining. To prepare dead cells, 1 ml of 1 N HCl was added to 9 ml of cell suspension5. Afterwards, dead cells were washed twice with 10 ml PBS.

3.2.2 Preparation of cell seeded collagen gels (CSCGs)

CSCGs were produced by mixing 255 μl of acid-solubilized rat-tail tendon collagen type I solution (2 mg/ml final collagen concentration, BD Biosciences), 245 μl SM with 1 g/l glucose, and 6 μl of 1 N NAOH and the isolated cell solutions of either live or dead NP cells at 2 x 106 cells/ml. Subsequently, the collagen-cell mixtures were cast (18mm diameter, 500 μl collagen-cell mix/chamber) into the chambers of a 4-chambered coverglass (LabTek, Thermo Fisher Scientific, U.S.A). Gels were allowed to polymerize for 30 min at 37^oC before 2 ml of SM with 1 g/l glucose was added. The construct was put back into the incubator for 2 h before imaging.

3.2.3 NP explant culture

SM osmolarity was adjusted by adding 13.3% w/v polyethylene glycol (20 kDa molecular weight, Sigma)(van Dijk et al., 2011). Four culture groups were then defined by supplementing SM with 0, 0.25, 0.5 and 1 g/l glucose. All media were filter sterilized and the pH was adjusted to 7.1, the pH of a healthy human disc (van Dijk et al., 2011). NP explants were placed inside dialysis tubing (15 kDa molecular weight cut-off; Spectra-Por, USA) and closed with custom-made plastic rings (van Dijk et al., 2011). Samples were cultured for 6 days at 37^oC, 5% O2, and 5% CO2 and media

were changed at day 3. For every culture condition, five NP explants (corresponding to five donors) were cultured. After culture, NP samples were cut into halves. One half was left unlabelled and immediately imaged using two-photon microscopy. The other was put into 10 μM Calcein-AM (Sigma) and 10 μM Propidium Iodide (Sigma) in PBS and incubated first for 1h at 4^oC, followed by 1h at 37^oC to allow hydrolysis of Calcein-AM.

3.2.4 Two-photon and confocal microscopy

Two photon microscopy images of the unlabeled CSCGs and NP halves were acquired on a Zeiss LSM 510 META laser scanning microscope with a 62x, 1.2 numerical aperture (NA) water immersion objective (Carl Zeiss, Germany). Images were taken at random locations approximately 40 μm deep into the CSCGs and 100 μm deep into the NP samples. Samples were excited at 730 nm and the fluorescence emission was discriminated with a 650 nm short-pass dichroic mirror and transmitted to the appropriate detector unit. Two photon spectral images and emission spectra were acquired as previously described5. Confocal images of the Calcein-AM/Propidium Iodide stained NP halves were obtained on the same microscope with a 10x, 0.3 NA objective (Carl Zeiss) and the laser tuned to excitation wavelengths of 488 nm (Calcein-AM) and 543 nm (Propidium Iodide), respectively. Images were taken approximately 100 μm deep into the stained NP samples.

3.2.5 Threshold and CV determination

Receiver operating characteristics (ROC) analysis was performed to identify an autofluorescence threshold value to distinguish live from dead NP cells. Emission spectra of cells in CSCGs with 0% CV and 100% CV were obtained (n = 50 spectra per CSCG). Per spectra, the ratio of the intensities at 470/560 nm was determined and a ROC curve was calculated in SPSS 18.0 (SPSS, Inc., www.spss.com) (Hennings et al., 2009). The ratio corresponding to the maximum sum of sensitivity and specificity on the ROC curve was identified as the threshold value. The number of live and dead cells per two-photon spectral image (n = 20 - 30 images/ with at least 50 cells imaged) of each unlabeled NP half (n = 5) was counted. Likewise, live and dead cells were quantified per confocal image (n = 5 images / with at least 150 cells imaged) of the corresponding stained NP halves using the "cellcounter3D" macro in ImageJ (Gantenbein-Ritter et al., 2008). Subsequently, all living and dead cells were summed, and CV per imaged unlabeled or stained NP explant was calculated.

3.2.6 Statistical analysis

The measured CV values obtained were examined for significant differences using a two-way ANOVA. The two factors were defined as the method to assess CV and the glucose concentration. If no significant interaction effect was found, Fischer-HSD post-hoc testing was employed. Statistical significance was assumed for $p < 0.05$. All statistical tests were performed using SPSS 18.0 (SPSS, Inc., www.spss.com).

3.3 Results

3.3.1 Auto-fluorescence characterization in CSCGs

Live and dead isolated NP cells systematically emitted fluorescent light with distinct spectral characteristics. Living NP cells showed predominantly blue fluorescence with peak emission around 470 nm, the typical emission wavelength of NADH (Fig. 3.1A, C). In contrast, dead cells appeared to mainly emit green fluorescent light with peak intensity around 560nm, characteristic for FP fluorescence (Fig. 3.1B, C).

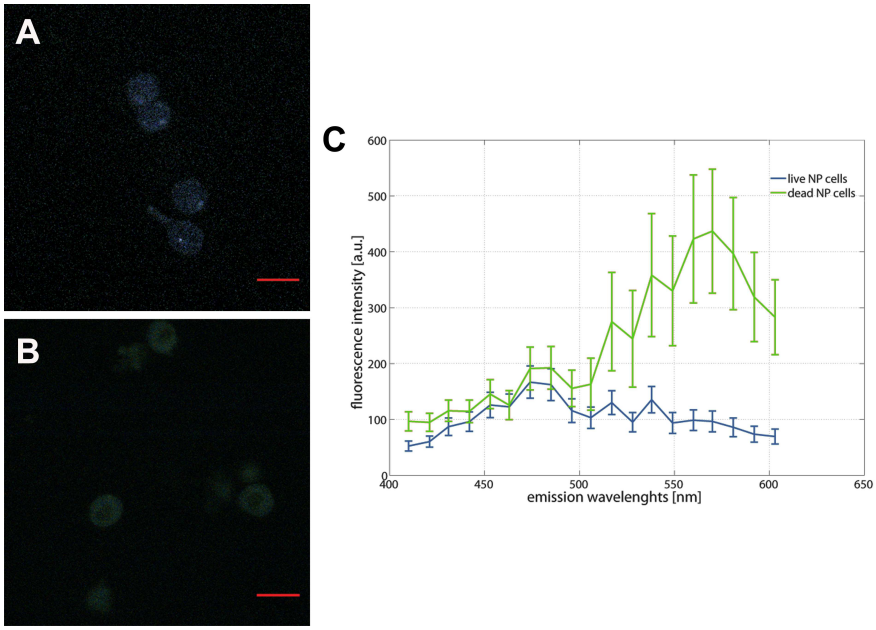

Figure 3.1: Characteristic two-photon spectral images of isolated NP cells seeded in collagen gels with A) 100% cell viability (CV) and B) 0% CV. Bar is 20 μm, Magnification 630x. C) Respective emission spectra of 50 live (blue) and 50 dead (green) NP cells illustrating distinct spectral differences between live and dead cells. Values are means +/- standard deviations.

These spectral differences resulted in live cells appearing blue and dead cells appearing green on the color-coded two-photon images, allowing an easy and direct cell classification (Fig. 3.1A, B). This observation was further manifested by live NP cells having larger intensity ratios (470/560 nm) than dead cells (Fig. 3.2).

The distribution of intensity ratios of live and dead NP cells indicated a good potential to classify them using a threshold intensity ratio. Using ROC analysis, the best combination of sensitivity and specificity was attained for a threshold ratio between 0.72 and 0.92, corresponding to 100% sensitivity (50 of the 50 live cells correctly identified) and 100% specificity (50 of the 50 dead cells correctly identified). For practicality, a final threshold ratio of 0.82 was defined and consequently, when assessing CV using label-free two-photon spectral imaging, cells with intensity ratio above 0.82

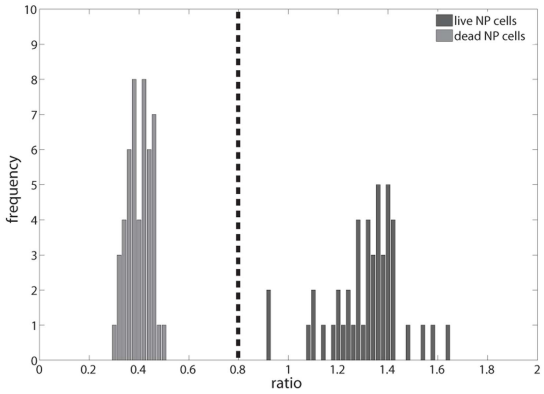

Figure 3.2: Histogram of the intensity ratios of the CSCGs with 0% CV and 100% CV. Dashed line represents the threshold ratio of 0.82 as calculated by Receiver operating characteristics (ROC) analysis. At this value the sum of sensitivity (number of correctly identified live cells / total number of live cells) and specificity (number of correctly identified dead cells / total number of dead cells) is maximized (100% and 100%, respectively).

were classified as viable, whereas cells with a lower intensity ratio were classified as dead.

3.3.2 Viability assessment in cultured NP explants

Auto-fluorescence emission of NP cells in cultured explants showed the typical characteristics as determined for isolated NP cells seeded into collagen gels. However, a few cells (usually 2-3 cells out of 50 cells imaged) emitted auto-fluorescent light with peak emission at 530 nm (Fig. 3.3A, B).

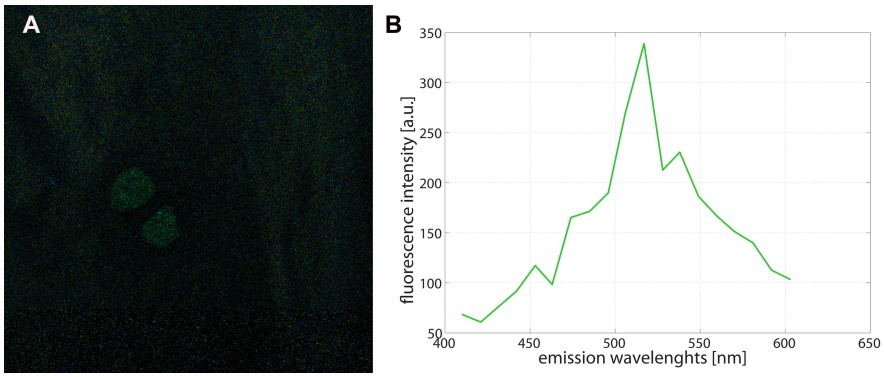

Figure 3.3: (A) Two-photon spectral image of "special" auto-fluorescence emission of presumably dead NP cells in cultured NP explants. B) Corresponding emission spectrum of one NP cell.

Cells exhibiting this "special" case of auto-fluorescence were classified as dead cells since their intensity ratios were below the threshold value. Also, emission in this spectral range is more characteristic for FPs than NADH, and this elevated FP contribution to the fluorescence signal further suggests that these cells are almost dead or dying. In a trial study, the number of cells required for obtaining a representative CV measurement of the cultured NP explants was determined. Results show that the more cells that are imaged the more accurate the CV estimation becomes as the standard deviation of the CV values decreases with increasing number of cells visualized. Here, for maximum accuracy, images of at least 50 cells per cultured NP sample were recorded. Culturing excised bovine NP tissue in different glucose concentrations resulted in NP explants with CV ranging from ca. 10% to 85% (Fig.3.4).

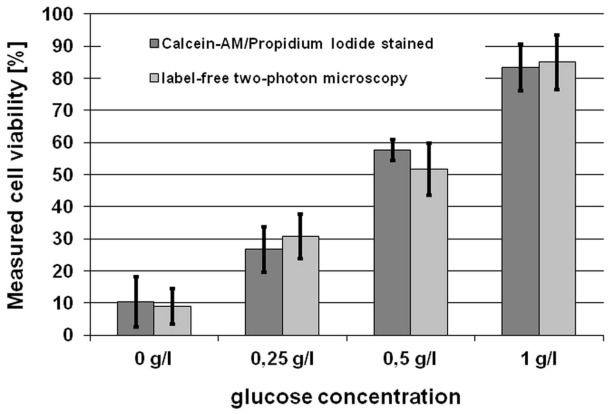

Figure 3.4: Measured cell viabilities as evaluated using two methods, Calcein-AM/Propidium Iodide staining and label-free two-photon microscopy, for cultured NP explants in four different glucose concentrations (0, 0.25, 0.5 and 1 g/l). Values are means +/- standard deviations, n=5.

Since the measured CVs at each glucose concentration were all significantly different from each other, glucose supplementation had a significant effect on the obtained CV values using both label-free two-photon microscopy and conventional Calcein-AM/Propidium-Iodide staining. In other words, both techniques could accurately distinguish CVs between explants cultured in the four different glucose concentrations. More importantly, no significant differences in assessing CV were found between the two methods, i.e. both techniques showed similar accuracy in determining CV. Furthermore, no significant interaction between the two CV assessment methods was found.

3.4 Discussion

Reference spectra of isolated NP cells seeded in collagen gels clearly demonstrated that live and dead NP cells emit auto-fluorescent light with distinct spectral differences. Using label-free two-photon microscopy, these spectral differences could be exploited to accurately differentiate viable from dead cells in NP tissue in-situ without requiring

additional staining. In fact, CV values obtained with either label-free two-photon spectral imaging or the gold standard, that is Calcein-AM/Propidium Iodide staining, were not significantly different from each other. Therefore, these results provide the first evidence, that CV can be non-invasively and accurately assessed even in highly light scattering NP tissue containing low metabolically active live cells and dead cells. The exact underlying mechanism that causes the measured differences in auto-fluorescence emission between live and dead NP cells remains to be investigated. One possible explanation may be the oxidation of FPs upon cell death. As cells become necrotic, they lose the integrity of their mitochondrial membranes leaving proteins or compounds unprotected to oxidation5. Unlike NADH, FPs are fluorescent in their oxidized form only and do not fluoresce in their reduced state11. Therefore, as shown in this study and our previous study with fibroblasts, dead cells appear to emit green auto-fluorescent light, characteristic for oxidized FPs. Thus, the enhanced FP contribution to the total fluorescence signal of dead cells may be explained by increased levels of oxidized FP present in nonviable cells.

Generally, an ongoing uncertainness exists about the proper interpretation of auto-fluorescence variations found in live and dead cells (Wang et al., 2009). Some studies report an increased auto-fluorescence intensity of dead cells as compared to living cells similar to our results (Fig. 3.1), while others report the opposite. In our study, a few cells in the NP explants exhibited an atypical emission spectrum with single peak at 530 nm (Fig. 3.3). Instead, living cells are generally characterized by emitting auto-fluorescent light with NADH emission peaking around 470 nm and show negligible fluorescence at 530 nm (Heikal, 2010), a wavelength typical for FP fluorescence. This suggests that these "special" cells are at least not in the same metabolic state as regular living cells, since their emission spectra are clearly different. Still, classification was achieved by examining their intensity ratios and applying the threshold, which resulted in these "special" cells being identified as dead cells. This classification resulted in CV assessments that did not differ from classical fluorescent staining methods. Furthermore, NP cells cultured in collagen gels or in tissue could potentially show different auto-fluorescence emission spectra depending on the mechanism of their demise. However, NP cells killed by "acidic shock" (exposing live cells to 1 N HCl for 10 min) as well as dead myofibroblasts also killed by "acidic shock" and seeded in collagen gels in vitro5 exhibited similar auto-fluorescence spectra as dead NP cells killed by limited glucose supplementation. Since the objective of this study was to introduce and demonstrate a new method to non-invasively assess CV in NP explants in situ, auto-fluorescence patterns and their relationship to cell death pathways were not investigated further.

Intervertebral disc tissue typically exhibits collagen auto-fluorescence particularly when irradiated with ultra-violet light sources (Dittmar et al., 2012). Here, by tuning the two-photon excitation to 730 nm, the collagen auto-fluorescence signal was much weaker than the emission due to cellular sources, i.e. NADH and FPs. Collagen structures were hardly visible (Fig. 3.1 and 3.3) and mainly contributed to background noise in the two-photon spectral images. This background signal could potentially be elevated in human NP tissue due to presence of auto-fluorescent advanced glycation end products (AGEs) that accumulate with age in aggrecan and collagen (Sivan et al., 2006). However, as AGE fluorescence does not overlap cellular FP auto-fluorescence and NP cells were discriminated mainly based on differences in their FP auto-fluorescence, this novel cell viability assay would likely not be significantly affected by aging or age-related AGE fluorescence. Also, by applying spectral un-

mixing, the individual components comprising the total recorded auto-fluorescence could be deciphered (Grosberg et al., 2011) and consequently any interference from AGE fluorescence could be reduced. Furthermore, one of the main advantages of two-photon microscopy is the localization of excitation, i.e. the density of scattered excitation photons is generally too low to produce significant signal (Helmchen and Denk, 2005). By utilizing near-infrared excitation, undesired light scattering was reduced and the cellular auto-fluorescence signal was captured. Moreover, two-photon microscopy is known to be less photo-damaging than other one-photon excitation microscopy techniques, e.g. confocal microscopy (Helmchen and Denk, 2005). No direct cell death due to two-photon microscopy was observed and since other reports have shown that long-term imaging does not comprise CV even in highly photosensitive specimens (Squirrell et al., 1999), we do not expect any (long-term) detrimental effects of this method on CV. In consequence, due to intrinsic properties of two-photon microscopy in conjunction with a carefully selected excitation wavelength, cells could be non-invasively visualized even in strongly scattering NP explants.

A few factors may have influenced the good accuracy of two-photon spectral imaging that could be considered bias. Here, only a reasonable number of NP samples (n = 5 for each glucose concentration) were imaged. Visualization of more specimens with subsequent CV assessment could potentially show that the two-photon microscopy and Calcein-AM/Propidium Iodide staining do not express the same accuracy. However, such small differences requiring large sample sizes are often not actually meaningful differences in CV. Estimating the viability exploiting cellular auto-fluorescence depends on visualizing representative numbers of live and dead cells. However, cells from a limited number of regions within the NP samples were visualized possibly overlooking zones of accumulated live or dead cells. Here, special care was taken to visualize cells from randomly selected regions within the tissue and therefore it took 30 - 60 min to complete two-photon imaging of one sample. Also, a trial study was performed to estimate how many cells needed to be visualized in order to obtain a representative CV measurement utilizing two-photon microscopy. Results showed that for evaluating ca. 10% differences in CV utilizing auto-fluorescence, images of at least 50 cells should be acquired, as done in this study.

Finally, a high NA objective was required to capture the weak auto-fluorescence emission in this study, but its depth penetration was limited to 280 μm. Future in-situ or in-vivo applications using auto-fluorescence to assess CV may want to consider employing objectives with high enough NA and large enough working distances to image cell populations deeper within the tissue. However, even the most advanced two-photon microscopes do not penetrate even low light-scattering tissues deeper than 1mm (Theer et al., 2003). Therefore, any clinical application of label-free two-photon microscopy to estimate CV requiring deeper tissue penetration will likely rely on the development of endoscopic probes (Wu et al., 2009). In conclusion, our results provide the first evidence of using differences in auto-fluorescence to distinguish live from dead cells and accurately assess CV in NP tissue in-situ. Consequently, the effect of various regenerative therapies, e.g. growth factor injection, on CV and potentially cell activity could be non-invasively monitored in pre-clinical explant culture systems mimicking in-vivo conditions. As samples could be utilized for other analyses without discarding them after CV assessment, this technique may potentially better facilitate a high-throughput screening of intervertebral disc regeneration approaches.

Chapter 4

Loss of collagen heterogeneity in moderately degenerated human intervertebtal discs

While severely degenerated intervertebral discs suffer from dramatic structural changes, less is known about the tissue architecture in moderately degenerated discs. As collagen organization strongly affects disc biomechanics and mechanobiology of disc cells, long-term success of regenerative therapies will likely depend on its thorough understanding. Here, we quantified collagen orientation and its spatial distribution in the annulus fibrosus of moderately degenerated human discs (Pfirrmann grade III). Tissue samples were dissected from four circumferential (anterior, left/right lateral and posterior) and two radial (outer and inner) locations. Cryo-sections were imaged using Second Harmonic Generation microscopy and the collagen fiber orientations per location were determined. Also, the proportionality between fibers aligned in the primary direction vs. other oriented fibers was determined. In contrast to healthy intervertebral discs, collagen orientation of moderately degenerated discs did not exhibit a spatial heterogeneity. Mean primary fiber orientations at circumferential locations were only significantly different from each other at two locations. Similarly, fiber angles at radial locations were only significantly different posteriorly. Fiber orientation proportionality did not show large variations either. Thus, the results of this study provide the first quantitative evidence that moderately degenerated discs are characterized by a spatially homogeneous collagen fiber orientation.

The content of this chapter is based on the publication: Dittmar, R., van Rijsbergen, M. M. and Ito, K.: Loss of collagen heterogeneity in moderately degenerated human intervertebtal discs, *J. Orthop. Res.*, **(submitted)**.

4.1 Introduction

Degeneration of intervertebral discs (IVDs), the pads of fibrocartilage located between the vertebral bodies of the spine, is commonly thought of being a major source of low back pain1. This multi-faceted condition involves cell-mediated biochemical and structural changes to both the center of the IVD, the nucleus pulposus (NP), and its surrounding ring of tissue, the annulus fibrosus (AF)(Urban and Roberts, 2003). Based on cellular and structural differences, the AF can be further divided into an outer AF (OAF) and an inner AF (IAF)(Marchand and Ahmed, 1990). Measured from the disc periphery, the OAF consists of the first 18 lamellae, whereas the IAF comprises the next 20 lamellae (Cassidy et al., 1989). Within each lamella, collagen fibers are oriented with a distinct mean angle of 30^o (alternating between lamellae) with respect to the transverse plane of the spine (Marchand and Ahmed, 1990; Holzapfel et al., 2005; Guerin and Elliott, 2006). As shown by Cassidy et al. and Holzapfel et al., this angle varies with location, both radially and circumferentially, leading to a spatially heterogeneous collagen fiber organization in healthy AF tissue. In other words, collagen fiber angle increases from the OAF towards the IAF (radially) and it also increases from the anterior to posterior location (circumferentially). The unique lamellar collagen organization of the AF is affected during IVD degeneration. As discs degenerate, structural damage and injury occurs including fissures and tears specifically in the AF (Videman and Nurminen, 2004). Around these severe annular defects, the collagen architecture is remodeled as part of an attempted repair process. Likely, this process is governed by extracellular matrix degrading enzymes, e.g. matrix metalloproteinases (MMPs), as previous studies have found a clear association between MMP expression and tear formation (Weiler et al., 2002). Furthermore, degenerated discs are characterized by a less apparent distinction between the NP and the AF due to tissue fibrosis. Consequently, the number of distinct lamellae in the AF decreases, whereas the thickness of the remaining concentric layers increases (Marchand and Ahmed, 1990). Computational studies have shown that the mechanical properties of the AF and consequently of the entire disc are dramatically affected when the fiber orientation is altered (Guerin and Elliott, 2006; Noailly et al., 2011). While it is well established that the collagen organization experiences dramatic changes in severely degenerated discs, less is known about (possible) effects of degeneration on the collagen fiber architecture in the AF of moderately degenerated IVDs. As mechanics directly influences disc cell metabolism (Fernando et al., 2011) and thus cellular function and survival, long-term success of e.g. novel regenerative therapies aiming at treating early/mild degeneration will likely also depend on a thorough understanding of the biomechanical environment they are exposed to (Kandel et al., 2008). Furthermore, potential changes to the AF collagen organization may serve as a biomarker for improved diagnosis of moderate IVD degeneration, where with the advent of novel imaging techniques such as Diffusion Tensor Imaging (Hsu and Setton, 1999), collagen orientation may potentially be assessed in the clinic. Hence, the aim of this study was to quantify the AF collagen orientation in moderately degenerated discs (Pfirrmann grade III). Cryosections of AF tissue from human cadaveric discs were obtained and visualized using Second Harmonic Generation (SHG) microscopy. Images were obtained of samples from four circumferential locations (anterior, left lateral, right lateral and posterior) and two different radial locations (OAF and IAF). Using a collagen fiber tracking algorithm, the primary collagen fiber orientation per location as well as the proportionality between fibers aligned in the primary direction

vs. other oriented fibers was determined.

4.2 Materials and Methods

4.2.1 Sample preparation

Cadaveric human lumbar spines (L1-S1) were provided by the Anatomy Department of the University Medical Center Utrecht (Utrecht, The Netherlands) following an IRB approved protocol. T2-weighted MRI images of the spines were acquired and all IVDs were graded by a senior radiologist of the Polyclinique Saint-Cme (Compiegne, France) according to the Pfirrmann scale (Pfirrmann et al., 2001). Only grade III discs were utilized for further analysis. In total, seven IVDs (levels L1-L2 and L3-L4) from five different donors (all male, mean age 62.8 ± 12 years) were dissected by cutting transversally underneath the superior endplate using a scalpel. IVD pieces containing both OAF and IAF were dissected by making vertical incision and cutting transversally above the inferior endplate. For each disc, samples were obtained from the anterior, left and right lateral, and posterior location (Fig. 4.1a). Specimens were split into an OAF sample and an IAF sample by cutting the dissected IVD piece at 2 mm from the outside (Fig. 4.1b).

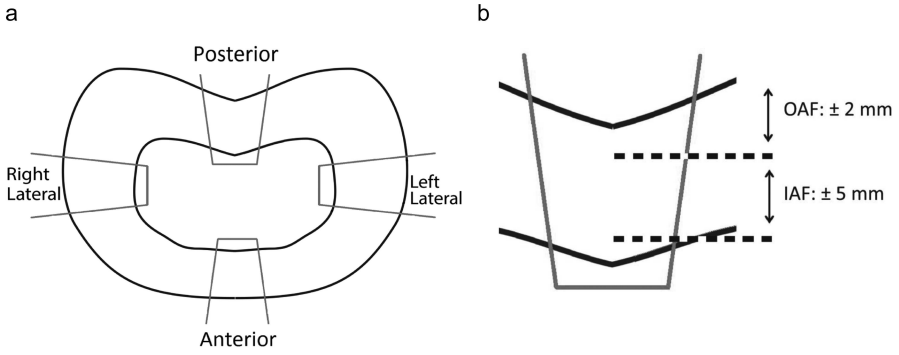

Figure 4.1: Schematic representation of the sample isolation and preparation. a) Per IVD, 4 wedge-shaped pieces containing both OAF and IAF were dissected. b) After isolation, each IVD piece (posterior sample shown in schematic) was split in an OAF and IAF sample. Dotted lines represent razor blade dissection sites.

Samples were then directly put into cryo-molds (Gibco, The Netherlands) with OAF pieces having their outermost circumferential surfaces tangent to the faces of the molds. Instead, IAF samples were put into molds with their innermost circumferential surfaces tangent to the faces of the molds. Samples were embedded in cryo-glue (Sakura Finetek Europe, The Netherlands) together with three 0.3 mm diameter graphite leads (Pentel, Japan) next to them (Fig. 4.2). These leads were used as markers of each sample when they were taken out of the molds and mounted on the cryotome. After freezing overnight at -30C, samples were mounted on a cryotome (Fisher Scientific,

The Netherlands) and 50 μ thick tangential cryo-sections of the OAF and IAF were obtained.

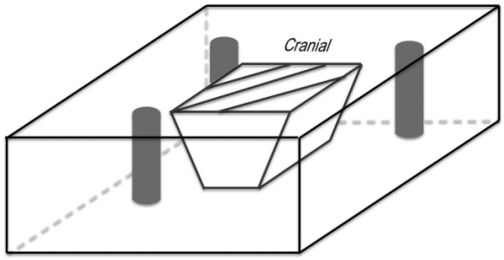

Figure 4.2: Schematic drawing of sample embedding. Each isolated OAF and IAF piece was put into a cryo-mold and embedded in cryo-glue. Graphite leads (grey bars) were inserted next to samples.

4.2.2 SHG microscopy

SHG images of the OAF and IAF cryo-sections were acquired on a Leica TCS SP5X laser scanning microscope (Leica, Germany) with a 10x, 0.4 numerical aperture (NA) objective and excitation light tuned to 810 nm. The SHG signal was collected through a tunable hybrid detector set to 390-420 nm. Tiled scans usually comprising 80 individual SHG images were obtained to cover the entire cryo-section.

4.2.3 Image registration and analysis

Tiled SHG scans were stitched into a so-called mosaic image of the entire OAF or IAF cryo-section (Fig. 4.3). Mosaic images were loaded into a custom written Matlab (Matlab, U.S.A) script. First, the vertical edges of the OAF or IAF sample were defined by manually selecting two points, P1 and P2, located on the edge of the sample (Fig. 4.3a). Second, three other points, P3, P4 and P5, located equally distributed between these initial two points and on the edge of the sample, were automatically determined. A line was plotted through P1 and P2, then P3 was defined as a point on the sample edge with y-coordinate equal to the center of the plotted line (Fig. 4.3b). Next, lines through P1 to P3 and P3 to P2 were plotted (Fig. 4.3c). First the center points of the lines through P1 to P3 and P3 to P2 were calculated, respectively. Then the points on the sample edge with y-coordinate equal to the center points were defined as P4 and P5 (Fig. 4.3c). Finally, a line was fitted through all five points using a linear least squares fitting technique (Fig. 4.3d). The same approach was repeated for the opposite edge of the sample leading to two reference lines with a certain angle with respect to the transverse plane (Fig. 4.3d). A third, final line was calculated by averaging both reference lines (Fig. 4.3d). Mosaic images were rotated until this third, final reference line was aligned in vertical direction (Fig. 4.3e). The first mosaic image, into the depth of the section, containing aligned collagen fibers was used for fiber orientation analysis. A sub-image was cropped out of the mosaic

image (Fig. 4.3f) and an in-house-developed algorithm (Daniels F, 2006) was used for quantifying the collagen fiber orientations in the cropped image(s) (Fig. 4.4a). Based on this algorithm, a histogram was created of each sample and the primary collagen fiber orientation was defined as the angle value with maximum number of counts (Fig. 4.4b). To determine the proportionality of the collagen fibers in the primary direction vs. other directions, the root mean square (RMS) of the total counted angle values was used to distinguish between the different orientations. Fiber orientations with counts lower than the RMS were classified as oriented in the other directions, whereas angles with counts larger than the RMS were identified as fibers in the primary direction (Fig. 4.4b). This approach was validated by creating multiple idealized distribution ratios (Gaussian shaped curves) from which the distribution was known and comparing the calculated ratio to the known distribution ratio.

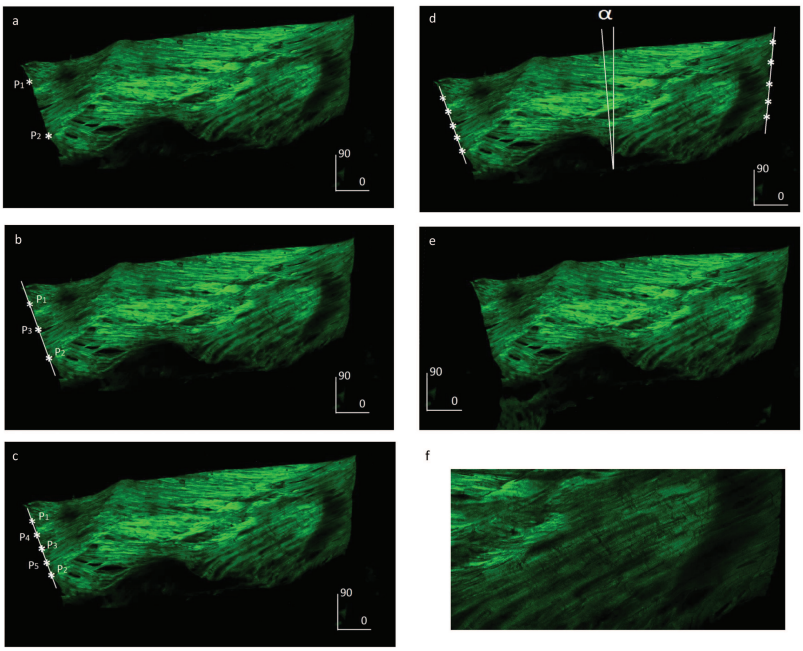

Figure 4.3: Image registration steps. a) Representative mosaic image prior to registration. Two points, P1 and P2 are manually selected on sample edge. b) Plotted line through P1 and P2. P3 is automatically determined as point on the sample edge with y-coordinate equal to the line center. c) P4 and P5 are determined in the same procedure resulting in five equally distributed points on sample edge. d) Steps a)-c) are repeated on opposite sample edge leading to two reference lines. Average of both reference lines is calculated: third reference line. e) Mosaic image is rotated until third reference line is aligned in vertical direction. f) Sub-image is cropped out of aligned mosaic image for collagen fiber orientation and proportionality analysis.

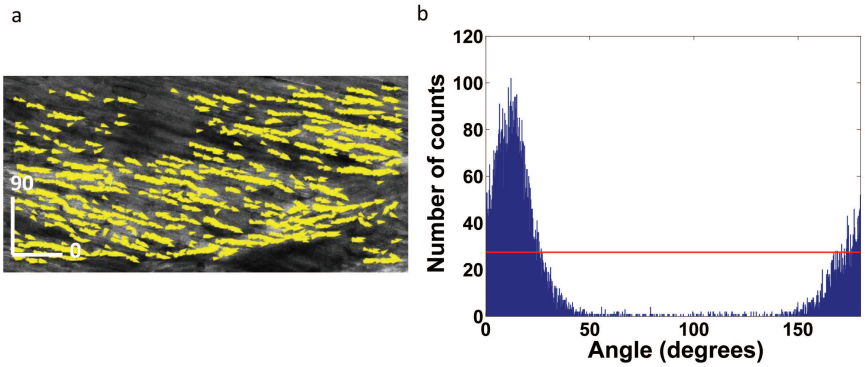

Figure 4.4: Collagen orientation and fiber proportionality calculation a) Collagen fiber orientation in cropped sub-image containing aligned collagen. Yellow arrows indicate calculated fiber orientations. b) Corresponding histogram of detected fiber orientations; angle values are with respect to the transverse plane. Red line indicates RMS value used for determining proportionality between fibers aligned in primary direction vs. other directions.

4.2.4 Statistical analysis

To determine differences in fiber primary angles and proportionality between locations blocked two-way analysis of variance (ANOVA; blocked per disc) was performed. For comparing fiber values and proportionality between locations, one-sided paired t-tests were performed, using the Fisher's LSD correction. Normality and sphericity were checked using the Shapiro-Wilk resp. Mauchly's test. All statistical analysis was performed using SPSS 20 (IBM, USA) and statistical significance was assumed for $p < 0.05$.

4.3 Results

Mean primary collagen fiber angles were between 15^o to 31^o throughout the AF and exhibited a rather large variance at the posterior position (Table 4.1).

Table 4.1: Measured primary collagen fiber orientation for both OAF and IAF samples at the various circumferential locations. Values are means standard deviations (n = 7 for anterior and posterior, n = 14 for lateral).

	OAF (mean ±SD)	**IAF (mean ±SD)**
Anterior	21.0 ± 8.2^o	15.4 ± 2.7^o
Lateral	21.7 ± 4.2^o	19.5 ± 5.0^o
Posterior	31.5 ± 14.9^o	19.2 ± 9.4^o

No statistically significant differences were found between the mean primary collagen orientations of OAF specimens at the various circumferential locations (Fig. 4.5). Still, a trend for increasing mean primary angle from anterior to posterior position was

observed, since angle values at anterior and lateral locations showed great similarity and were generally smaller than those at the posterior position. In the IAF, mean primary angle values were significantly different from each other between anterior and lateral locations (p=0.032) (Fig. 4.5). In contrast to the OAF, mean primary angle values in the IAF at lateral and posterior locations were very similar and larger as compared to the anterior location. Also, differences in the mean collagen orientation between the different circumferential locations were smaller than in the OAF. In the radial direction, i.e. from OAF to IAF, fiber angles did not show strong alterations depending on the position. A radial gradient in collagen orientation was observed only at the posterior location where OAF and IAF angles were significantly different from each other (p=0.008) (Fig. 4.6). In both the OAF and IAF, mean primary fiber proportionality was 70 ± 20% (Table 4.2). OAF samples showed significantly larger fiber proportionality posteriorly than laterally (p=0.030). No other statistically significant differences in proportionality depending on circumferential locations were observed (Table 4.2). In contrast, IAF samples showed very similar mean fiber proportionalities for all circumferential locations and no statistically significant differences were observed. Also, in radial direction, no statistically significant differences in collagen fiber proportionality between the OAF and IAF at the various locations were found.

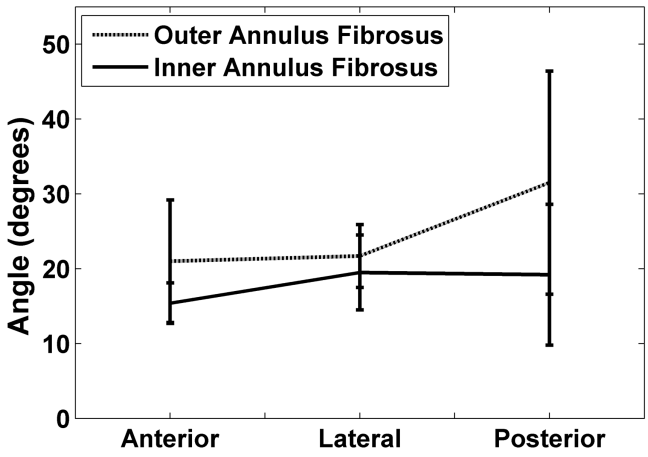

Figure 4.5: Calculated collagen orientations at various circumferential locations. Mean primary collagen fiber orientation for OAF and IAF samples at the various circumferential locations. Values are means standard deviations (n = 7 for anterior and posterior, n = 14 for lateral).

4.4 Discussion

Using SHG microscopy and subsequent image analysis, the collagen fiber architecture in moderately degenerated IVDs was quantified. Primary fiber angles ranged between 21^o to 31^o for the OAF and 15^o to 19^o for IAF samples, respectively. Although

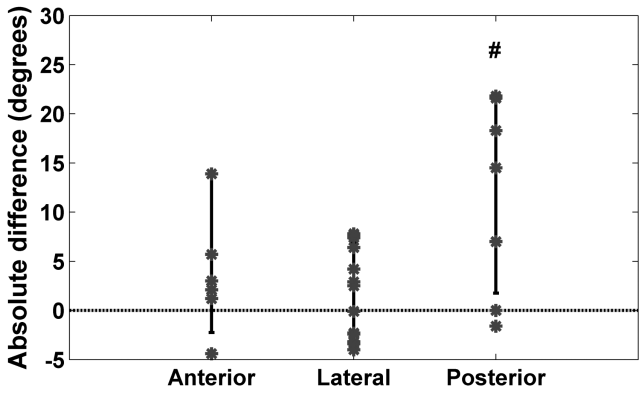

Figure 4.6: Calculated collagen orientations at various radial locations. Absolute difference in primary collagen fiber orientation between OAF and IAF at various circumferential locations. Values are means standard deviations, including the individual measurements (; n = 7 for anterior and posterior, n = 14 for lateral). At posterior location, a significant difference in fiber orientation between OAF and IAF was determined (p=0.008,#).

Table 4.2: Measured collagen fiber proportionality. Collagen fiber proportionality (in %) at various circumferential locations. Values are means standard deviations (n = 7 for anterior and posterior, n = 14 for lateral). A significant difference between posterior and lateral location of the OAF was found (p=0.030, #).

	OAF (mean ±SD)	**IAF (mean ±SD)**
Anterior	70 ± 9	72 ± 9
Lateral	66 ± 12$^{\#}$	71 ± 9
Posterior	80 ± 10$^{\#}$	74 ± 12

there was a pattern of increasing fiber angle from anterior to posterior, statistically no significant general gradient in collagen orientation in the circumferential direction was found. Only in the IAF a significant difference in mean primary collagen orientation between anterior and lateral location was observed. Similarly, in radial direction mean fiber angles exhibited only small alternations depending on the circumferential position. Only at the posterior location, a significant radial gradient in collagen orientation was observed. Also, the degree of collagen anisotropy, as measured by the fiber direction proportionality, did not exhibit large variations between the OAF and IAF and the various circumferential locations. Except for a statistically significant difference in fiber proportionality between OAF posterior and lateral position, no other circumferential or radial gradients were measured. The unique heterogeneous collagen organization of healthy IVDs was first described in the reports of (Cassidy et al., 1989; Holzapfel et al., 2005). They showed that fiber orientation in the AF follows both radial and circumferential gradients. In other words, mean fiber angle increases from the OAF towards the IAF and also depends on the circumferential location within the AF. As such, both studies established that healthy discs are characterized by collagen fiber gradients which are essential to disc biomechanics and function. Our results indicate that this unique collagen fiber architecture in the mod-

erately degenerated AF is strongly influenced by disc degeneration. Whereas healthy discs are characterized by a spatially heterogeneous AF collagen fiber orientation, moderately degenerated IVDs appear to comprise a more homogenous AF collagen architecture. During degeneration, discs experience a number of structural changes connected to collagen remodeling. Examples of such changes include dehydration of the NP, loss of the distinction between the AF and NP due to tissue fibrosis and in later stages of degeneration the appearance of cracks and fissures, which in severe cases, may lead to neurovascular in-growth and the formation of granulation tissue (Urban and Roberts, 2003). Consequently, these cell-mediated degenerative processes affect the lamellar organization of the AF. As the transition between NP and AF fades away, degenerated discs are reported to have less and thicker lamellae (Marchand and Ahmed, 1990). Also, as the NP becomes dehydrated, discs height and pressure within discs decrease causing the lamellae of the inner AF to bulge inwards. This in turn may affect the load distribution onto these lamellae, potentially inducing or accelerating the remodeling of the AF collagen architecture in order to cope with the altered biomechanical environment. Here, albeit not significantly, mean primary fiber angle in the OAF of moderately degenerated IVDs was larger than in the IAF, which is opposite to the reported increasing fiber angle from the OAF to the IAF in healthy discs. Hence, the absence of strong spatial gradients in collagen fiber orientation in moderately degenerated discs may be explained by cell-mediated degenerative processes that affected disc biomechanics and triggered disc cells to remodel the AF collagen architecture. In general, our measurements of fiber angles showed a variance of up to 15^o at the different locations (Table 4.1, posterior location) similar to studies of healthy AF tissue4. As shown by Boos et al. (2002); Marchand and Ahmed (1990), this large variance may be explained by the natural heterogeneity of fiber orientations within the AF and is not related to the utilized imaging or orientation analysis technique. While the utilized algorithm was originally developed and validated to capture collagen orientations in tissue-engineered constructs, it has successfully been utilized to quantify collagen angles in mature collageneous tissues, e.g. the collagen organization of the carotid artery (Ghazanfari et al., 2012). Also, SHG microscopy has been extensively used to visualize fibrillar collagens and their organization with the resolution and detail of standard histology (Zipfel et al., 2003). Since the orientation of collagen fibers in the acquired SHG images was successfully quantified (Fig. 4), this further suggests that the determined large variance is of biological origin, i.e. characteristic of (human) degenerated AF tissue. Our results, obtained on moderately degenerated discs, showed a somewhat inhomogeneous variance distribution where the posterior samples showed larger variance than specimens from other locations. This is likely due to more severe morphological changes of degeneration in AF tissue typically found at the posterior position. Posteriorly, IVDs are much thinner and more prone to injury such as herniation (Holzapfel et al., 2005). As the large variance may have blurred our results and conclusion, especially since it is unknown how degeneration influences the primary fiber orientation and corresponding variance and since no AF tissue from healthy IVDs was tested, a power analysis on the obtained angle values was conducted. The calculated power for all comparisons, except for the test between anterior and lateral IAF, was below 80 % and, therefore, sample size would have to be doubled (n = 15) to increase power for all locations (to a minimum of 80 %). However, to detect similar differences between the locations as reported for healthy discs, n would also have to be increased and reports of collagen orientations in healthy AF tissue with larger n (n=11) showed similarly large variances (Holzapfel et al., 2005). Thus, such large sample sizes are indicative of the observed large variance in primary collagen

fiber orientation of both healthy and moderately degenerated IVDs, and not related to the used imaging, image processing technique or small sample size, suggesting that this is an intrinsic property of AF tissue. Loss of spatial heterogeneity in collagen architecture during degeneration as shown in this study will have severe implications on disc mechanical behavior and load-bearing function (Holzapfel et al., 2005; Guerin and Elliott, 2006). This in turn may induce more or accelerate degenerative changes in the IVD, as the biomechanical environment is known to directly influence disc cell metabolism (Fernando et al., 2011). Elaborate computational models describing healthy IVD mechanics exist that include collagen fiber orientation and in the case of Schroeder et al. (2006), also fiber proportionality. As other model parameters such as biochemical content (water, proteoglycans, and collagen) are known for degenerated discs, the results of this study may be incorporated to obtain a computational model of a (moderately) degenerated disc. This would further aid in improving the efficacy of novel regenerative medicine approaches, e.g. cell therapy, aiming at treating early degenerated discs. Since injected cells would be exposed to the same environment that promoted disc degeneration in the first place, a thorough understanding of how altered mechanics due to a more spatially homogenous collagen organization affects disc cell metabolism may increase long-term success of such regenerative approaches (Kandel et al., 2008). Also, the results of this study may be utilized to validate Diffusion Tensor Imaging as (clinical) tool for diagnosing moderately IVD degeneration. Hsu and Setton successfully applied this novel imaging technique to assess the collagen organization of healthy human IVDs. Diffusion Tensor Imaging provides information on both collagen orientation and anisotropy and, therefore, changes to the AF collagen organization, as shown in this study, may serve as biomarker for improved diagnosis of early IVD degeneration. In summary, the results of this study provide the first evidence that moderately degenerated IVDs are characterized by a spatially homogeneous collagen fiber orientation. No strong collagen fiber gradients in circumferential or radial direction were determined. Hence, quantitative data on how degeneration affects collagen architecture specifically in the AF is obtained. This may lead to a better understanding of the mechano-biological environment of moderately degenerated discs and, thus, key processes and risk factors involved in disc degeneration may be better understood potentially leading to improved therapy. Also, these findings may result in an earlier diagnosis of degenerative changes as homogenous fiber architecture may serve as a biomarker for mild disc degeneration.

Chapter 5

Characterization of a novel fluorescent probe for MMP-13 activity reveals MMP-13 independent cell-mediated cleavage

Evidence suggests that increased matrix metalloproteinase 13 activity plays a key role in progression of degenerative diseases including osteoarthritis and intervertebral disc degeneration. Current methods for measuring MMP-13 levels and activity are limited to measuring in aqueous media. Fluorescent probes may overcome these limitations and allow a non-destructive assessment of MMP-13 activity in intact cell-laden constructs and tissues. Hence, a fluorescent probe for assessing active MMP-13 levels in aqueous media and in three-dimensional cultures was synthesized. Its accuracy, sensitivity, detection limit and selectivity for measuring active MMP-13 was evaluated and compared to ELISA. Next, human OA chondrocytes were seeded into agarose constructs and cultured in media with different supplements. Active MMP-13 levels secreted into the culture media were evaluated using ELISA and compared to active MMP-13 levels inside intact constructs as evaluated by the novel fluorescent probe. Results show that no significant differences in measuring active MMP-13 levels were found between the novel probe and ELISA. However, despite its demonstrated selectivity for active MMP-13, results from three-dimensional cell culture indicated that the probe may be subjected to cleavage by other enzymes. Since other fluorescent probes exhibit a very similar design, these results may raise concerns regarding the applicability of such probes and may therefore prompt the re-evaluation of current probe designs.

The content of this chapter is based on: Dittmar, R., Janssen, B., Patil, S., Creemers, L., Merkx, M. and Ito, K.: Characterization of a novel fluorescent probe MMP-13 activity reveals MMP-13 independent cell-mediated cleavage, **(manuscript in preparation)**.

5.1 Introduction

Under normal physiological conditions in connective tissue, extracellular matrix (ECM) synthesis and breakdown are precisely regulated by a well-controlled balance between anabolic and catabolic enzyme activity (Visse and Nagase, 2003; Nagase et al., 2006). When this balance is deregulated, it can have severe implications and lead to the onset or progression of many diseases including cancer (Folgueras et al., 2004), cardiovascular diseases (Nagase et al., 2006) and musculoskeletal disorders such as osteoarthritis (Murphy and Nagase, 2008; Troeberg and Nagase, 2012) (OA) and intervertebral disc (IVD) degeneration (Vo et al., 2013). Various enzymes have been implicated in the maintenance of the ECM with so-called matrix metalloproteinases (MMPs) being commonly regarded as the major enzymes causing tissue breakdown (Visse and Nagase, 2003; Nagase et al., 2006). MMPs are zinc-dependent proteinases that are produced in latent form and require activation, often by other MMPs, to become active (Nagase et al., 2006; Murphy and Nagase, 2008). These enzymes are capable of breaking down all major matrix constituents including different types of collagens and proteoglycans (Nagase et al., 2006). Both levels and activities of most MMPs are low or negligible in the normal steady-state and they presumably contribute to the normal matrix turnover (Nagase et al., 2006; Murphy and Nagase, 2008). However, during OA and IVD degeneration, increased or unbalanced levels and activities of MMPs are widely thought to mediate ECM loss (Roughley, 2004; Maitre et al., 2007; Murphy and Nagase, 2008; Troeberg and Nagase, 2012; Vo et al., 2013). Evidence suggests that particularly MMP-13, also known as collagenase 3, plays a pivotal role in the depletion of the ECM collagen network in OA and IVD degeneration (Troeberg and Nagase, 2012; Vo et al., 2013). Of all MMPs, MMP-13 displays the strongest affinity for collagen type II (Mitchell et al., 1996) and is therefore suspected to be pivotal in the degradation of collagen type II - rich tissues such as cartilage and the inner part of IVDs (Murphy and Nagase, 2008; Troeberg and Nagase, 2012; Vo et al., 2013). Both MMP-13 gene and protein expression is elevated in degenerated discs and osteoarthritic cartilage (Wu et al., 2002; Kevorkian et al., 2004; Maitre et al., 2004; Bachmeier et al., 2009; Vo et al., 2013). Instead, healthy discs and cartilage show hardly any signs of MMP-13 presence (Kevorkian et al., 2004; Maitre et al., 2004).

However, while these reports indicate elevated expression of MMP-13 in degenerated disc and cartilage tissue, they often did not distinguish between the latent and active form of the enzyme (Maitre et al., 2004), let alone assess MMP-13 activity (Wu et al., 2002). Currently, for measuring active MMP-13, the so-called enzyme-linked immunosorbent assay (ELISA) is the gold-standard technique, whereas enzyme zymography is often employed for semi-quantitative measurements of MMP-13 activity (van Beurden and den Hoff, 2005; Bachmeier et al., 2009). However, both ELISA and in vitro zymography are mostly limited to measuring in vitro in aqueous media, e.g. cell culture supernatants or tissue homogenates, and can therefore not be utilized without destroying the constructs or tissues (van Beurden and den Hoff, 2005). Likewise, in situ zymography does not enable non-invasive MMP-13 activity determinations as this technique is generally applied utilizing histological sections (van Beurden and den Hoff, 2005). Fluorescent probes may overcome these limitations and allow a non-destructive assessment of MMP-13 activity (Lee et al., 2008; Zhu et al., 2011; Lim et al., 2014; Zhu et al., 2014). Typically, probes consist of a peptide linker that functions as a specific substrate to the target MMP, e.g. MMP-13, which connects a fluorescence donor and quencher (Lee et al., 2008; Zhu et al., 2011; Lim et al., 2014; Zhu et al., 2014). In the

absence of active MMP-13, no fluorescent light is emitted since the energy of the donor is transferred to the quencher by fluorescence resonance energy transfer. When the peptide linker is cleaved by active MMP-13, the fluorescence donor separates from the quencher and, therefore, the energy transfer from donor to quencher seizes resulting in a detectable fluorescence signal.

However, while several studies have demonstrated the potential of fluorescent probes for non-destructively monitoring the activity of MMP-13, the aforementioned studies focused mainly on demonstrating the in vivo applicability of fluorescent probes and provided little information on their ability and accuracy to quantify specific active MMP-13 levels in vitro as compared to existing techniques, i.e. ELISA (Lee et al., 2008; Zhu et al., 2011; Lim et al., 2014; Zhu et al., 2014).

Hence, the objectives of this study were to first synthesize a fluorescent probe for non-destructively assessing active MMP-13 levels in 3D in vitro cultures and to rigorously characterize its performance in vitro. On the basis of known MMP-13 fluorescent probes, a novel probe was designed. Its accuracy, sensitivity, detection limit and selectivity for measuring active MMP-13 was evaluated in vitro and in three-dimensional (3D) constructs and compared to a commercially available ELISA for active, human MMP-13. Then the feasibility of non-destructively measuring active MMP-13 levels in tissue culture constructs was examined. Human OA chondrocytes were seeded into 3D agarose constructs and cultured in media with different supplements to either stimulate MMP-13 generation or inhibit MMP-13 activity. Active MMP-13 levels secreted into the culture media were evaluated using ELISA and compared to active MMP-13 levels inside intact constructs as evaluated by the novel fluorescent probe.

5.2 Materials and methods

5.2.1 Synthesis of fluorescent probe

The fluorescent probe was prepared by conjugating the near-infrared fluorochrome, Atto680 NHS ester (ex/em; 680/700 nm, Sigma-Aldrich, Zwijndrecht, The Netherlands) and black hole quencher-3 (BHQ-3 NHS ester, abs. 650 nm, Biosearch Technologies, Inc., Petaluma, CA, U.S.A) to an MMP-13 specific substrate (GPLGMRGLG-K(Mmt)). Peptide synthesis was performed manually following the standard Fmoc peptide synthesis protocol using NovaSyn TGR resin (Novabiochem, Billerica, MA, U.S.A). Subsequently, 3.5 μmol of resin was used for the coupling of Atto680 and BHQ-3. First, Atto680 was coupled to the N-terminus of the peptide using 1.8- fold molar excess and stirred for two hours at room temperature in anhydrous dimethylformamide (DMF, Sigma-Aldrich). The Fmoc-Lys(Mmt)-OH building block was used in order to introduce BHQ-3. Selective de-protection of the Mmt-group was performed by repeatedly stirring in a mixture of Trifluoroacetic acid/ Triisopropylsilane/Dichloromethane (TFA/TIS/DCM, 2:5:93) for 5 minutes until the yellow color of the Mmt-carbocations disappeared. BHQ-3 was coupled to the ε-amine by stirring the reaction for 2 hours at room temperature using a 1.8-fold molar excess in anhydrous DMF. 8-fold molar excess of DIPEA was used in both coupling steps. Finally, the peptide was cleaved from the resin using TFA/TIS/H2O (95:2.5:2.5) and precipitated by adding ethyl ether. ESI-MS spectra were recorded on a mass spectrometer (Single Quadrupole Electrospray Ion-

ization Mass Spectrometer API-150EX, Applied Biosystems, Darmstadt, Germany) in positive mode (0.1% TFA, 2-70% Acetonitrile gradient)(Fig. 5.1). Semi-preparative reversed phase HPLC was performed (LC-8A HPLC system, Shimadzu Benlux, Den Bosch, The Netherlands) by using a GraceAlpha C18 column (250 mm x 4.6 mm) and 0.1% TFA (Fig. 5.2). The appropriate fractions were collected and lyophilized.

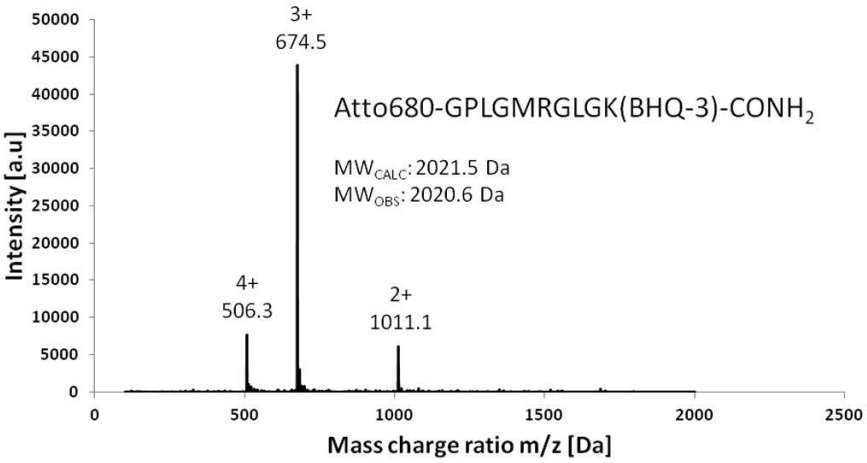

Figure 5.1: ESI-MS spectrum of synthesized fluorescent probe (Atto680-GPLGMRGLGK(BHQ-3)-$CONH_2$). Calculated molecular weight (MW_{CALC}) was 2021.5 Da and observed molecular weight (MW_{OBS}) was 2020.6 Da.

5.2.2 In vitro and in situ performance of the MMP-13 FRET probe

To determine the feasibility of measuring active MMP-13 using the probe, 10 nM active, recombinant, human MMP-13 (Calbiochem, Merk Millipore, Darmstadt, Germany) was incubated with 10 uM probe and the change in fluorescence intensity was recorded in a microplate reader (BioTek, Winooski, VT, U.S.A) every 5 min during the first half hour and then every 10 min during the second half hour. The excitation filter was set to 670/10 nm and the emission filter was set to 700/20 nm. To establish the newly synthesized fluorescent probe as basis for an assay for MMP-13 activity, the performance of the probe in vitro and in 3D constructs was evaluated following US Food and Drug Administration guidelines (www.fda.gov/downloads/Drugs /Guidances/ucm070107) for bio-analytical method validation whenever possible. For the assay performance in aqueous media, the relationship between assay response, i.e. fluorescence signal, and known concentrations of active MMP-13 (100, 50, 25, 12.5, 6.25 and 0 pM, n = 5/concentration) was analyzed by a calibration curve. Calibration curves were obtained by assaying fluorescent probe (10 μM) with serial dilutions of active, recombinant, human MMP-13 (Calbiochem, Merk Millipore, Darmstadt, Germany) diluted in assay buffer (500 mM HEPES, 10 mM CaCl2, 0.005% Brij 35 P, pH = 7) to the desired concentration and recording the fluorescence signal in a

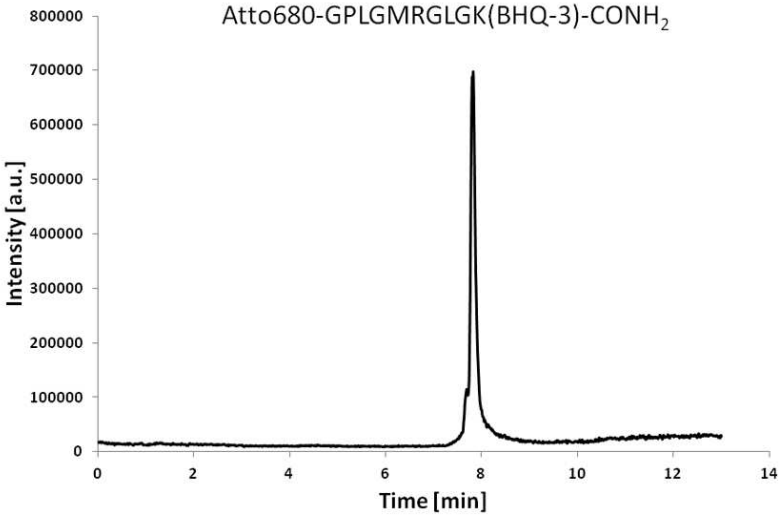

Figure 5.2: HPLC chromatogram of synthesized fluorescent probe (Atto680-GPLGMRGLGK(BHQ-3)-$CONH_2$).

microplate reader (BioTek, Winooski, VT, U.S.A) every 30 min for 9 hours. The excitation filter was set to 670/10 nm and the emission filter was set to 700/20 nm. Linearity of the calibration curve was evaluated using regression coefficients, R2, determined in Excel (Microsoft, Redmond, WA, U.S.A). The limit of detection (LOD) was defined as the mean value of the negative controls, i.e. 0 pM MMP-13 samples, plus three standard deviations of the mean (Armbruster and Pry, 2008). The limit of quantification (LOQ) was defined as the mean value of the negative controls plus five standard deviations (Armbruster and Pry, 2008). Assay precision was determined by calculating the coefficient of variation (%CV) values, i.e. standard deviation divided by the mean, in the high, mid and low assay range, i.e. at 100 pM, 25 pM and 6.25 pM. Assay accuracy was assessed as the nominal active MMP-13 concentrations divided by the corresponding calculated active MMP-13 values in the high, mid and low assay range and presented as percentage.

For the assay performance in 3D culture, a similar approach was followed. The relationship between fluorescence signal and known concentrations of active MMP-13 in 3D agarose constructs was analyzed by a calibration curve. Agarose constructs (2% w/v, Sigma-Aldrich) with known MMP-13 levels (100, 50, 25, 12.5, 6.25 and 0 pM, n = 5/concentration) were prepared by mixing active, recombinant, human MMP-13 diluted in assay buffer with agarose (3% w/v) in assay buffer at ratio 1:3. The agarose-MMP-13 mix (160 μl) was then transferred to a 96-well plate and allowed to polymerize for 5 min at room temperature. Calibration curves were obtained by incubating fluorescent probe (40 μl, 10 μM final concentration) with agarose constructs and recording the fluorescence signal in a microplate reader every 30 min for 9 hours. The excitation filter was set to 670/10 nm and the emission filter was set to 700/20 nm. Linearity, LOD, LOQ, assay precision and accuracy was defined and determined

as for the in vitro evaluation.

5.2.3 In vitro selectivity and comparison to ELISA

To confirm selectivity of the novel fluorescent probe, the enzyme kinetic parameter k_{cat}/K_M was determined. Different concentrations of the probe (0.125, 0.25, 0.5, 1 and 2 μM, n = 3/concentration) in assay buffer were incubated with 5 nM active, recombinant human MMP-13 (Calbiochem), MMP-1 MMP-2, MMP-3 (all Peptrotech, Rocky Hill, NJ, U.S.A.) or MMP-7 (ProSpec Bio, Ness-Ziona, Israel) and the fluorescence was measured every 1 min for 2 hours in a spectrophotometer (Varian, Agilent Inc., Santa Clara, CA, U.S.A). The excitation was set to 680 nm and emission spectra were recorded between 690 and 720 nm. The initial reaction rate v0 was defined as the slope of a linear curve fitted through the peak fluorescence intensity vs. time data of the first 20 min. The fluorescence of completely cleaved probe was used to convert fluorescent units into moles. Next, for each investigated MMP, a linear curve was fitted through the v_0 vs. [S] data, with [S] being the probe concentrations (0.125, 0.25, 0.5, 1 and 2 pM). Due to the relation $v_0 = (k_{cat} * [E] * [S])/(K_M + [S])$ and assuming $[S] << K_M$ it follows that $v_0 = (k_{cat}/K_M) * [E] * [S])$ (with [E] = 5 nM of the investigated MMP). Thus, K_{cat}/K_M can be calculated from the slope of this linear curve. All curve fitting was performed in Matlab (Mathworks Inc., Natick, MA, U.S.A)

To determine how well the fluorescent probe determines active MMP-13 levels in vitro in fluids as compared to ELISA, a range of nominal active MMP-13 concentrations (3600, 2880, 2160, 1440, 720, 360, 72, 36, 7.2 and 0 pM, n = 3/concentration) were assessed using the probe and ELISA specific for active, human MMP-13 (MD Bioproducts, Egg b. Zrich, Switzerland).

5.2.4 OA chondrocyte cell culture

Human OA chondrocytes were expanded at 5000 cells/cm^2 in monolayer in two passages in DMEM (4.5 g/L glucose, 25 mM HEPES, 1 mM sodium pyruvate, Gibco, Breda, The Netherlands) with 1% penicillin/streptomycin, 10% fetal bovine serum (FBS, Lonza, Verviers, Belgium), and 10 ng/mL basic fibroblast growth factor (bFGF, Peprotech). At 80% confluency, cells were trypsinized and after two passages, OA chondrocytes were seeded into agarose constructs. Cells were washed twice in phosphate-buffered-saline (PBS), trypsinized and counted. 6 x 10^6 cells were then re-suspended in 1 ml DMEM with 1% penicillin/streptomycin and 10% FBS. After centrifuging (7 min, 250 g), the cell pellet was mixed with 2.5% w/v agarose in PBS. Of this agarose-cell mix, 160 μl was cast into a 96-wells plate and allowed to polymerize for 5 min at room temperature (1 x 106 cells/construct). Cell-laden constructs were then transferred into a 6-well plate using a metal spatula. A total of 25 constructs was prepared and cultured in an incubator (37 C, 5% CO_2 and 95% humidity) for 1 week in 6 ml re-differentiation medium. Re-differentiation medium was prepared by adding 5 ng/ml transforming growth factor beta 2 (TGF-beta 2, Peprotech) to basal medium comprising DMEM (4.5 g/L glucose, 25 mM HEPES, 1 mM sodium pyruvate) with 1% penicillin/streptomycin, 2% v/v human serum albumin (Sanquin, Amsterdam, The Netherlands), 2% v/v Insulin-Transferrin-Selenium-Ethanolamine (ITS-X, Gibco) and

ascorbate acid-2-phosphate (50 ug/ml, Sigma-Aldrich). After re-differentiation, five different culture conditions were defined by adding to basal medium 1) no additions (basal medium) 2) interleukin-1beta (IL-1, 10 ng/ml, Peprotech) + phorbol-myristate-acetate (PMA, 100 nM, Abcam, Cambridge, UK) 3) IL-1 (10 ng/ml)) + PMA (100 nM) + specific MMP-13 inhibitor WAY 170523 (1 μM, RD Systems, Minneapolis, MN, U.S.A) 4) IL-1 (10 ng/ml)) + PMA (100 nM) + broad range MMP inhibitor Marimastat (10 μM, Sigma-Aldrich) and 5) IL-1 (10 ng/ml)) + PMA (100 nM) + aspartate, cysteine and serine proteinase inhibitor cocktail consisting of: pepstatin (1 μM) + leupeptin (100 μM) + E-64 (10 μM, all Enzo LifeSciences, Farmingdale, NY, U.S.A.). Per culture condition, five cell-laden agarose constructs (n = 5/condition) were cultured for another 4 days.

After culture, active MMP-13 levels inside the constructs were non-destructively evaluated using the novel fluorescent probe. First, cultured constructs were transferred into a 96-well plate using a metal spatula. Next, in the same plate, agarose constructs (2% w/v, 160 μl) with known MMP-13 levels (10000, 5000, 2500, 1000, 500, 250, 100, 50, 25, 12.5, 6.25 and 0 pM, n = 3/concentration) were prepared by mixing active, recombinant, human MMP-13 diluted with agarose (3% w/v) in assay buffer at ratio 1:3 and allowing the mix to polymerize for 5 min at room temperature. Fluorescent probe (10 μM) was then added to the cell-laden constructs and agarose samples with known MMP-13 concentration and the fluorescence was recorded in a microplate reader (excitation filter: 670/10 nm and emission filter: 700/20 nm) every 5 min for 4 hours. A calibration curve was obtained using the fluorescence signal from the agarose constructs with known active MMP-13 levels. Subsequently, this calibration curve was utilized to calculate the concentration of active MMP-13 inside the cell-laden agarose samples. In parallel, active MMP-13 levels inside the media of the different culture groups were assessed using ELISA. Culture medium samples were added to the ELISA plate and samples for an ELISA calibration curve were prepared by serial dilutions of provided active MMP-13 standard (0, 0.66, 1.3, 2.6, 5.2, 10.41, 20.83 and 41.66 pM). After completion of the ELISA protocol, the resulting ELISA standard curve relating absorbance vs. active MMP-13 concentration was utilized to calculate the MMP-13 levels of culture media samples.

5.2.5 Statistical Analysis

The measured active MMP-13 levels in vitro in assay buffer were examined for significant differences using a two-way ANOVA. The two factors were defined as the method to assess MMP-13 concentration (fluorescent probe and ELISA) and the nominal active MMP-13 concentration. If no significant interaction effect was found, Tukey-HSD post-hoc testing was employed. To determine differences in active MMP-13 levels inside the cultured cell-laden agarose constructs, one-way ANOVA was performed followed by Bonferroni-corrected independent t-tests. To determine differences in active MMP-13 levels inside culture media, Kruskal-Wallis test was performed followed by Bonferroni corrected Mann-Whitney U tests. Statistical significance was assumed for $p < 0.05$. All statistical tests were performed using SPSS 18.0 (SPSS, Inc., www.spss.com).

5.3 Results

5.3.1 Activation of fluorescent probe and selectivity

A fluorescent probe was successfully synthesized by attaching a near-infrared fluorescence donor, Atto680, and a fluorescence quencher, BHQ3, to a peptide linker comprising the amino-acid sequence PLGMRG that functions as substrate to active MMP-13. When incubated with active MMP-13, both in vitro and in 3D agarose constructs, the newly synthesized fluorescent probe was rapidly cleaved leading to a strong increase in fluorescence emission (Fig. 5.3 A and B). The detected fluorescent signal linearly increased with increasing active MMP-13 concentrations. Moreover, when incubating probe and active MMP-13 longer (540 min), fluorescent signals from even very small MMP-13 levels were detectable demonstrating the potential of using the probe as assay for MMP-13 activity (Fig. 5.3 C and D).

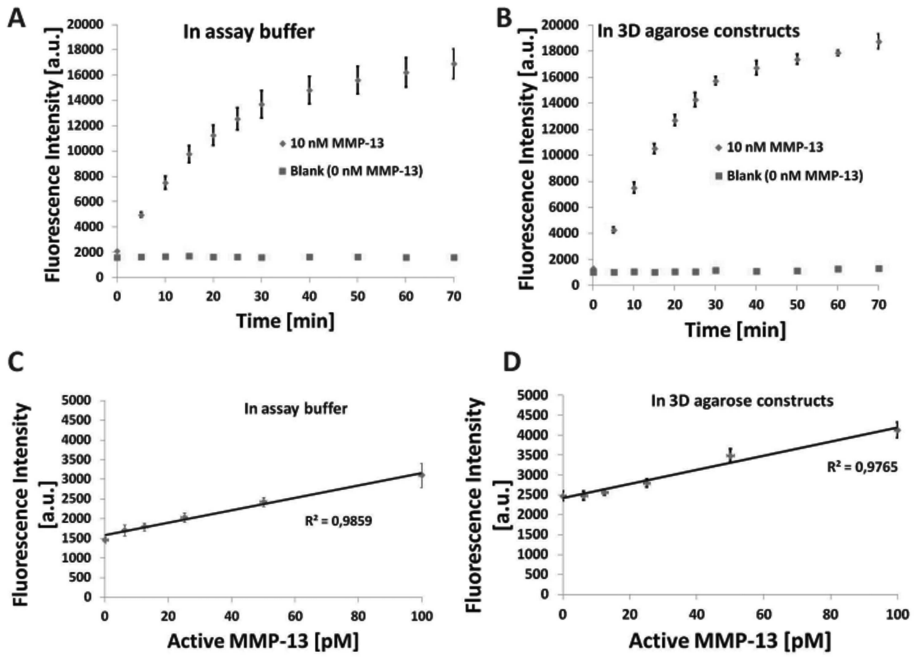

Figure 5.3: A) Change in fluorescence in vitro in assay buffer of fluorescent probe (10 μM) incubated with (blue dots) or without (red dots) active MMP-13 (10nM). B) Change in fluorescence of 3D agarose constructs loaded with (blue dots) or without (red dots) active MMP-13 (10 nM) and incubated with fluorescent probe (10 μM). C) Fluorescence intensities in vitro in assay buffer of fluorescent probe (10 μM) after incubating with different concentrations active MMP-13 (0, 6.25, 12.5, 25, 50 and 100 pM) for 540 min. Values are means $\pm$ standard deviations, n = 5. D) Fluorescence intensities of 3D agarose constructs loaded with different concentrations active MMP-13 (0, 6.25, 12.5, 25, 50 and 100 pM) and incubating with fluorescent probe (10 μM) for 540 min. Values are means $\pm$ standard deviations, n = 5.

Selectivity for MMP-13 activity as evaluated by K_{cat}/K_M was 4.7 $\text{min}^{-1}\mu\text{M}^{-1}$ and

therefore about 2x larger than for active MMP-2 (Table 5.1). Moreover, incubation of the probe with MMP-1, MMP-3 and MMP-7 resulted in a very low signal and thus very low K_{cat}/K_M values of 0.5 $\text{min}^{-1}\mu\text{M}^{-1}$, 0.4 $\text{min}^{-1}\mu\text{M}^{-1}$ and 0.6 $\text{min}^{-1}\mu\text{M}^{-1}$ further demonstrating the small sensitivity of the probe to other major MMPs.

Table 5.1: Fluorescent probe selectivity in vitro against active MMP-13 and other common active MMPs.

Enzyme	K_{cat}/K_M $[\mathbf{min}^{-1}\mu\mathbf{M}^{-1}]$
MMP-1	0.5
MMP-2	2.4
MMP-3	0.4
MMP-7	0.6
MMP-13	4.7

5.3.2 Probe as active MMP-13 assay in vitro and in 3D constructs

Performance of the fluorescent probe is given in Table 5.2. In vitro, the fluorescent probe assay showed very good linearity with R^2 greater than 0.98. Mean LOD was 6.5 pM and mean LOQ was 16 pM indicating that active MMP-13 can be evaluated in vitro down to the picomolar range. Assay precision was 20 % CV, 24 % CV and 43.4% CV in the high, mid and low assay range, thereby above the maximum 15% CV criterion for bio-analytical assays. Furthermore, in vitro accuracy was found to be excellent with 97%, 115% and 109% accuracy in the high, mid and low assay range and thus meeting the 100 ±15% accuracy requirement. In 3D constructs, similar performance characteristics were obtained. A fluorescent signal was detected from all agarose constructs containing known active MMP-13 levels and the assay showed good linearity with $\text{R}^2 = 0.97$. More importantly, mean LOD was 22 pM and mean LOQ was 35 pM demonstrating the potential of measuring active MMP-13 concentrations in the picomolar range in intact 3D constructs. Assay precision was 11% CV in the high assay range, better than in vitro and meeting the maximum 15% CV criterion for bio-analytical assays. In the mid assay range, precision was 25% CV, slightly less than in aqueous media only but not meeting the requirement. In the low assay range, precision was 173% CV indicating that in the low picomolar range, MMP-13 assessments are subjected to very large variations. Also, assay accuracy was slightly less than in aqueous media only. In the mid - and high assay range, in situ accuracy was 96% and 86% and therefore within the 100 ±15% requirement. In the low assay range, accuracy was 57% and therefore much lower than in aqueous media.

5.3.3 Comparison to ELISA

Measured active MMP-13 concentrations using the fluorescent probe and ELISA all matched well (Fig. 5.4). The obtained values show a clear gradient from 0 to 3600 pM with a significant effect of (the nominal) active MMP-13 level. More importantly, the fluorescent probe showed similar accuracy in determining active MMP-13

Table 5.2: Fluorescent probe assay performance results in vitro in aqueous media (assay buffer) and in 3D constructs. Precision and accuracy was calculated in high (100 pM), mid (25 pM) and low (6.25 pM) assay range.

Performance parameter	**In vitro**	**In 3D constructs**
Linearity	0.986 (R^2)	0.976 (R^2)
LOD	6.5 pM	22 pM
LOQ	16 pM	35 pM
Precision	20 % CV High 24 % CV Mid 43 % CV Low	11 % CV High 25 % CV Mid 173 % CV Low
Accuracy	97 % CV High 115 % CV Mid 109 % CV Low	96 % CV High 86 % CV Mid 57 % CV Low

concentrations in vitro as compared to the established ELISA technique. No significant differences in measuring MMP-13 levels over the range of nominal MMP-13 concentrations were found between the two methods. However, the individual set of active MMP-13 values obtained with the probe did not show significant differences for nominal concentrations below 72 pM, i.e. between 72 and 36 pM, 36 and 7.2 pM and 7.2 and 0 pM (Fig. 5.4 insert). In contrast, all active MMP-13 concentration values obtained with ELISA were significantly different from each other.

5.3.4 OA chondrocyte culture

Secreted MMP-13 levels as measured by ELISA in the culture media of cell-laden agarose constructs were rather low, ranging from 0.04 - 0.6 pM (Fig. 5.5). This is likely due to the utilized large volume (6 ml) of the culture media causing MMP-13 protein to be diluted. Still, determined active MMP-13 levels were within the ELISA detection range. In basal culture media, low active MMP-13 levels were determined indicating that OA chondrocytes produce low levels of MMP-13 in absence of pro-inflammatory stimuli. In contrast, IL-1 and PMA stimulation induced significantly higher active MMP-13 levels in the culture medium as compared to concentrations found in constructs without stimulation or in the presence of specific MMP-13 inhibitor WAY 170523 or broad-range MMP inhibitor Marimastat. Furthermore, the presence of aspartate, cysteine and serine protease inhibitors did not appear to influence active MMP-13 in constructs stimulated with IL-1 and PMA. Values were similar to those obtained from media samples of constructs cultured with IL-1 and PMA stimulation and significantly higher than in the other three groups. Instead, WAY 170523 or Marimastat significantly reduced active MMP-13 levels in the culture medium as compared to constructs that were stimulated but not supplemented with MMP inhibitors.

Active MMP-13 levels inside agarose constructs as evaluated using the fluorescent probe exhibited a different pattern than values determined by ELISA in corresponding culture conditions (Fig. 5.6). Active MMP-13 levels in intact constructs were much larger than in culture media ranging from 20,000 - 35,000 pM. Moreover, constructs cultured in basal medium already exhibited a strong fluorescent signal, suggesting high active MMP-13 concentration. Surprisingly, IL-1 and PMA stimulation did not result

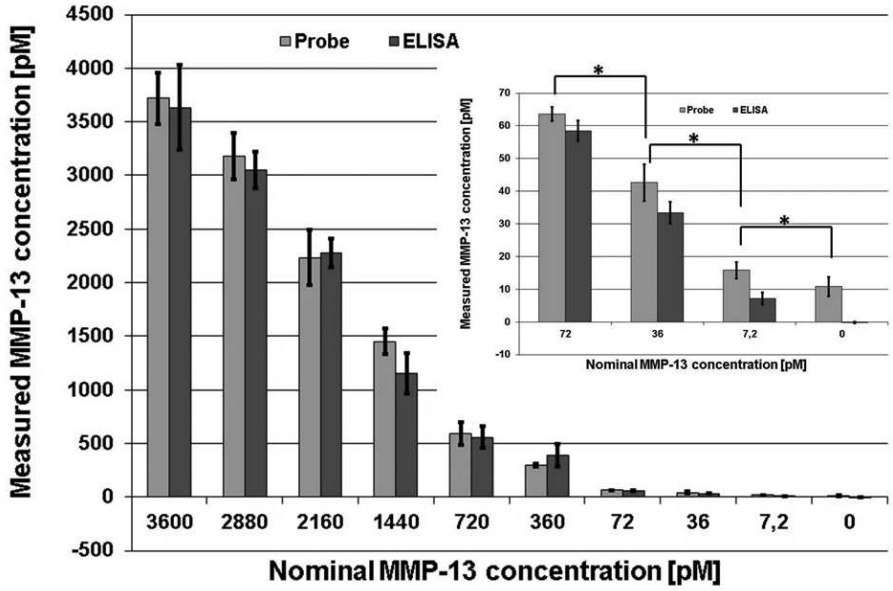

Figure 5.4: Measured active MMP-13 concentration as evaluated using two methods, fluorescent probe and ELISA, for ten different nominal active MM-13 levels. Figure insert highlights measured concentrations of 72 pM and below. Values are means ± standard deviations, n = 3. ∗ denotes $p > 0.05$ between determined MMP-13 levels as measured using fluorescent probe.

in significantly larger active MMP-13 levels inside constructs as compared to constructs cultured in basal medium or basal medium with inhibitors. Likewise, co-incubation with Marimastat or aspartate, cysteine and serine protease inhibitors had no effect on measured active MMP-13 levels. However, WAY 170523 significantly decreased active MMP-13 levels as compared to constructs cultured in medium with Marimastat. No other significant differences in measured active MMP-13 levels inside intact constructs were found.

5.4 Discussion

A novel fluorescent probe for non-destructively assaying active MMP-13 levels and activity was successfully synthesized. Similar to other probe designs, we chose to attach a near-infrared fluorescence donor, Atto680, and a fluorescence quencher, BHQ3, to a protein linker comprising the amino-acid sequence PLGMRG that functions as substrate to active MMP-13 (Deng et al., 2000). To fully validate this probe for use in a non-destructive assay for active MMP-13, assay characteristics including linearity, detection and quantification limits, precision and accuracy were obtained. Both in vitro and in 3D constructs, performance parameters largely met requirements for introducing novel bio-analytical assays (Table 5.2). The assay's detection limit

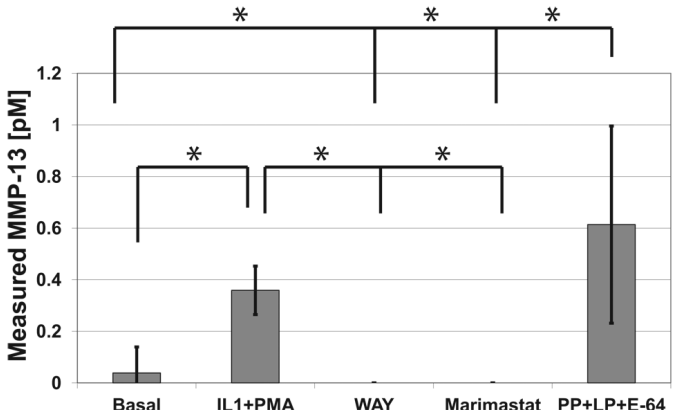

Figure 5.5: Measured active MMP-13 concentrations in culture media of cell laden agarose constructs as determined by ELISA. Constructs were cultured in media with different supplementation: 1) basal, i.e. no supplements 2) IL-1 + PMA 3) IL-1 + PMA + WAY 170523 (specific MMP-13 inhibitor) 4) IL-1 + PMA + Marimastat (broad range MMP inhibitor) 5) IL-1 + PMA + Pepstatin, Leupeptin and E-64 (aspartate, cysteine and serine protease inhibitors). Values are means ± standard deviations, n = 5. $*$ denotes $p < 0.05$ between determined MMP-13 levels as measured using ELISA.

was found to be in the picomolar range similar to that of the gold standard technique, i.e. ELISA, and therefore even small changes in active MMP-13 levels or activity may be detected without disintegrating samples. Furthermore, over a large range of concentrations in vitro, no significant differences in measuring active MMP-13 levels were found between the fluorescent probe and ELISA illustrating the good accuracy of this assay in detecting active MMP-13 concentrations (Fig. 5.4). Still, for active MMP-13 levels lower than 72 pM, ELISA remains the more accurate technique since the fluorescent probe did not succeed in distinguishing enzyme levels. The novel probe also exhibited good selectivity (Table 5.1) over other MMPs commonly found in (degenerated) cartilage and IVD tissue. Probe selectivity for active MMP-13 expressed as K_{cat}/K_M was 4.7 $\text{min}^{-1}\mu\text{M}^{-1}$ and therefore similar to the K_{cat}/K_M value of 4.46 $\text{min}^{-1}\mu\text{M}^{-1}$ reported by Lim et al. (2014) for their probe design. Only MMP-2 did show some cross-reactivity with our fluorescent probe, similar to other probe designs (Lee et al., 2008; Zhu et al., 2011), yet K_{cat}/K_M was about 2x larger for MMP-13.

As these initial results showed great potential for utilizing the novel probe as basis for a non-destructive assay for MMP-13 activity, the feasibility of measuring cell-produced MMP-13 levels using the fluorescent probe was evaluated. Human OA chondrocytes were seeded into 3D agarose constructs and samples were cultured in medium with different supplements. After culture, active MMP-13 levels inside the constructs were assessed using the probe, whereas active MMP-13 leaked from the constructs into the culture medium was evaluated using ELISA. As expected, ELISA measurements showed that IL-1+PMA significantly increased MMP-13 production while constructs cultured without IL-1 and PMA stimulation exhibited rather low levels of active MMP-13 in their medium (Fig. 5.5). Likely, OA chondrocytes produce these basal MMP-13 levels since cells were obtained from OA cartilage and therefore cells may be pre-conditioned to generate catabolic enzymes including MMP-13 (Tardif et al.,

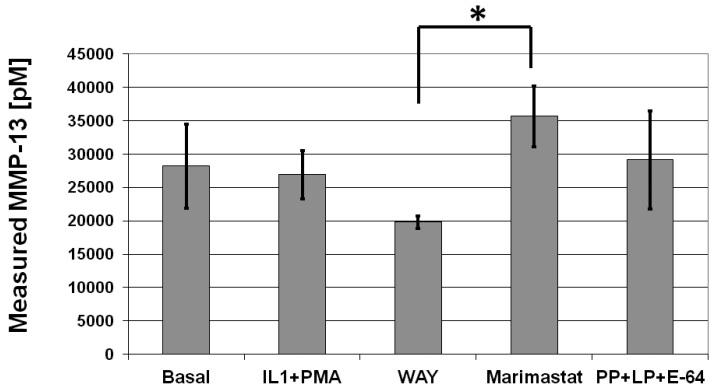

Figure 5.6: Active MMP-13 concentrations inside cell laden agarose constructs as determined by fluorescent probe. Constructs were cultured in media with different supplementation: 1) basal, i.e. no supplements 2) IL-1 + PMA 3) IL-1 + PMA + WAY 170523 (specific MMP-13 inhibitor) 4) IL-1 + PMA + Marimastat (broad range MMP inhibitor) 5) IL-1 + PMA + Pepstatin, Leupeptin and E-64 (aspartate cysteine and serine protease inhibitors). Values are means +/- standard deviations, n = 5. $*$ denotes $p < 0.05$ between determined MMP-13 levels as measured using fluorescent probe.

1999). Surprisingly, addition of both specific MMP-13 inhibitor WAY 170523 and the broad-range MMP inhibitor Marimastat resulted in complete loss of active MMP-13 as determined by ELISA. This is rather counterintuitive as ELISAs are thought to be specific for an enzyme form (either latent or active) and not sensitive to enzyme activity. The utilized inhibitors were expected to inhibit the (catalytic) activity of active MMP-13 but not its production or activation and consequently the ELISA should have detected the same active MMP-13 levels in samples cultured with or without inhibitors. Broad range MMP inhibitor Marimastat is a pseudopeptide compound mimicking the structure of collagen and inhibiting MMP activity by binding at the active site and chelating the zinc atom (Engel et al., 2005). As the catalytic domains of all MMPs are highly homologous with sequence similarities in the range 50-88% (Engel et al., 2005) MMP-13 specific inhibitors such as WAY 170523 do not bind at the active site and chelate the catalytic zinc. Instead, they bind into the so-called S1' pocket, a relatively large and hydrophobic groove within the 3D enzyme structure and presumably unique to MMP-13 (Engel et al., 2005). Potentially, binding of WAY 170523 and Marimastat to MMP-13 may have induced some conformational change in the enzyme that could have affected the ELISA's ability to detect (active) MMP-13. However, since it is unknown which exact part of enzyme is recognized by the antibody of the ELISA, it remains speculative whether inhibitor binding influenced ELISA assessments.

While our ELISA measurements support our hypothesis that IL-1+PMA stimulation leads to increased levels of active MMP-13 and that both WAY 170523 and Marimastat significantly inhibit MMP-13 activity (Fig. 5.5), this was not confirmed by MMP-13 activity assessment using the fluorescent probe (Fig. 5.6). No significant differences in measured active MMP-13 levels inside constructs were found between samples receiving no stimulation or IL-1+PMA stimulation. Surprisingly, nether WAY 170523 nor Marimastat had a significant effect on active MMP-13 levels as compared to samples

cultured without. Here, OA chondrocytes in agarose constructs were cultured in media containing both potent stimulators of MMP-13 production, i.e. IL-1 and PMA (Tardif et al., 1999), and specific MMP-13 inhibitor WAY 170523 or Marimastat, a non-specific MMP inhibitor. WAY 170523 is known to selectively inhibit MMP-13 activity (Engel et al., 2005), whereas Marimastat efficiently inhibits the activity of a broad-range of MMPs including MMP-13 (Folgueras et al., 2004). We had hypothesized that cells would be strongly stimulated to generate (active) MMP-13, yet WAY 170523 and Marimastat would efficiently inhibit any proteolytic activity of MMP-13 and in the case of Marimastat also of other produced MMPs. Hence, measured active MMP-13 levels as evaluated using our fluorescent probe should have been minimal as MMP-modulated probe cleavage would hardly occur. Instead, results show that the probe is cleaved upon incubation with cell-laden agarose constructs cultured in media with either WAY 170523 or Marimastat leading to the high measured MMP-13 levels (Fig. 5.6). The measured high active MMP-13 levels of all cell-laden agarose samples and the ineffectiveness known MMP-13 inhibitors could be due to several causes, e.g. non-functional inhibitors, ineffective inhibitor concentrations and probe cleavage resulting from some other unknown effect or enzyme. Marimastat functionality was, however, confirmed by incubating active MMP-13 with this compound and fluorescent probe in solution and in 3D agar constructs (without cells) resulting in no detectable fluorescent signal (data not shown). Furthermore, WAY 170523 and Marimastat concentration of 1 μM and 10 μM was well above levels commonly known to efficiently inhibit MMP-13 and a variety of other MMPs, respectively (Rasmussen and McCann, 1997). Thus, although selectivity measurements showed that the fluorescent probe is also cleaved by other MMPs (Table 5.2), Marimastat concentration was likely large enough to efficiently suppress any MMP activity and consequently probe cleavage by (other) MMPs. Taken together, it is therefore unlikely that the detected large active MMP-13 concentrations of agarose constructs cultured in media with MMP inhibitors are due to non-functional inhibitors, too low inhibitor levels or probe cleavage by other MMPs.

Possibly, OA cells produce some enzyme other than active MMP-13 and/or other MMPs capable of cleaving our newly synthesized fluorescent probe. One potential source of undesired probe cleavage may be enzymes such as aspartate, cysteine or serine proteases (Troeberg and Nagase, 2012). However, fluorescent probe measurements on intact agarose constructs cultured with a protease inhibitor cocktail exhibited the same fluorescence signal as constructs cultured without (Fig. 5.6). Moreover, inhibiting aspartate, cysteine and serine proteases had no effect on active MMP-13 levels as demonstrated by ELISA (Fig. 5.5). In fact, determined levels were as large as MMP-13 concentrations found in samples stimulated with IL-1+PMA. Therefore, aspartate, cysteine or serine proteases are unlikely candidates for causing the undesired probe cleavage. One other potential source for undesired or non-specific cleavage of the fluorescent probe that may explain our results are lysosomal enzymes. These enzymes can break down virtually any biomolecule and may be secreted upon cell necrosis (Boya and Kroemer, 2008). In our study, cell-laden constructs were transferred from a 6-well plate to a 96-well plate prior to adding fluorescent probe for assessing MMP-13 levels. Potentially, OA chondrocytes in agarose constructs undergo necrosis during this process as cells are not supplied with culture medium and thus nutrients. However, the process of transferring constructs from well-plate to well-plate takes only a few minutes and upon addition of fluorescent probe, a strong signal is immediately detected in all experimental groups. It is highly unlikely that within this short time window massive

cell necrosis took place and consequently the detected fluorescence is probably caused by some agent other than lysosomal enzymes. Recently, Zhu et al. (2014) also reported on the non-specific cleavage of a fluorescent probe designed for measuring MMP-13 activity. Similar to our probe, their design comprised a near-infrared fluorescence donor, Cy 5.5, a fluorescence quencher, BHQ3 and the amino-acid sequence PLGVRG as MMP-13 substrate (Zhu et al., 2011, 2014). When in-vivo profiling the probe metabolites, i.e. the probe fragments after presumably MMP-13 cleavage, suggested that the protein linker of their probe consisted of two cleavage sites, a specific MMP cleavage site and a non-specific site. Since our fluorescent probe comprises a protein linker with a very similar amino-acid sequence, it is also possible that our probe similarly carries a specific and non-specific cleavage site. However, since Zhu et al. (2014) did not further investigate the mechanism underlying the non-specific cleavage of their probe, it remains speculative which enzyme other than MMPs is capable of catabolizing fluorescent probes such as the probe developed in this study.

The results of this study may have some wider implications. Various research groups reported on the successful development of fluorescent probes for both in vitro and in vivo measurements of MMP-13 activity (Lee et al., 2008; Zhu et al., 2011; Lim et al., 2014). Based on the well-known substrate for MMP-13, both Lee et al. (2008), Zhu et al. (2011) and Lim et al. (2014) chose to incorporate the amino-acid sequence PLGMRG or a slightly modified version into their MMP-13 specific peptide linker of their fluorescent probes. However, the results of this study and the findings of Zhu et al. (2014) suggest that probes comprising this particular amino-acid sequence may be subjected to non-specific cleavage. Furthermore, our results indicate that this non-specific cleavage is due to enzymes other than MMPs and/or aspartate, cysteine and serine proteases. Previous studies generally characterized fluorescent probes in vitro using (recombinant) MMPs including MMP-13 followed by administering probes into tissue/animal models to demonstrate the feasibility for MMP-13 measurements in vivo. Since our results indicate non-specific cleavage of our fluorescent probe by some cell-produced agent, this raises concerns whether the reported fluorescence of very similar probes in vivo is in fact due to MMP-13 presence and activity or whether other cellular agents caused probe cleavage. Moreover, in this report, the newly synthesized fluorescent probe was rigorously characterized in vitro and in 3D OA chondrocyte culture. Instead, other studies often directly performed in vivo measurements in animal/tissue models after characterizing their probes using recombinant MMPs only (Lee et al., 2008; Zhu et al., 2011; Lim et al., 2014) and therefore non-specific probe cleavage may have been overlooked. Therefore, future studies may want to include (3D) cell culture experiments for better characterizing the suitability of fluorescent probes for MMP-13 activity assessments. Cell culture studies may also allow a more controlled environment without interference of pre-existing conditions and less potential agents causing undesired probe cleavage. This may significantly help in the quest of determining the underlying mechanism causing the observed cleavage and therefore contribute to improving future probe designs for MMP-13 activity assessments.

In summary, a novel fluorescent probe for non-destructively assaying MMP-13 activity was successfully synthesized and rigorously characterized. In vitro and 3D assay parameters such as accuracy and precision comply with guidelines for bio-analytical assays and the fluorescent probe detection limit is similar to that of the gold standard technique, i.e. ELISA. Moreover, no significant differences in measuring active MMP-13 levels in vitro were found between the novel probe and ELISA indicating the good accuracy in vitro of this novel MMP-13 assay. However, while measurements in

vitro aqueous media demonstrated the selectivity of this novel fluorescent probe for active MMP-13, results from 3D OA chondrocyte culture indicate that the probe may be subjected to non-specific cleavage and therefore selectivity is lost. Since other fluorescent probes exhibit a very similar design, these results may raise concerns regarding the feasibility of measuring cell-produced MMP-13 utilizing such probes and may therefore prompt the re-evaluation of current probe designs.

Chapter 6

General Discussion

6.1 Main findings

The general objective of this thesis was to introduce and apply novel strategies for monitoring IVD regeneration and degeneration. As IVD degeneration is a multifactorial disease, a wide array of both structural and biochemical alterations characterize degenerated IVDs and different (potential) strategies exist to target and monitor biomarkers of disc degeneration. Typical biomarkers include (decreased) cell viability (CV), (increased) catabolic enzyme levels and activity and changes to the disc's collagen network. Concomitantly, these biomarkers of IVD degeneration may represent interesting parameters for monitoring and evaluating the effects of different regenerative therapies on (degenerated) IVDs. Thus, we focused on developing and applying techniques to detect and monitor parameters of disc homeostasis that constitute biomarkers for evaluating disc regeneration and (early) degeneration.

In a first study, we sought to determine the potential of non-invasively assessing CV using cellular auto-fluorescence. Current CV assays are rather invasive as they require potentially harmful dyes and in some cases even the disintegration of scaffold/tissue prior to quantifying living and dead cells (Gantenbein-Ritter et al., 2008). Recent studies showed that the metabolic state of living cells can be non-destructively probed by measuring cellular auto-fluorescence originating from endogenous proteins, i.e. nicotinamide adenine dinucleotide (NADH) and flavoproteins (FPs) (Rocheleau et al., 2004; Tiede et al., 2007; Heikal, 2010). Consequently, researchers exploited this intrinsic cellular property to visualize and/or determine different metabolic states of living cells, e.g. by determining different cellular reduction-oxidation (redox) states (Quesada et al., 2006; Skala et al., 2007). In chapter 2, we demonstrate that also live and dead cells can be discriminated by measuring their auto-fluorescence using advanced microscopy tools. Mixtures of live and dead C2C12 myoblasts were prepared and CV was determined before seeding cells into collagen carriers using the trypan blue assay. Both two-photon and confocal microscopy images of the cell seeded collagen gels were acquired and the cellular auto-fluorescence emission was analyzed. Live and dead cells systematically emitted auto-fluorescent light with different spectral characteristics. Based on these spectral differences, cells were classified as viable or dead. Since no dyes were required to stain cells, CV could be determined without disintegrating the constructs resulting in an accurate and non-invasive CV assessment.

To become a useful technique for longitudinally evaluating the effects of regenerative stimuli on CV in pre-clinical or even clinical settings, monitoring cellular auto-fluorescence must first prove its applicability in mature tissue containing a dense extracellular matrix. Recording auto-fluorescent light in such tissues may be considerably more difficult due to increased light scattering (Durr et al., 2011), interfering collagen auto-fluorescence (Hoell et al., 2006) and low metabolic activity of IVD cells (Gruber et al., 2012). Therefore, in chapter 3, we assessed the feasibility and accuracy of measuring CV using this novel assay in an IVD explant model that better resembles the IVD in-vivo environment (van Dijk et al., 2011). First, we characterized the auto-fluorescence emission of (bovine) nucleus pulposus (NP) cells seeded into collagen gels. Similar to our previous study (chapter 2) employing myoblasts, living and dead NP cells exhibited distinct spectral differences in their auto-fluorescence emission. Live NP cells emitted mainly blue fluorescent light, whereas dead NP cells showed predominantly green auto-fluorescence. Subsequently, (bovine) NP explants were isolated and cultured for 6 days in media with different glucose supplementation

to induce different degrees of cell death. After culture, samples were split and CV was assessed using conventional staining and auto-fluorescence measurements using two-photon microscopy. The obtained CV values were not significantly different from each other indicating that viability assessments using cellular auto-fluorescence are not limited to 3D constructs. In fact, CV can be non-invasively and accurately assessed even in highly light scattering NP tissue in-situ containing low metabolically active live cells and dead cells.

A second biomarker relevant for potentially detecting early IVD degeneration and monitoring regeneration is the organization of the disc's collagen network. Healthy IVDs consist of a specific, spatially heterogeneous collagen fiber orientation in the annulus fibrosus (AF) (Cassidy et al., 1989). Mean fiber angle is $\pm\ 30^o$ with respect to the transverse plane of the spine (Cassidy et al., 1989; Marchand and Ahmed, 1990; Holzapfel et al., 2005). However, this mean fiber orientation varies both in radial direction (disc periphery to center) and circumferentially (from anterior to posterior location) (Cassidy et al., 1989; Holzapfel et al., 2005). While it is well established that severely degenerated IVDs suffer from dramatic changes to their collagen network (Urban and Roberts, 2003; Videman and Nurminen, 2004; Vernon-Roberts et al., 2007), less is known about effects of degeneration on the tissue architecture in moderately degenerated discs. Therefore, in chapter 4, we hypothesized that degeneration also affects the collagen fiber organization of moderately degenerated human IVDs and quantified the AF collagen orientation using advanced optical microscopy, i.e. Second Harmonic Generation (SHG) microscopy, with subsequent image analysis. Results indicate that moderately degenerated human discs are characterized by a spatially homogeneous collagen fiber orientation. Mean collagen orientation did not change strongly in radial or in circumferential direction supporting the hypothesis that the disc tissue architecture is affected during (early) degeneration. As the mechanical properties of the AF and consequently of the entire disc depend on the collagen fiber organization (Holzapfel et al., 2005; Guerin and Elliott, 2006; Noailly et al., 2011), these findings support the hypothesis that moderately degenerated discs are subject to an altered mechano-biological environment which in its turn may induce more or accelerate degenerative changes in the IVD (Urban and Roberts, 2003; Adams and Roughley, 2006).

Finally, in chapter 5, we describe the development and characterization of a novel-fluorescent probe for detecting and monitoring matrix metalloproteinase 13 (MMP-13) activity, a catabolic enzyme involved in IVD degeneration (Vo et al., 2013). Both levels and activities of MMP-13 are rather low or negligible in the normal steady-state, however during IVD degeneration increased or unbalanced levels and activities of MMP-13 are widely thought to mediate disc matrix breakdown particularly in the NP (Maitre et al., 2004; Bachmeier et al., 2009; Vo et al., 2013). Recently, fluorescent probes have been developed for non-destructively measuring MMP-13 levels and activity in vivo (Lee et al., 2008; Zhu et al., 2011; Lim et al., 2014), yet concerns exist regarding the selectivity against MMP-13 of the method (Zhu et al., 2014) and how probes perform as compared to traditional (destructive) techniques, e.g. ELISA. Therefore, based on existing probe designs, a novel probe was synthesized consisting of a peptide linker that functions as a specific substrate to MMP-13 and a fluorescence donor and quencher. In the absence of active MMP-13, no fluorescent light is emitted since the energy of the donor is transferred to the quencher by fluorescence resonance energy transfer. When the peptide linker is cleaved by active MMP-13, the fluorescence donor separates from the quencher and, therefore, the energy transfer from donor to quencher

seizes resulting in a detectable fluorescence signal. Probe performance parameters of measuring active MMP-13 in vitro and in situ largely complied with relevant guidelines and fluorescent probe detection limit is similar to that of the gold standard technique, i.e. ELISA. Moreover, no significant differences in measuring active MMP-13 levels in vitro were found between the novel probe and ELISA indicating the good accuracy of this novel method for assaying active MMP-13. However, while in vitro measurements demonstrated the selectivity of the fluorescent probe for active MMP-13, results from 3D cell culture indicate that the probe may be subjected to non-specific cleavage and therefore selectivity is lost. Since other fluorescent probes exhibit a very similar design (Lee et al., 2008; Zhu et al., 2011; Lim et al., 2014), these results may raise concerns regarding the feasibility of measuring cell-produced MMP-13 utilizing such probes and may therefore prompt the re-evaluation of current probe designs.

6.2 Limitations

6.2.1 Cell viability

Choosing the appropriate method/assay for measuring CV depends on several factors including the experimental design, the research question, time, infrastructure and costs. In chapters 2 and 3, a novel CV assay based on (differences in) cellular auto-fluorescence was introduced and evaluated. This technique combines accuracy in measuring CV with being non-invasive, i.e. no dyes are required to stain cells and samples may be repeatedly and non-destructively assessed. However, while this certainly represents a strong advantage as compared to conventional CV methods, there are some major disadvantages related to the applicability and (daily) usage of this novel technique. Established viability assays such as the trypan blue method and Calcein-AM/Propidium Iodide staining are advantageous to monitoring cellular auto-fluorescence in terms of simplicity, needed infrastructure, and required lab time. Aside from specialized equipment, i.e. a two-photon microscope with a spectral detector, the cell auto-fluorescence assay requires fluorescence emission spectra of cells to be obtained for characterizing the emitted auto-fluorescent light and classifying cells as dead or alive. Accurate determination of these reference spectra is essential, since various cell types may be present in tissues and intracellular contents of endogenous fluorophores may vary between cell types and species. Furthermore, a representative cell population from different regions within the sample needs to be visualized for obtaining accurate CV assessment and to avoid overlooking zones of for instance accumulated cell death. This increases lab time and thus costs, especially when the microscopy image acquisition and processing is not automated. Therefore, we do not envision cellular auto-fluorescence measurements replacing conventional CV assays. Albeit being rather invasive, traditional CV assays allow for a (relatively) fast and accurate CV assessment (Gantenbein-Ritter et al., 2008) that will satisfy the demands of many researchers. Instead, monitoring auto-fluorescence constitutes a complementary technique that will likely be utilized in situations when conventional CV methods are not applicable. Examples include longitudinal CV measurements where viability is repeatedly determined over time and screening of cells or tissue-engineered constructs prior to transplantation.

6.2.2 Collagen orientation

In healthy IVDs, both the (tensile) properties and collagen fiber angles of AF tissue exhibit a specific spatial heterogeneity which essentially determines the mechanics of IVDs (Holzapfel et al., 2005). Using SHG microscopy and subsequent image analysis, we showed that this spatial heterogeneity is affected even in moderately degenerated human discs (chapter 4). However, these findings have to be interpreted with care as there are two major limitations of this study. First of all, our measurements of collagen fiber angles of moderately degenerated IVDs exhibited a rather large variance. This may raise concerns regarding the conclusion of this study, as the large variance may have blurred our results, A power analysis on the obtained angle values revealed that indeed more samples should have been analyzed to increase statistical power and thus confidence in our observations. However, studies on collagen angles of healthy IVDs employing larger sample sizes exhibited a variance similar to our findings (Holzapfel et al., 2005). Thus, such large sample sizes are indicative of the observed large variance in collagen fiber orientation of both healthy and moderately degenerated IVDs suggesting that this is an intrinsic property of AF tissue. Furthermore, SHG microscopy has been extensively used to visualize fibrillar collagens and their organization with the resolution and detail of standard histology (Zipfel et al., 2003). This also suggests that the observed large variance is of biological origin and not due to the chosen imaging technique, image processing method and sample size. A second major concern of this study is the absence of data on healthy disc tissue specimens. Measurements were performed solely on (moderately) degenerated IVDs and since this is the first study of its kind, no data exists in literature to directly compare our findings to. Applying the same methodology on healthy IVDs may have alleviated doubts regarding the usefulness and accuracy our methodology, i.e. SHG microscopy with subsequent image processing, in accurately determining collagen fiber orientations since data exists on the spatial distribution of collagen fiber angles within healthy AF tissues (Cassidy et al., 1989; Holzapfel et al., 2005). However, even if we had assessed the collagen orientation of healthy AF tissue using our approach, it remains speculative whether this would have led to more conclusive results. Direct comparison to the aforementioned studies is cumbersome, since differences in measurement methods, sample selection and locations to measure collagen orientations would make comparisons between studies rather complicated. Furthermore, in our study, a macroscopic grading system (Pfirrmann et al. (2001) grading) was used to classify IVDs as moderately degenerated (grade III). The studies of Cassidy et al. (1989) and Holzapfel et al. (2005) either used no or a different (histologic) grading system and therefore it is questionable whether results would be comparable at all. In summary, we believe that our findings, i.e. the presence of a spatially homogenous collagen orientation in moderately degenerated IVDs, are likely a real effect of tissue remodeling and not an artifact due to measuring too few samples and/or an inappropriate measurement technique.

6.2.3 Enzyme levels and activity

Traditionally, destructive methods have been employed to determine levels and activity of MMPs thought to be involved in IVD degeneration (Vo et al., 2013). Recently, peptide-based fluorescent probes have been developed for non-destructively monitoring MMP activity and thus, in chapter 5, we describe the development and characterization of such a probe for specifically assessing MMP-13 levels and activity. As the success of

this probe largely depends on its selectivity against MMP-13, we chose to incorporate the amino-acid sequence PLGVRG into our probe's peptide linker since this particular sequence is known to function as MMP-13 specific substrate (Deng et al., 2000). Not surprisingly, the probe exhibited good selectivity for MMP-13 in vitro and therefore corroborated results of similar probe designs (Lee et al., 2008; Zhu et al., 2011; Lim et al., 2014). However, when assessing cell-laden agarose constructs for MMP-13 levels using this novel fluorescent probe, we found that selectivity is lost. Our probe appears to be subjected to non-specific cleavage since even in the presence of a potent inhibitor of MMP-13 activity a strong fluorescence signal is detected. Apparently, cells produce some agent other than active MMP-13 capable of cleaving our newly synthesized fluorescent probe. Naturally, other MMPs would make prime suspects in causing this undesired probe cleavage as different MMPs are capable of breaking-down the same substrate (Visse and Nagase, 2003; Nagase et al., 2006). However, culturing cell-laden constructs in media containing the broad-range MMP inhibitor Marimastat and subsequently assessing constructs using our probe also resulted in a strong fluorescence signal. Marimastat functionality was confirmed in experiments in vitro and chosen Marimastat concentration of 10 μM was well above levels commonly known to efficiently inhibit MMP-13 and a variety of other MMPs, respectively (Rasmussen and McCann, 1997). Thus, it is unlikely that the observed non-specific probe is cleavage results from proteolytic activity of MMPs. Another potential source of undesired probe cleavage may be other enzymes such as cysteine or serine proteases (Troeberg and Nagase, 2012). However, fluorescent probe measurements on intact agarose constructs cultured in media supplemented with a cysteine and serine protease inhibitor cocktail exhibited the same fluorescence signal as constructs cultured in media with Marimastat supplementation. Agarose itself could have caused some unforeseen effect on the newly developed fluorescent probe, yet measurements on blank agarose constructs exhibited only background fluorescence excluding any influence of agarose. Taken together, these findings suggest that the observed non-specific cleavage of our novel fluorescent probe is due to probe cross-reactivity with some unknown agent or effect. Our results are supported by the findings of Zhu et al. (2014) who also reported on the non-specific cleavage of a fluorescent probe designed for measuring MMP-13 activity. Similar to our probe, their design comprised a near-infrared fluorescence donor, Cy 5.5, a fluorescence quencher, BHQ3 and the amino-acid sequence PLGVRG as MMP-13 substrate. However, in-vivo profiling the probe metabolites, i.e. the probe fragments after presumably MMP-13 cleavage, suggested that the protein linker of their probe consisted of two cleavage sites, a specific MMP cleavage site and a non-specific site (Zhu et al., 2014). Since our fluorescent probe comprises a protein linker with a very similar amino-acid sequence, it is straightforward to assume that also our probe carries a specific and non-specific cleavage site. However, since Zhu et al. (2014) did not further investigate the mechanism underlying the non-specific cleavage of their probe, it remains speculative which agent and/or effect is capable of catabolizing fluorescent probes such as the probe developed in this thesis. Therefore, more research is necessary to validate the suitability of current fluorescent probes and to potentially improve existing probe designs.

6.2.4 In vivo applicability

The clinical success of the developed and applied strategies in terms of monitoring regeneration and (early) detection of IVD degeneration in vivo will depend on whether

these techniques can be translated into clinics to evaluate patients. As far as the novel CV assay (chapter 2 and 3) and the method to evaluate collagen organization in the AF is concerned (chapter 4), advanced microscopy tools were applied that cannot be directly transferred into a clinical setting. Even in pre-clinical environments, a high numerical aperture objective was required to capture the weak auto-fluorescence emission for measuring CV (chapter 2 and 3). As the depth penetration of such an objective is limited to 280 μm, future in situ and in vivo applications using auto-fluorescence to assess CV will rely on employing either different objectives with larger depth penetration or endoscopic probes. In recent years, endoscopes equipped with optical fibers have been developed that can be utilized to record advanced microscopy images (Wu et al., 2009). Great advances have been made including compact and flexible endoscopic probes offering the potential to acquire two-photon microscopy images of unstained tissues and cellular auto-fluorescence in vivo (Rivera et al., 2011). This may ultimately lead to clinical tools allowing physicians to perform "optical biopsies" on degenerated IVDs and non-invasively assess their CV and collagen network in vivo. However, there are many challenges facing the development of such endoscopic probes. One main issue that needs to be addressed is whether these probes can be miniaturized enough to allow in vivo measurements of IVDs without causing (more) harm. There has been a lot of controversy regarding the safety of inserting "needles" during discography surgery into discs and whether puncturing leads to or accelerates IVD degeneration (Carragee et al., 2009; Michalek et al., 2010; Iatridis and Hecht, 2012; Lipscomb et al., 2014). Provocative discography involves inserting a 22 - 25 gauge needle into the IVD and injecting contrast medium to induce a pain response and thereby identifying the pain source, i.e. the disc (Carragee et al., 2009). Computational studies have shown that puncturing causes drastic changes in IVD biomechanics that may directly initiate degeneration or lead to progressive degenerative processes (Michalek et al., 2010; Lipscomb et al., 2014). In fact, needle puncture is an accepted experimental animal model of IVD degeneration (Masuda et al., 2005; Sobajima et al., 2005) and Carragee et al. (2009) found increased signs of degeneration in patients that underwent discography as compared to an untreated control group. Still, it is unclear to what extent these degenerative changes are caused by the actual needle puncture or by injecting contrast fluid that may be responsible for the deleterious effects (Gruber et al., 2012; Iatridis and Hecht, 2012). Finally, endoscopes may utilize optical fibers smaller in diameter than typical needles used during discography and thus avoid harmful effects.

Another issue potentially complicating in vivo measurements using our novel CV assay and SHG microscopy for evaluating the collagen network is the presence of interfering fluorescence and absorbance sources. Mature IVDs typically exhibit collagen auto-fluorescence particularly when irradiated with ultra-violet light sources (Hoell et al., 2006). Also, auto-fluorescent advanced glycation end products (AGEs) that accumulate with age in aggrecan and collagen (Meerwaldt et al., 2004; Sivan et al., 2006) may interfere with recordings of cellular auto-fluorescence. Likewise, blood is known to broadly absorb of fluorescence excitation signals and hence may complicate attempts to obtain measurements in vivo (Hoell et al., 2006). However, by tuning the laser light source to an appropriate wavelength, collagen auto-fluorescence signal in bovine NP explants was much weaker than the emission due to cellular sources, i.e. NADH and FPs (chapter 3). Furthermore, AGE fluorescence does largely not overlap cellular FP auto-fluorescence95 and cells were mainly classified as living or dead depending on (differences in) their FP signal. Finally, IVDs are largely

avascular (Roughley, 2004; Grunhagen et al., 2011) and two-photon microscopy utilizes near-infrared excitation (wavelengths 690-1060nm) that is less prone to undesired absorbance by blood (Helmchen and Denk, 2005).

6.2.5 Patient selection / time of intervention

Assuming that all issues regarding the in vivo applicability of the aforementioned techniques (cell auto-fluorescence, SHG microscopy and fluorescent probe) are solved one day, there is still a major concern with respect to time of intervention, i.e. at what point would one apply these methods to diagnose (painful) IVD degeneration in patients? Generally, people with acute low back pain recover rather quickly and only the about 10-15% of that develop chronic symptoms are given a more thorough investigation (Balague et al., 2012). Aside from the patient's history and physical examination, this may involve imaging techniques, e.g. MRI, to diagnose and monitor structural, degenerative changes to the IVD that presumably cause pain syndromes. However, as mentioned in the Introduction of this thesis (chapter 1), once patients suffer from (chronic) pain, diagnoses may be too late for preventative or regenerative interventions (Urban and Winlove, 2007; Emch and Modic, 2011). On the other hand, finding the appropriate moment to screen people for degenerative changes is extremely challenging since currently no criteria other than pain syndromes exist that would justify a diagnostic intervention. In other words, even if we did have improved and non-invasive diagnostic methods available in the clinic, we would still be oblivious as to when to use them since the etiology of disc degeneration is poorly understood and physicians will, for example, refuse to insert endoscopes for in vivo CV assessments without having strong indications. This dilemma of on the one hand the need for earlier diagnosis to have better treatment options, and on the other hand the plausible hesitation to use (improved) methods without having clear reasons represents a significant challenge. However, recent advances in genetics may help to better estimate one's risk of developing degenerated IVDs and thus justify diagnostic intervention even in the absence of pain syndromes. Genetic studies with twins have shown that heritability could be as high as 70% (Battie et al., 1995) and once candidate genes associated with disc degeneration have been identified, patients could be screened prior to developing symptoms similar to routine scans of people with high risk of developing breast cancer (Force, 2009). Still, searching for genetic determinants of disc degeneration is challenging and the information so far indicates that disc degeneration is complex and polygenic (Battie and Videman, 2006; Mayer et al., 2013). It likely involves multiple, interacting genetic and environmental determinants and therefore it is remains speculative whether clear (genetic) criteria will become available that may prompt diagnostic interventions.

6.3 Future directions

6.3.1 Cell auto-fluorescence

In chapters 2 and 3, a new method to accurately and non-invasively measure CV using cellular auto-fluorescence was introduced and evaluated. Results show that this technique allows CV assessments without staining or scaffold/tissue disintegration

and, therefore, represents a promising method for longitudinal viability measurements. However, actual longitudinal CV determinations were not performed since these studies focused on demonstrating the feasibility and accuracy of this novel CV assay. Clearly, to further demonstrate the potential and suitability of this technique, repeated measurements over time of CV in 3D constructs and in cultured disc explants are warranted. If successful, such longitudinal CV assessments would also alleviate any concerns regarding the safety or true non-invasive nature of utilizing two-photon microscopy to record cellular auto-fluorescence. While it is generally believed that this microscopy technique is less harmful than for instance confocal microscopy (Squirrell et al., 1999; Hellum et al., 2011) potential adverse effects of repeated laser irradiation on cells and tissues need to be investigated.

Virtually all cells are auto-fluorescent and therefore this novel CV assay may be applicable to other cell types as well (Ying, 2008; Heikal, 2010). However, for each individual cell type the auto-fluorescence emission of living and dead cells has to be thoroughly characterized. Furthermore, cell auto-fluorescence measurements are not limited to distinguishing merely live from dead cells. In fact, advanced microscopy tools have been successfully applied to assess the metabolic state of living cells by measuring differences in auto-fluorescence resulting from changes in cellular metabolic activity, i.e. different levels of NADH and FPs (Rocheleau et al., 2004; Quesada et al., 2006; Skala et al., 2007). Future investigations could therefore focus on determining different metabolic states of for example IVD cells. Likewise, different cell death mechanisms could potentially be identified using differences in cellular auto-fluorescence (Levitt et al., 2006). For instance apoptotic disc cells may emit auto-fluorescent light with different (spectral) characteristics as compared to necrotic IVD cells. Since one hallmark of IVD degeneration is a decreased cellularity due to apoptosis (Ding et al., 2013), distinguishing apoptotic from necrotic cells and monitoring them in unstained disc tissue may help in understanding the underlying mechanism of disc degenerative disease. This also counts for IVD cell senescence, another hallmark of disc degeneration (Roberts et al., 2006; Kepler et al., 2013). Senescence, or a cell's inability to replicate, is an inevitable part of cellular aging, yet studies indicate that this process is accelerated in degenerated IVDs (Roberts et al., 2006; Maitre et al., 2007). A common feature of cell senescence or aging is the accumulation of so-called lipofuscin (Yasuma et al., 1992). These lipid-protein aggregates are found in the cytoplasm of senescent cells and exhibit auto-fluorescence (Cho and Hwang, 2011). Therefore, measuring the relative contributions of NADH, FPs and lipofuscin to the total cellular auto-fluorescence signal, may provide an elegant technique to distinguish different cellular metabolic states, i.e. living, senescent, apoptotic and or/nectrotic. Finally, recent studies have demonstrated that cellular auto-fluorescence can be utilized to monitor stem cell differentiation (Quinn et al., 2012, 2013). This may be of high interest in both pre-clinical and clinical settings since the cell differentiation state can be non-invasively followed, e.g. to evaluate the fate and status of transplanted mesenchymal stem cells for IVD regeneration (Yoshikawa et al., 2010).

6.3.2 Collagen

From literature, it is known that the collagen orientation within healthy AF is heterogeneous (Cassidy et al., 1989; Marchand and Ahmed, 1990; Holzapfel et al., 2005), whereas our results suggest that moderately degenerated AF exhibit a spatially ho-

mogenous collagen fiber orientation (chapter 4). These changes in collagen network architecture during degeneration will have severe implications on disc mechanical behavior and potentially induce more, or accelerate, degenerative changes in the IVD as the biomechanical environment is known to directly influence disc cell metabolism (Fernando et al., 2011). For better understanding the (long-term) outcome of such fiber angle changes, future investigations could incorporate our findings in elaborate computational models describing a (moderately) degenerated disc. For instance Schroeder et al. (2006) describe a numerical model of the healthy IVD that also includes collagen fibers and their orientation. Since other model parameters such as biochemical content (water, proteoglycans, and collagen) are known for degenerated discs, the results of chapter 4 may be utilized for modeling a (moderately) degenerated IVD. If successful, this could help in elucidating the adverse biomechanical environment that cells inside degenerated discs are exposed to. In its turn, an improved understanding of the altered mechanics could help with increasing long-term success of regenerative approaches, since for example transplanted stem cells will be exposed to the same adverse environment that promoted degeneration in the first place.

Our findings on IVD collagen orientation could also be utilized in future (clinical) validation studies of advanced MRI techniques such as Diffusion Tensor Imaging and high-resolution MRI. These techniques have successfully been applied to measure the collagen organization of healthy IVDs (Hsu and Setton, 1999; Haughton, 2006). However, measurements were performed ex vivo in pre-clinical or animal MRI scanners employing large magnetic field strengths with 7T and more. Still, with more powerful clinical scanners on the horizon that exert similar large magnetic fields (Krug et al., 2009; Vossen et al., 2011), these advanced MRI methods may soon become readily available in the clinic.

Future pre-clinical investigations could also focus on using non-invasive SHG microscopy to evaluate and monitor the development of a collagen network for example in tissue engineered IVD replacements. Next to collagen and proteoglycan content, one of the key parameters in assessing the quality of an engineered construct is the collagen organization (Bowles et al., 2010). Since SHG microscopy can be applied onto unstained specimens, constructs could be repeatedly assessed enabling a longitudinal monitoring of the (developing) collagen network. Moreover, SHG microscopy can be combined with other (non-invasive) imaging modalities, e.g. to simultaneously image cells and collagen without adding dyes (Zoumi et al., 2002; Schenke-Layland et al., 2006). In this regard, one could non-invasively assess both CV (using cellular autofluorescence) and the collagen network by choosing appropriate excitation wavelengths and therefore improve quality control of engineered constructs prior to implantation. Also, the effect of different growth factors and other stimuli on the collagen content and architecture could be assessed utilizing SHG microscopy and thus possibly leading to improved regenerative therapies.

6.3.3 Enzyme levels and activity

Various research groups reported on the successful development of fluorescent probes for both in vitro and in vivo measurements of MMP-13 activity (Lee et al., 2008; Zhu et al., 2011; Lim et al., 2014). In chapter 5, we describe the development and rigorous characterization of a similar probe for measuring active MMP-13 levels and activity. In vitro using recombinant active MMP-13, probe performance exhibited

great promise as active MMP-13 levels could be assessed with similar accuracy as the gold standard technique, i.e. ELISA. However, when characterizing the fluorescent probe using cell-laden agarose constructs, probe performance was rather poor since results indicate that the probe is subject to non-specific cleavage. In other words, some cellular agent or process other than the target enzyme that is MMP-13 is capable of cleaving the probe and therefore probe selectivity is lost. Consequently, this finding seriously compromises any potential usage of the newly synthesized probe to monitor active MMP-13 levels and activity for instance in studies aiming to elucidate MMP-13 function and regulation during IVD degeneration and regeneration. Therefore, future investigations of this novel probe should focus on elucidating the agent or process responsible for the observed un-specific probe cleavage. In a first step, experiments employing 2D cell culture could be performed to stimulate active MMP-13 production and to analyze culture supernatants for (active) MMP-13 and other agents using established techniques such as western blotting, enzyme zymography and ELISA. This would significantly help in establishing which enzymes and agents are produced when OA chondrocytes are stimulated by IL-1 and PMA and therefore aid in identifying potential sources of non-specific fluorescent probe cleavage. Simultaneously, the process of probe cleavage, or more specifically which cleavage site(s) our probe comprises, must be thoroughly investigated. Zhu et al. (2014) utilized a liquid chromatography - mass spectroscopy approach to identify fragments after cleavage of a probe very similar to our probe design. They could demonstrate that their probe exhibited a MMP-13 specific and a non-specific cleavage site prompting them to re-design their fluorescent probe to increase selectivity against MMP-13. Thus, future investigations may want to focus on profiling probe fragments after cleavage to determine which kind(s) of cleavage site our probe comprises. Together with a thorough understanding of the enzymes/agents produced by IL-1 + PMA, this may help in determining whether our probe also requires re-designing or if different (physiological more relevant) experimental conditions should be chosen to characterize the probe.

Bibliography

Adams MA, Roughley PJ. 2006. What is intervertebral disc degeneration, and what causes it?. Spine (Phila Pa 1976.) 31:2151–2161.

Antoniou J, Steffen T, Nelson F, Winterbottom N, Hollander AP, Poole RA, Aebi M, Alini M. 1996. The human lumbar intervertebral disc: evidence for changes in the biosynthesis and denaturation of the extracellular matrix with growth, maturation, ageing, and degeneration. J.Clin.Invest 98:996–1003.

Appel AA, Anastasio MA, Larson JC, Brey EM. 2013. Imaging challenges in biomaterials and tissue engineering. Biomaterials 34:6615–6630.

Armbruster DA, Pry T. 2008. Limit of blank, limit of detection and limit of quantitation. Clin.Biochem.Rev. 29 Suppl 1:S49–S52.

Bachmeier BE, Nerlich A, Mittermaier N, Weiler C, Lumenta C, Wuertz K, Boos N. 2009. Matrix metalloproteinase expression levels suggest distinct enzyme roles during lumbar disc herniation and degeneration. Eur.Spine J. 18:1573–1586.

Bader AN, Pena AM, vanJohan V, Palero JA, Leroy F, Colonna A, Gerritsen HC. 2011. Fast nonlinear spectral microscopy of in vivo human skin. Biomed.Opt.Express 2:365–373.

Bae WC, Masuda K. 2011. Emerging technologies for molecular therapy for intervertebral disk degeneration. Orthop.Clin.North Am. 42:585–601, ix.

Balague F, Mannion AF, Pellise F, Cedraschi C. 2012. Non-specific low back pain. Lancet 379:482–491.

Battie MC, Videman T. 2006. Lumbar disc degeneration: epidemiology and genetics. J.Bone Joint Surg.Am. 88 Suppl 2:3–9.

Battie MC, Videman T, Gibbons LE, Fisher LD, Manninen H, Gill K. 1995. 1995 Volvo Award in clinical sciences. Determinants of lumbar disc degeneration. A study relating lifetime exposures and magnetic resonance imaging findings in identical twins. Spine (Phila Pa 1976.) 20:2601–2612.

Bibby SR, Jones DA, Ripley RM, Urban JP. 2005. Metabolism of the intervertebral disc: effects of low levels of oxygen, glucose, and pH on rates of energy metabolism of bovine nucleus pulposus cells. Spine (Phila Pa 1976.) 30:487–496.

Bibby SR, Urban JP. 2004. Effect of nutrient deprivation on the viability of intervertebral disc cells. Eur.Spine J. 13:695–701.

Blumenthal S, McAfee PC, Guyer RD, Hochschuler SH, Geisler FH, Holt RT, R. Garcia J, Regan JJ, Ohnmeiss DD. 2005. A prospective, randomized, multicenter Food and Drug Administration investigational device exemptions study of lumbar total disc replacement with the CHARITE artificial disc versus lumbar fusion: part I: evaluation of clinical outcomes. Spine (Phila Pa 1976.) 30:1565–1575.

Boden SD. 2002. Overview of the biology of lumbar spine fusion and principles for selecting a bone graft substitute. Spine (Phila Pa 1976.) 27:S26–S31.

Boos N, Weissbach S, Rohrbach H, Weiler C, Spratt KF, Nerlich AG. 2002. Classification of age-related changes in lumbar intervertebral discs: 2002 Volvo Award in basic science. Spine (Phila Pa 1976.) 27:2631–2644.

Bowles RD, Gebhard HH, Hartl R, Bonassar LJ. 2011. Tissue-engineered intervertebral discs produce new matrix, maintain disc height, and restore biomechanical function to the rodent spine. Proc.Natl.Acad.Sci.U.S.A 108:13106–13111.

Bowles RD, Williams RM, Zipfel WR, Bonassar LJ. 2010. Self-assembly of aligned tissue-engineered annulus fibrosus and intervertebral disc composite via collagen gel contraction. Tissue Eng Part A 16:1339–1348.

Boya P, Kroemer G. 2008. Lysosomal membrane permeabilization in cell death. Oncogene 27:6434–6451.

Brewer M, Utzinger U, Li Y, Atkinson EN, Satterfield W, Auersperg N, Richards-Kortum R, Follen M, Bast R. 2002. Fluorescence spectroscopy as a biomarker in a cell culture and in a nonhuman primate model for ovarian cancer chemopreventive agents. J.Biomed.Opt. 7:20–26.

Bron JL, Helder MN, Meisel HJ, Royen BJV, Smit TH. 2009. Repair, regenerative and supportive therapies of the annulus fibrosus: achievements and challenges. Eur.Spine J. 18:301–313.

Brox JI, Nygaard OP, Holm I, Keller A, Ingebrigtsen T, Reikeras O. 2010. Four-year follow-up of surgical versus non-surgical therapy for chronic low back pain. Ann.Rheum.Dis. 69:1643–1648.

Bruehlmann SB, Rattner JB, Matyas JR, Duncan NA. 2002. Regional variations in the cellular matrix of the annulus fibrosus of the intervertebral disc. J.Anat. 201:159–171.

Buckwalter JA. 1995. Aging and degeneration of the human intervertebral disc. Spine (Phila Pa 1976.) 20:1307–1314.

Carragee EJ, Don AS, Hurwitz EL, Cuellar JM, Carrino JA, Herzog R. 2009. 2009 ISSLS Prize Winner: Does discography cause accelerated progression of degeneration changes in the lumbar disc: a ten-year matched cohort study. Spine (Phila Pa 1976.) 34:2338–2345.

Cassidy JJ, Hiltner A, Baer E. 1989. Hierarchical structure of the intervertebral disc. Connect.Tissue Res. 23:75–88.

Chen J, Zhuo S, Luo T, Jiang X, Zhao J. 2006. Spectral characteristics of autofluorescence and second harmonic generation from ex vivo human skin induced by femtosecond laser and visible lasers. Scanning 28:319–326.

Chen R, Chen JY, Zhou LW. 2008. Metabolic patterns (NAD(P)H) in rat basophilic leukemia (RBL-2H3) cells and human hepatocellular carcinoma (Hep G2) cells with autofluorescence imaging. Ultrastruct.Pathol. 32:193–198.

Chen WL, Huang CH, Chiou LL, Chen TH, Huang YY, Jiang CC, Lee HS, Dong CY. 2010. Multiphoton imaging and quantitative analysis of collagen production by chondrogenic human mesenchymal stem cells cultured in chitosan scaffold. Tissue Eng Part C.Methods 16:913–920.

Chernyavskiy O, Vannucci L, Bianchini P, Difato F, Saieh M, Kubinova L. 2009. Imaging of mouse experimental melanoma in vivo and ex vivo by combination of confocal and nonlinear microscopy. Microsc.Res.Tech. 72:411–423.

Cho S, Hwang ES. 2011. Fluorescence-based detection and quantification of features of cellular senescence. Methods Cell Biol. 103:149–188.

Coric D, Mummaneni PV. 2008. Nucleus replacement technologies. J.Neurosurg.Spine 8:115–120.

, Ter Haar Romeny BMDaniels F RMvAH. 2006. Quantification of collagen orientation in 3D engineerd tissue .

Degroot J, Verzijl N, vanWijk MJW, Jacobs KM, Van EB, Roermund PMV, Bank RA, Bijlsma JW, TeKoppele JM, Lafeber FP. 2004. Accumulation of advanced glycation end products as a molecular mechanism for aging as a risk factor in osteoarthritis. Arthritis Rheum. 50:1207–1215.

Deng SJ, Bickett DM, Mitchell JL, Lambert MH, Blackburn RK, H. L. Carter I, Neugebauer J, Pahel G, Weiner MP, Moss ML. 2000. Substrate specificity of human collagenase 3 assessed using a phage-displayed peptide library. J.Biol.Chem. 275:31422–31427.

Ding F, Shao ZW, Xiong LM. 2013. Cell death in intervertebral disc degeneration. Apoptosis. 18:777–785.

Dittmar R, Potier E, van ZM, Ito K. 2012. Assessment of cell viability in three-dimensional scaffolds using cellular auto-fluorescence. Tissue Eng Part C.Methods 18:198–204.

Drezek R, Sokolov K, Utzinger U, Boiko I, Malpica A, Follen M, Richards-Kortum R. 2001. Understanding the contributions of NADH and collagen to cervical tissue fluorescence spectra: modeling, measurements, and implications. J.Biomed.Opt. 6:385–396.

Duance VC, Crean JK, Sims TJ, Avery N, Smith S, Menage J, Eisenstein SM, Roberts S. 1998. Changes in collagen cross-linking in degenerative disc disease and scoliosis. Spine (Phila Pa 1976.) 23:2545–2551.

Durr NJ, Weisspfennig CT, Holfeld BA, Ben-Yakar A. 2011. Maximum imaging depth of two-photon autofluorescence microscopy in epithelial tissues. J.Biomed.Opt. 16:026008.

Eijkelkamp MF, vanDonkelaar CC, Veldhuizen AG, vanHorn JR, Huyghe JM, Verkerke GJ. 2001. Requirements for an artificial intervertebral disc. Int.J.Artif.Organs 24:311–321.

Emch TM, Modic MT. 2011. Imaging of lumbar degenerative disk disease: history and current state. Skeletal Radiol. 40:1175–1189.

Eng J, Lynch RM, Balaban RS. 1989. Nicotinamide adenine dinucleotide fluorescence spectroscopy and imaging of isolated cardiac myocytes. Biophys.J. 55:621–630.

Engel CK, Pirard B, Schimanski S, Kirsch R, Habermann J, Klingler O, Schlotte V, Weithmann KU, Wendt KU. 2005. Structural basis for the highly selective inhibition of MMP-13. Chem.Biol. 12:181–189.

Fairbank J, Frost H, Wilson-MacDonald J, Yu LM, Barker K, Collins R. 2005. Randomised controlled trial to compare surgical stabilisation of the lumbar spine with an intensive rehabilitation programme for patients with chronic low back pain: the MRC spine stabilisation trial. BMJ 330:1233–.

Feng H, Danfelter M, Stromqvist B, Heinegard D. 2006. Extracellular matrix in disc degeneration. J.Bone Joint Surg.Am. 88 Suppl 2:25–29.

Fernando HN, Czamanski J, Yuan TY, Gu W, Salahadin A, Huang CY. 2011. Mechanical loading affects the energy metabolism of intervertebral disc cells. J.Orthop.Res. 29:1634–1641.

Finch P. 2006. Technology Insight: imaging of low back pain. Nat.Clin.Pract.Rheumatol. 2:554–561.

Folgueras AR, Pendas AM, Sanchez LM, Lopez-Otin C. 2004. Matrix metalloproteinases in cancer: from new functions to improved inhibition strategies. Int.J.Dev.Biol. 48:411–424.

Force UPST. 2009. Screening for Breast Cancer: U.S. Preventive Services Task Force Recommendation Statement. Annals of Internal Medicine 151(10):716–726.

Gantenbein-Ritter B, Potier E, Zeiter S, vander WM, Sprecher CM, Ito K. 2008. Accuracy of three techniques to determine cell viability in 3D tissues or scaffolds. Tissue Eng Part C.Methods 14:353–358.

Georgakoudi I, Jacobson BC, Muller MG, Sheets EE, Badizadegan K, Carr-Locke DL, Crum CP, Boone CW, Dasari RR, Van DJ, et al.. 2002. NAD(P)H and collagen as in vivo quantitative fluorescent biomarkers of epithelial precancerous changes. Cancer Res. 62:682–687.

Georgakoudi I, Levitt J, Baldwin A, Papadakis A, Munger K. 2005. Intrinsic fluorescence changes associated with apoptosis of human epithelial keratinocytes. Gynecol.Oncol. 99:S54–S57.

Ghazanfari S, Driessen-Mol A, Strijkers GJ, Kanters FM, Baaijens FP, Bouten CV. 2012. A comparative analysis of the collagen architecture in the carotid artery: second harmonic generation versus diffusion tensor imaging. Biochem.Biophys.Res.Commun. 426:54–58.

Ghukasyan VV, Kao FJ. 2009. Monitoring Cellular Metabolism with Fluorescence Lifetime of Reduced Nicotinamide Adenine Dinucleotide. Journal of Physical Chemistry C 113:11532–11540.

Grosberg LE, Radosevich AJ, Asfaha S, Wang TC, Hillman EM. 2011. Spectral characterization and unmixing of intrinsic contrast in intact normal and diseased gastric tissues using hyperspectral two-photon microscopy. PLoS.One. 6:e19925.

Gruber HE, A. L. Rhyne I, Hansen KJ, Phillips RC, Hoelscher GL, Ingram JA, Norton HJ, E. N. Hanley J. 2012. Deleterious effects of discography radiocontrast solution on human annulus cell in vitro: changes in cell viability, proliferation, and apoptosis in exposed cells. Spine J. 12:329–335.

Gruber HE, Watts JA, Riley FE, Fulkerson MB, Norton HJ, E. N. Hanley J. 2013. Mitochondrial Bioenergetics, Mass, and Morphology Are Altered in Cells of the Degenerating Human Annulus. J.Orthop.Res. .

Grunhagen T, Shirazi-Adl A, Fairbank JC, Urban JP. 2011. Intervertebral disk nutrition: a review of factors influencing concentrations of nutrients and metabolites. Orthop.Clin.North Am. 42:465–77, vii.

Guerin HA, Elliott DM. 2006. Degeneration affects the fiber reorientation of human annulus fibrosus under tensile load. J.Biomech. 39:1410–1418.

Halloran DO, Grad S, Stoddart M, Dockery P, Alini M, Pandit AS. 2008. An injectable cross-linked scaffold for nucleus pulposus regeneration. Biomaterials 29:438–447.

Haughton V. 2006. Imaging intervertebral disc degeneration. J.Bone Joint Surg.Am. 88 Suppl 2:15–20.

Heikal AA. 2010. Intracellular coenzymes as natural biomarkers for metabolic activities and mitochondrial anomalies. Biomark.Med. 4:241–263.

Hellum C, Johnsen LG, Storheim K, Nygaard OP, Brox JI, Rossvoll I, Ro M, Sandvik L, Grundnes O. 2011. Surgery with disc prosthesis versus rehabilitation in patients with low back pain and degenerative disc: two year follow-up of randomised study. BMJ 342:d2786–.

Helmchen F, Denk W. 2005. Deep tissue two-photon microscopy. Nat.Methods 2:932–940.

Hennings L, Kaufmann Y, Griffin R, Siegel E, Novak P, Corry P, Moros EG, Shafirstein G. 2009. Dead or alive? Autofluorescence distinguishes heat-fixed from viable cells. Int.J.Hyperthermia 25:355–363.

Hoell T, Huschak G, Beier A, Huttmann G, Minkus Y, Holzhausen HJ, Meisel HJ. 2006. Auto fluorescence of intervertebral disc tissue: a new diagnostic tool. Eur.Spine J. 15 Suppl 3:S345–S353.

Holzapfel GA, Schulze-Bauer CA, Feigl G, Regitnig P. 2005. Single lamellar mechanics of the human lumbar anulus fibrosus. Biomech.Model.Mechanobiol. 3:125–140.

Hsu EW, Setton LA. 1999. Diffusion tensor microscopy of the intervertebral disc anulus fibrosus. Magn Reson.Med. 41:992–999.

Huang S, Heikal AA, Webb WW. 2002. Two-photon fluorescence spectroscopy and microscopy of NAD(P)H and flavoprotein. Biophys.J. 82:2811–2825.

Hudson KD, Alimi M, Grunert P, Hartl R, Bonassar LJ. 2013. Recent advances in biological therapies for disc degeneration: tissue engineering of the annulus fibrosus, nucleus pulposus and whole intervertebral discs. Curr.Opin.Biotechnol. 24:872–879.

Iatridis JC, Hecht AC. 2012. Commentary: Does needle injection cause disc degeneration? News in the continuing debate regarding pathophysiology associated with intradiscal injections. Spine J. 12:336–338.

Iatridis JC, Nicoll SB, Michalek AJ, Walter BA, Gupta MS. 2013. Role of biomechanics in intervertebral disc degeneration and regenerative therapies: what needs repairing in the disc and what are promising biomaterials for its repair?. Spine J. 13:243–262.

K. K, H. S. 1994. Laser-induced autofluorescence for medical diagnosis. J.Fluoresc 4:17–40.

Kandel R, Roberts S, Urban JP. 2008. Tissue engineering and the intervertebral disc: the challenges. Eur.Spine J. 17 Suppl 4:480–491.

Kepler CK, Ponnappan RK, Tannoury CA, Risbud MV, Anderson DG. 2013. The molecular basis of intervertebral disc degeneration. Spine J. 13:318–330.

Kevorkian L, Young DA, Darrah C, Donell ST, Shepstone L, Porter S, Brockbank SM, Edwards DR, Parker AE, Clark IM. 2004. Expression profiling of metalloproteinases and their inhibitors in cartilage. Arthritis Rheum. 50:131–141.

Kierdaszuk B, Malak H, Gryczynski I, Callis P, Lakowicz JR. 1996. Fluorescence of reduced nicotinamides using one- and two-photon excitation. Biophys.Chem. 62:1–13.

Kirkpatrick ND, Zou C, Brewer MA, Brands WR, Drezek RA, Utzinger U. 2005. Endogenous fluorescence spectroscopy of cell suspensions for chemopreventive drug monitoring. Photochem.Photobiol. 81:125–134.

Krug R, Stehling C, Kelley DA, Majumdar S, Link TM. 2009. Imaging of the musculoskeletal system in vivo using ultra-high field magnetic resonance at 7 T. Invest Radiol. 44:613–618.

Kwan AC, Duff K, Gouras GK, Webb WW. 2009. Optical visualization of Alzheimer's pathology via multiphoton-excited intrinsic fluorescence and second harmonic generation. Opt.Express 17:3679–3689.

Lee S, Park K, Lee SY, Ryu JH, Park JW, Ahn HJ, Kwon IC, Youn IC, Kim K, Choi K. 2008. Dark quenched matrix metalloproteinase fluorogenic probe for imaging osteoarthritis development in vivo. Bioconjug.Chem. 19:1743–1747.

Leo BM, Li X, Balian G, Anderson DG. 2004. In vivo bioluminescent imaging of virus-mediated gene transfer and transduced cell transplantation in the intervertebral disc. Spine (Phila Pa 1976.) 29:838–844.

Levitt JM, Baldwin A, Papadakis A, Puri S, Xylas J, Munger K, Georgakoudi I. 2006. Intrinsic fluorescence and redox changes associated with apoptosis of primary human epithelial cells. J.Biomed.Opt. 11:064012–064014.

Li Q, Seeger S. 2010. Autofluorescence Detection in Analytical Chemistry and Biochemistry. Applied Spectroscopy Reviews 45:12–43.

Lim NH, Meinjohanns E, Bou-Gharios G, Gompels LL, Nuti E, Rossello A, Devel L, Dive V, Meldal M, Nagase H. 2014. In vivo imaging of matrix metalloproteinase 12 and matrix metalloproteinase 13 activities in the mouse model of collagen-induced arthritis. Arthritis Rheumatol. 66:589–598.

Lipscomb KE, Sarigul-Klijn N, Klineberg E, Mohan V. 2014. Biomechanical Effects of Human Lumbar Discography: In-vitro Experiments and Their Finite Element Validation. J.Spinal Disord.Tech. pp. –.

Maitre CLL, Freemont AJ, Hoyland JA. 2004. Localization of degradative enzymes and their inhibitors in the degenerate human intervertebral disc. J.Pathol. 204:47–54.

———. 2007. Accelerated cellular senescence in degenerate intervertebral discs: a possible role in the pathogenesis of intervertebral disc degeneration. Arthritis Res.Ther. 9:R45.

Marchand F, Ahmed AM. 1990. Investigation of the laminate structure of lumbar disc anulus fibrosus. Spine (Phila Pa 1976.) 15:402–410.

Masters BR. 2009. Correlation of histology and linear and nonlinear microscopy of the living human cornea. J.Biophotonics. 2:127–139.

Masters BR, So PT, Gratton E. 1997. Multiphoton excitation fluorescence microscopy and spectroscopy of in vivo human skin. Biophys.J. 72:2405–2412.

Masuda K, An HS. 2004. Growth factors and the intervertebral disc. Spine J. 4:330S–340S.

Masuda K, Aota Y, Muehleman C, Imai Y, Okuma M, Thonar EJ, Andersson GB, An HS. 2005. A novel rabbit model of mild, reproducible disc degeneration by an anulus needle puncture: correlation between the degree of disc injury and radiological and histological appearances of disc degeneration. Spine (Phila Pa 1976.) 30:5–14.

Masuda K, Lotz JC. 2010. New challenges for intervertebral disc treatment using regenerative medicine. Tissue Eng Part B Rev. 16:147–158.

Mayer JE, Iatridis JC, Chan D, Qureshi SA, Gottesman O, Hecht AC. 2013. Genetic polymorphisms associated with intervertebral disc degeneration. Spine J. 13:299–317.

Meerwaldt R, Graaff R, Oomen PH, Links TP, Jager JJ, Alderson NL, Thorpe SR, Baynes JW, Gans RO, Smit AJ. 2004. Simple non-invasive assessment of advanced glycation endproduct accumulation. Diabetologia 47:1324–1330.

Meisel HJ, Siodla V, Ganey T, Minkus Y, Hutton WC, Alasevic OJ. 2007. Clinical experience in cell-based therapeutics: disc chondrocyte transplantation A treatment for degenerated or damaged intervertebral disc. Biomol.Eng 24:5–21.

Michalek AJ, Buckley MR, Bonassar LJ, Cohen I, Iatridis JC. 2010. The effects of needle puncture injury on microscale shear strain in the intervertebral disc annulus fibrosus. Spine J. 10:1098–1105.

Mitchell PG, Magna HA, Reeves LM, Lopresti-Morrow LL, Yocum SA, Rosner PJ, Geoghegan KF, Hambor JE. 1996. Cloning, expression, and type II collagenolytic activity of matrix metalloproteinase-13 from human osteoarthritic cartilage. J.Clin.Invest 97:761–768.

Mujat C, Greiner C, Baldwin A, Levitt JM, Tian F, Stucenski LA, Hunter M, Kim YL, Backman V, Feld M, et al.. 2008. Endogenous optical biomarkers of normal and human papillomavirus immortalized epithelial cells. Int.J.Cancer 122:363–371.

Murphy G, Nagase H. 2008. Reappraising metalloproteinases in rheumatoid arthritis and osteoarthritis: destruction or repair?. Nat.Clin.Pract.Rheumatol. 4:128–135.

Nagase H, Visse R, Murphy G. 2006. Structure and function of matrix metalloproteinases and TIMPs. Cardiovasc.Res. 69:562–573.

Nerurkar NL, Baker BM, Sen S, Wible EE, Elliott DM, Mauck RL. 2009. Nanofibrous biologic laminates replicate the form and function of the annulus fibrosus. Nat.Mater. 8:986–992.

Neumann DA. 2009Kinesiology of the musculoskeletal system. Mosby.

Noailly J, Planell JA, Lacroix D. 2011. On the collagen criss-cross angles in the annuli fibrosi of lumbar spine finite element models. Biomech.Model.Mechanobiol. 10:203–219.

Palero JA, deBruijn HS, van der Ploeg van denHeuvel, Sterenborg HJ, Gerritsen HC. 2007. Spectrally resolved multiphoton imaging of in vivo and excised mouse skin tissues. Biophys.J. 93:992–1007.

Park CY, Zhu Z, Zhang C, Moon CS, Chuck RS. 2006. Cellular redox state predicts in vitro corneal endothelial cell proliferation capacity. Exp.Eye Res. 83:903–910.

Pfirrmann CW, Metzdorf A, Zanetti M, Hodler J, Boos N. 2001. Magnetic resonance classification of lumbar intervertebral disc degeneration. Spine (Phila Pa 1976.) 26:1873–1878.

Pogue BW, Pitts JD, Mycek MA, Sloboda RD, Wilmot CM, Brandsema JF, O'Hara JA. 2001. In vivo NADH fluorescence monitoring as an assay for cellular damage in photodynamic therapy. Photochem.Photobiol. 74:817–824.

Quesada I, Todorova MG, Soria B. 2006. Different metabolic responses in alpha-, beta-, and delta-cells of the islet of Langerhans monitored by redox confocal microscopy. Biophys.J. 90:2641–2650.

Quinn KP, Bellas E, Fourligas N, Lee K, Kaplan DL, Georgakoudi I. 2012. Characterization of metabolic changes associated with the functional development of 3D engineered tissues by non-invasive, dynamic measurement of individual cell redox ratios. Biomaterials 33:5341–5348.

Quinn KP, Sridharan GV, Hayden RS, Kaplan DL, Lee K, Georgakoudi I. 2013. Quantitative metabolic imaging using endogenous fluorescence to detect stem cell differentiation. Sci.Rep. 3:3432–.

Rajwa B, Bernas T, Acker H, Dobrucki J, Robinson JP. 2007. Single- and two-photon spectral imaging of intrinsic fluorescence of transformed human hepatocytes. Microsc.Res.Tech. 70:869–879.

Rasmussen HS, McCann PP. 1997. Matrix metalloproteinase inhibition as a novel anticancer strategy: a review with special focus on batimastat and marimastat. Pharmacol.Ther. 75:69–75.

Rauch B, Edwards RB, Lu Y, Hao Z, Muir P, Markel MD. 2006. Comparison of techniques for determination of chondrocyte viability after thermal injury. Am.J.Vet.Res. 67:1280–1285.

Risbud MV, Schaer TP, Shapiro IM. 2010. Toward an understanding of the role of notochordal cells in the adult intervertebral disc: from discord to accord. Dev.Dyn. 239:2141–2148.

Rivera DR, Brown CM, Ouzounov DG, Pavlova I, Kobat D, Webb WW, Xu C. 2011. Compact and flexible raster scanning multiphoton endoscope capable of imaging unstained tissue. Proc.Natl.Acad.Sci.U.S.A 108:17598–17603.

Roberts S, Evans H, Trivedi J, Menage J. 2006. Histology and pathology of the human intervertebral disc. J.Bone Joint Surg.Am. 88 Suppl 2:10–14.

Rocheleau JV, Head WS, Piston DW. 2004. Quantitative NAD(P)H/flavoprotein autofluorescence imaging reveals metabolic mechanisms of pancreatic islet pyruvate response. J.Biol.Chem. 279:31780–31787.

Roughley PJ. 2004. Biology of intervertebral disc aging and degeneration: involvement of the extracellular matrix. Spine (Phila Pa 1976.) 29:2691–2699.

Schenke-Layland K, Riemann I, Damour O, Stock UA, Konig K. 2006. Two-photon microscopes and in vivo multiphoton tomographs–powerful diagnostic tools for tissue engineering and drug delivery. Adv.Drug Deliv.Rev. 58:878–896.

Schroeder Y, Wilson W, Huyghe JM, Baaijens FP. 2006. Osmoviscoelastic finite element model of the intervertebral disc. Eur.Spine J. 15 Suppl 3:S361–S371.

Sivan SS, Tsitron E, Wachtel E, Roughley P, Sakkee N, van derHam F, Degroot J, Maroudas A. 2006. Age-related accumulation of pentosidine in aggrecan and collagen from normal and degenerate human intervertebral discs. Biochem.J. 399:29–35.

Skala MC, Riching KM, Gendron-Fitzpatrick A, Eickhoff J, Eliceiri KW, White JG, Ramanujam N. 2007. In vivo multiphoton microscopy of NADH and FAD redox states, fluorescence lifetimes, and cellular morphology in precancerous epithelia. Proc.Natl.Acad.Sci.U.S.A 104:19494–19499.

Sobajima S, Kompel JF, Kim JS, Wallach CJ, Robertson DD, Vogt MT, Kang JD, Gilbertson LG. 2005. A slowly progressive and reproducible animal model of intervertebral disc degeneration characterized by MRI, X-ray, and histology. Spine (Phila Pa 1976.) 30:15–24.

Squirrell JM, Wokosin DL, White JG, Bavister BD. 1999. Long-term two-photon fluorescence imaging of mammalian embryos without compromising viability. Nat.Biotechnol. 17:763–767.

Tardif G, Pelletier JP, Dupuis M, Geng C, Cloutier JM, Martel-Pelletier J. 1999. Collagenase 3 production by human osteoarthritic chondrocytes in response to growth factors and cytokines is a function of the physiologic state of the cells. Arthritis Rheum. 42:1147–1158.

Theer P, Hasan MT, Denk W. 2003. Two-photon imaging to a depth of 1000 microm in living brains by use of a Ti:Al2O3 regenerative amplifier. Opt.Lett. 28:1022–1024.

Thompson JP, Pearce RH, Schechter MT, Adams ME, Tsang IK, Bishop PB. 1990. Preliminary evaluation of a scheme for grading the gross morphology of the human intervertebral disc. Spine (Phila Pa 1976.) 15:411–415.

Tiede LM, Rocha-Sanchez SM, Hallworth R, Nichols MG, Beisel K. 2007. Determination of hair cell metabolic state in isolated cochlear preparations by two-photon microscopy. J.Biomed.Opt. 12:021004–021008.

Troeberg L, Nagase H. 2012. Proteases involved in cartilage matrix degradation in osteoarthritis. Biochim.Biophys.Acta 1824:133–145.

Urban JP, Roberts S. 2003. Degeneration of the intervertebral disc. Arthritis Res.Ther. 5:120–130.

Urban JP, Winlove CP. 2007. Pathophysiology of the intervertebral disc and the challenges for MRI. J.Magn Reson.Imaging 25:419–432.

vanBeurden PAS, denHoff JWV. 2005. Zymographic techniques for the analysis of matrix metalloproteinases and their inhibitors. Biotechniques 38:73–83.

vanDijk B, Potier E, Ito K. 2011. Culturing bovine nucleus pulposus explants by balancing medium osmolarity. Tissue Eng Part C.Methods 17:1089–1096.

Vernon-Roberts B, Moore RJ, Fraser RD. 2007. The natural history of age-related disc degeneration: the pathology and sequelae of tears. Spine (Phila Pa 1976.) 32:2797–2804.

———. 2008. The natural history of age-related disc degeneration: the influence of age and pathology on cell populations in the L4-L5 disc. Spine (Phila Pa 1976.) 33:2767–2773.

Videman T, Nurminen M. 2004. The occurrence of anular tears and their relation to lifetime back pain history: a cadaveric study using barium sulfate discography. Spine (Phila Pa 1976.) 29:2668–2676.

Visse R, Nagase H. 2003. Matrix metalloproteinases and tissue inhibitors of metalloproteinases: structure, function, and biochemistry. Circ.Res. 92:827–839.

Vo NV, Hartman RA, Yurube T, Jacobs LJ, Sowa GA, Kang JD. 2013. Expression and regulation of metalloproteinases and their inhibitors in intervertebral disc aging and degeneration. Spine J. 13:331–341.

Vossen M, Teeuwisse W, Reijnierse M, Collins CM, Smith NB, Webb AG. 2011. A radiofrequency coil configuration for imaging the human vertebral column at 7 T. J.Magn Reson. 208:291–297.

Wang HW, Wei YH, Guo HW. 2009. Reduced nicotinamide adenine dinucleotide (NADH) fluorescence for the detection of cell death. Anticancer Agents Med.Chem. 9:1012–1017.

Weiler C, Nerlich AG, Zipperer J, Bachmeier BE, Boos N. 2002. 2002 SSE Award Competition in Basic Science: expression of major matrix metalloproteinases is associated with intervertebral disc degradation and resorption. Eur.Spine J. 11:308–320.

Wu W, Billinghurst RC, Pidoux I, Antoniou J, Zukor D, Tanzer M, Poole AR. 2002. Sites of collagenase cleavage and denaturation of type II collagen in aging and osteoarthritic articular cartilage and their relationship to the distribution of matrix metalloproteinase 1 and matrix metalloproteinase 13. Arthritis Rheum. 46:2087–2094.

Wu Y, Leng Y, Xi J, Li X. 2009. Scanning all-fiber-optic endomicroscopy system for 3D nonlinear optical imaging of biological tissues. Opt.Express 17:7907–7915.

Yasuma T, Arai K, Suzuki F. 1992. Age-related phenomena in the lumbar intervertebral discs. Lipofuscin and amyloid deposition. Spine (Phila Pa 1976.) 17:1194–1198.

Ying W. 2008. NAD+/NADH and NADP+/NADPH in cellular functions and cell death: regulation and biological consequences. Antioxid.Redox.Signal. 10:179–206.

Yoon ST, Patel NM. 2006. Molecular therapy of the intervertebral disc. Eur.Spine J. 15 Suppl 3:S379–S388.

Yoshikawa T, Ueda Y, Miyazaki K, Koizumi M, Takakura Y. 2010. Disc regeneration therapy using marrow mesenchymal cell transplantation: a report of two case studies. Spine (Phila Pa 1976.) 35:E475–E480.

Yu Q, Heikal AA. 2009. Two-photon autofluorescence dynamics imaging reveals sensitivity of intracellular NADH concentration and conformation to cell physiology at the single-cell level. J.Photochem.Photobiol.B 95:46–57.

Zhang Y, Chee A, Thonar EJ, An HS. 2011. Intervertebral disk repair by protein, gene, or cell injection: a framework for rehabilitation-focused biologics in the spine. PM.R. 3:S88–S94.

Zhang Y, Li Z, Thonar EJ, An HS, He TC, Pietryla D, Phillips FM. 2005. Transduced bovine articular chondrocytes affect the metabolism of cocultured nucleus pulposus cells in vitro: implications for chondrocyte transplantation into the intervertebral disc. Spine (Phila Pa 1976.) 30:2601–2607.

Zhang YG, Guo TM, Guo X, Wu SX. 2009. Clinical diagnosis for discogenic low back pain. Int.J.Biol.Sci. 5:647–658.

Zhu L, Ma Y, Kiesewetter DO, Wang Y, Lang L, Lee S, Niu G, Chen X. 2014. Rational design of matrix metalloproteinase-13 activatable probes for enhanced specificity. ACS Chem.Biol. 9:510–516.

Zhu L, Xie J, Swierczewska M, Zhang F, Quan Q, Ma Y, Fang X, Kim K, Lee S, Chen X. 2011. Real-time video imaging of protease expression in vivo. Theranostics. 1:18–27.

Zipfel WR, Williams RM, Christie R, Nikitin AY, Hyman BT, Webb WW. 2003. Live tissue intrinsic emission microscopy using multiphoton-excited native fluorescence and second harmonic generation. Proc.Natl.Acad.Sci.U.S.A 100:7075–7080.

Zoumi A, Yeh A, Tromberg BJ. 2002. Imaging cells and extracellular matrix in vivo by using second-harmonic generation and two-photon excited fluorescence. Proc.Natl.Acad.Sci.U.S.A 99:11014–11019.

Acknowledgments

In contrasts to common belief, research is very much a collaborative effort and many people have knowingly or not contributed to the realization of this thesis. First and foremost, a very special "Thank You" goes out to Prof. Dr. Keita Ito. Keita, thank you very much for giving me the opportunity to pursue a doctorate under your guidance and supervision and believing in me even in times of despair. I do not only value your extensive knowledge on all research related matters but I can truly say that these 4.5 working with you have shaped my way of "thinking". Sometimes, I even catch myself asking people "what is your research question?" ☺. Thank you for always having an open door, pushing me and our work to a higher level, and putting things in perspective when all I saw was confusion.

Next, I'd like to thank the PhD committee members for taking their time to not only read this thesis but also giving valuable input. Prof. Iatridis, I was very happy that you accepted to take part in this PhD defense. I truly appreciate your input and it feels somewhat like closing a circle since at the very beginning of my PhD I got the chance to talk to you personally at the ORS. Dr. Creemers of zou ik zeggen Laura, helaas ben jij pas in het derde jaar betrokken geraakt aan dit project. Wat mij betreft had jij al vanaf het begin erbij mogen zijn! Ik weet niet hoe vaak ik al "dank je wel" heb gezegd, maar zonder jou hulp was hoofdstuk 5 nooit zo ver gekomen. Ik sta nogs stets versteld hoeveel tijd en moeite je hebt genomen, om mij met mijn onderzoek te helpen. Ik heb onze samenwerking en jouw optimisme erg gewaardeerd en het is jou gelukt om het grote puzzle "matrix metalloproteinasen" iets verstandiger te maken. Dr, Merkx, Maarten, ook aan jou een groot dank je wel voor al jouw moeite en hulp. Je bent eigenlijk vanaf het begin bij deze proefschift betrokken geweest. Soms iets meer op het achtergrond en zeker de laatste 1.5 jaren helemaal vorop. Haartelijk bedankt voor al jouw inzet, vooral als het wat minder ging met mijn onderzoek. Ook voor jou geld, hoofdstuk fijf was zonder jouw ondersteuning nooit zo ver gekomen. Dr. Van Zandvoort, Marc, ik vind het heel prettig dat onze samenwerking tot twee leuke artikelen heeft geleidt. Je bijdrage was heel belangrijk en ik vond het heel leuk jij niet alleen als docent te heb leren kennen maar ook als collega onderzoeker. Last but not least. Dr. Van Donkelaar, Rene, hoewel je niet direct bij de verschillende projecten betrokken was, heb ik heel erg veel van jou kunnen leren en jou input tijdens groepdiscussiies enzovoort heeft ervoor gezorgd dat jij toch overal binnen dit proefschift aanwezig bent. Jouw oprecht interesse in ons project en je kritische vragen hebben mij veel geholpen en je deur stond altijd open voor vragen en brainstorm sessies.

As I mentioned earlier, research is a collaborative endeavor. This PhD thesis is very much the result of a larger cooperation as it was part of a European FP7 research project on intervertebral disc degeneration and back pain entitled "GENODISC". I feel very fortunate to having had the opportunity of getting to know so many different people with different backgrounds all interested in advancing our understanding of disc degeneration and regeneration. I would like to give a special thank you to Prof. Jill Urban, Prof. Sally Roberts, Prof. Dimitris Kletsas and Dr. Cornelia Neidlinger-Wilke whose fruitful input during various GENODISC meetings was very much appreciated.

Dr. Huyghe, Jacques, heel erg bedankt dat jij niet naar mij luisterde en mij de kans gaf om met een twee-fotonen microscoop te spleen toen ik pas in het eerste jaar van mijn Master zat. Zonder jou had ik waarschijnlijk nooit een microscoop in de handen gekregen. Dr. van Rietbergen, Bert, dank je wel voor de leuke gesprekken tijdens groepsuitingen etc. en voor jou advies wat betreft carriere paden. Janneke, wat ik moet ik zeggen, ik denk ik overtrijf niet als ik jou de "ziel" van onze groep mage noemen. Ik denk geen enkele proefschrift zou zonder al jouw werk tot stand komen. Daarnaast straal jij een optimisme uit en sta je altijd klaar als iemand hulp nodig heeft. Dus bij deze ook een super groot dank je wel aan jou en wie weet komen wij elkaar nog eens op een Electro feestje tegen ☺!. Dr. de Liefde-van Beest, Moniek, hoe vaak ben ik met een "spoed" bestelling bij jou lansgekomen en heb jij mij altijd geholpen? Heel erg bedankt! Ook wil ik je bedanken dat jij altijd veel begrip toont als er weer een student van Keita de nacht door moet werken ☺.

One very important factor that made me truly enjoy the countless hours in and around the lab were the people that call "Whoog" (I really cannot get used to calling it Gemini-Zuid) their second (?) home. Marc, onze samenwerking heft tot hoofdstuk vier geleidt. Naast deze prettige samenwerking was het erg leuk om jou beter te leren kennen. Alvast veel success met het afronden van jouw proefschift! Brian, hoewel je niet in Whoog zit, was jij mijn "partner in crime" wat betreft de FRET probe. Veel zweet en tranen zit in hoofdstuk vijf en zonder jouw syntheseskills waren we nooit zo ver gekomen. Heel erg bedankt! A very special thank you to all the PhD's and PostDocs of the Orthopedic Biomechanics group. We all share the same joy and pains and without that companionship PhD life could sometimes seem very futile. Linda, Stefan and Irene, my lab buddies, while I'm writing this, I truly hope you made it home early tonight. The Iranian "Mafia", Pooya, Reza and Javad, it was great having you guys around and even if I hardly understood whatever you guys were trying to "simulate", it was always fun hanging out. Juan, I wish we could have watched the World Cup final together. All the best to you and Sol and your son! May he revenge Argentina in 20 years ☺! Veronique, I know these last months were pretty tough. I'm very impressed how you've kept your head up high and never gave up. Good luck with finishing up your thesis and all the best to Nicola. Anthal, Renate, Rene en Menno wij hadden een leuke tijd als "Hora Estenaaren"! Professor Anita van de Loo, bedankt voor de gezelligheid in het lab. Dr. Nicky, Dr. Jasper and soon to be Dr. Chiara, thanks for sharing the joy and pain of "nightstalking" a.k.a. microscopy!

Eindhoven is sometimes compared to a black hole. Once you are in it, it won't ever let you go. During these 11 (!) years, I was very fortunate to have met a lot of awesome people and made friends for life. First of all, Agnese, I could write a chapter about you. Life in and outside TUE would not have been the same without you. You know the best and worst sides of me and throughout these years you've always been the one person that not only I, but pretty much everyone can rely on. It's amazing to see

how you never lose your good spirits and how you make this world a better place. I am very excited to see what the future will hold for you and Ozcan and I'm already looking forward to our next coffee chats, holiday trips and celebrations. Patrik, jij was de eerste kerel die mij en mijn gebrekkig Nederlands begreep ☺. Weet jij nog: blue eyes, Eagle, Cadzand, "Studeren" ☺! Vanaf het eerste dag was het lachen met jou en ook al ben je de laatste jaren je eigen weg gegaan, hebben wij ons nooit uit het oog verloren. Ik ben heel trots op jou dat je jouw eigen bedrijfje samen met Willem hebt opgebouwd. En natuurlijk wens ik jou en Saskia het beste voor de toekomst met jullie dochterjeto binnekort in Zwarte Woud. Rapha, my man, who would have thought you'd outlast me in Eindhoven? ☺ Since our Philips times, it's been a trip! I'm very happy things have turned out so well for you and Eszti. I'm looking forward to sharing a few "Gewrztraminers" with you! Dr. Potier, Esther, you started as my supervisor and soon enough become a good friend. Thank you for all your guidance and always having an answer ☺. I'm looking forward to seeing you soon in Paris. And tell Raymond, he's always invited to watch "Deadliest Catch" or even go on a survival trip! Carlos, the bookworm, I don't know if I should say "thanks" for all the jokes on my account ☺. Thanks for showing me how to play football and your patience regarding my "shot"☺. I really enjoyed our trips together notably to Germany and I hope we'll soon go on another journey together. Mamoun, I'm sorry I still can't pronounce your last name! Thank you for lifting the level of our conversations to a higher level. And don't listen to Carlos ☹! I will never forget our trip together to Jordan and Israel and I'm excited to hit the road again with you soon. Maria, you are one half of the Northern Alliance. Thanks for always backing me up! And I will finally admit that girls can play football ☺. Patty and Lolly, I'm sorry I never danced Salsa with you. That being said, I will never dance Salsa. Thanks for bringing some South American flavor to the group. George and Brano, the "professors", now that I switched to the dark side of the force, I wish you all the best in academia. I'm looking forward to seeing you here in Freiburg. Faysal, you know how it is being with a Portuguese lady! Don't worry, one day you will enjoy "salpicao" ☺. All the best to you and Ana. Fernando and Ana, it was great seeing you here in Germany. Los Pedros, Mariana and Pedro, we've met already a long time ago and each year your family is growing. You make parenting look easy! Manu and Valerio, soon we'll almost be neighbors again. I'm looking forward to seeing you in Switzerland. Ginny and that red-haired boy supposedly being Italian called Alberto ☺, I really enjoyed the countless parties with you. And yes Ginny, you finally joined the right research group ☺!

Last but not least, I would like to thank my family or should I say families ☺! Janny, Tonnis, Ielke en Tom, jullie waren en zijn nog stets een tweede familie voor mij. Helaas kan Tonnis er niet bij zijn, maar ik weet dat hij heel erg blij voor me is. "Obrigado" aos meus "pais" acorianos Lucia e Paulo. Ate ja em Horta! Tanja, meine groe Schwester, auch wenn wir uns nicht so hufig sehen, wei ich, dass du mir immer die Daumen drckst. Ben, noch bist du ein bisschen zu jung, um dir dieses Bchlein zu erklren. Aber auch du hattest deinen Anteil daran, denn dein Puzzleball hat mir immer geholfen. Peer, ich htte mir keinen besseren groen Bruder wnschen knnen. Du hast immer ein offenes Ohr, und hilfst mir wo du helfen kannst. Ich freue mich sehr fr dich und Christine. Rosa und Luisa, meinen beiden Zwillingsnichten, ich freue mich darauf euch bald fters zu sehen und hoffentlich sprecht ihr dann ganz langsam, weil woher soll Eurer Onkel wissen was "Anke" ist? Auch meinen beiden Eltern, Christel und Rainer, mchte ich herzlichst fr Ihre Liebe, Untersttzung und Vertrauen danken. Ich freue mich darauf

euch bald wiederzusehen und euch den Schwarzwald, die Vogesen und den Elsass zu zeigen.

Finally, Ana ☺! Obrigado pelo teu amor e por sempre me fazeres sorrir. *É*s a minha melhor amiga e juntos podemos conquistar o mundo.

Eindhoven, Maastricht and Freiburg January - September 2014

Roman